Development of malaria detection methods using *Plasmodium falciparum* histidine rich protein II as target biomarker

A thesis

Submitted by

Babina Chakma

For the award of the degree

Of

Doctor of Philosophy

Department of Biosciences and Bioengineering

Indian Institute of Technology Guwahati

Guwahati – 781039, Assam, India

February, 2018

INDIAN INSTITUTE OF TECHNOLOGY GUWAHATI

Department of Biosciences and Bioengineering

Guwahati - 781039

STATEMENT

I do hereby declare that the matter embodied in this thesis is the result of investigations carried out by me in the Department of Biosciences and Bioengineering, Indian Institute of Technology Guwahati, Assam, India, under the guidance of Prof. Pranab Goswami.

In keeping with the general practice of reporting scientific observations, due acknowledgements have been made wherever the work described is based on the findings of other investigators.

February, 2018

Babina Chakma

INDIAN INSTITUTE OF TECHNOLOGY GUWAHATI

Department of Biosciences and Bioengineering

Guwahati - 781 039, India

Phone: +91-361-2582202(Office)

Fax: +91-361-2582249 (Office)

E-mail: pgoswami@iitg.ernet.in

Pranab Goswami, PhD

Professor (Higher Academic Grade)

CERTIFICATE

It is certified that the work described in this thesis, entitled "Development of malaria detection methods using *Plasmodium falciparum* histidine rich protein II as target biomarker", performed by Babina Chakma for the award of degree of Doctor of Philosophy is an authentic record of the results obtained from the research work carried out under my supervision, in the Department of Biosciences and Bioengineering, Indian Institute of Technology Guwahati India. The results embodied in this thesis have not been submitted to any other University or Institute for the award of any degree.

Prof. Pranab Goswami, Ph.D

(Supervisor)

Acknowledgement

This PhD work presented here would not have been possible without the support of many people and I am truly indebted and thankful to all those who have contributed their time and effort throughout my journey of completing PhD.

I would like to extend my deepest gratitude towards my thesis advisor ***Prof. Pranab Goswami*** for mentoring me to think like a researcher and teaching me to never lose my patience. His esteemed guidance, advice and encouragement at every step has helped me to propel my work in a fruitful direction. His optimism and down to earth nature has kept me grounded and made this journey much bearable and memorable. I would also like to thank him for the well-equipped laboratory, vast resources and dedicated work culture that has made working in his laboratory a pleasant experience.

I would also like to extend my gratitude towards my doctoral committee members ***Prof. Utpal Bora***, ***Prof. Vikash Kumar Dubey***, and ***Prof. G. Krishnamoorthy*** for their critical assessments and valuable suggestions that helped me focus on the weaker areas of my research.

During this work I had great time with our research group who have helped me as well as cheered me during my hard days. I would like to give my warm thanks to my fellow lab members ***Priyamvada***, ***Ankana***, ***Phurpa***, ***Lightson***, ***Santhosh***, ***Naveen***, ***Sharbani***, ***Priyanki*** and ***Mrinal*** for their constant support professionally and emotionally. Special thanks to my seniors ***Mitun***, ***Madhuri***, ***Urimla***, ***Seeraj*** and ***Reddy Bhaiya*** for guiding me well around the laboratory. Also to my beloved juniors ***Smita***, ***Torsha***, ***Farhan***, ***Anil***, ***Naveen*** and ***Pooja*** to brighten up my days with their youthful energy.

Along with this I wish to extend my appreciation to the staff members of ***Dept. BSBE***, ***CIF*** and ***COE*** for their technical support.

Friends, who have always brightened my days, enriched my career and cheered my heart during hard days I want to acknowledge them all. I would like to especially thank ***Priyamvada*** and ***Ruchika*** for sharing with me the best memories of my life in IITG campus and realizing what friends for life are meant. I also want to appreciate ***Phurpa***, ***Nama*** and ***Beth*** who showed me there is so much to do in a life of a PhD scholar. Lastly to my hostel wing mates ***Rupali***, ***Mitali***, ***Anu, Neha***, ***Ruchira***, ***Ananya*** and ***Rakhi*** with whom I shared numerous cooked lunches and dinners, late night TV shows, birthday parties and moments of both happiness and sadness.

At the very end, I express my profound debt to my family members, to ***Papa***, ***Mama*** and ***Nikki*** who kept on encouraging me to pursue this path. Special thanks to my husband ***Prout*** and his family for supporting and showing great patience while I pursued my PhD. Their unconditional love, encouragement, sacrifices, and faith in my capabilities had always kept me going and made me fulfil this journey.

Babina Chakma

Table of Contents

Abstract

The current investigation focuses on the development of chemical and aptamer recognition systems to detect histidine rich protein-II (HRP-II) with an aim of developing efficient diagnostic systems for malaria caused by *P.falciparum*. Based on our investigation we put forwarded three independent proof of concepts which will be further discussed below : (A) development of an indicator displacement based optical detection of malaria for application in point-of-care settings, (B) quantitative detection of histidine-rich proteins using silver nanoparticle-based sensitive competitive binding assay following spectroscopic approach and lastly (C) development of a specific aptamer against HRP-II and an electrochemical impedance spectroscopy based aptasensor for malaria using HRP-II as target biomarker. The biomarker HRP-II required for the experiments was sub-cloned, expressed, purified and finally characterized to validate the natural integrity of the protein. The novel ssDNA aptamer against HRP-II namely B4 was generated following a systematic molecular approach starting from SELEX (Systemic evolution of ligands by exponential enrichment), cloning and screening of the enriched candidates and then finally, validated the specificity by analysing the binding affinity using ITC.

(A) Development of an indicator displacement based optical detection of malaria for application in point-of-care settings.

This approach is based on competitive displacement of murexide dye from its complex with Ni^{2+} by HRP-II present in serum samples. The binding constant (K_d) discerned for the dye and HRP-II to Ni^{2+} were 1.4×10^{-6} M^{-1} and 6.8×10^{-9} M^{-1}, respectively. The progress of the reaction could be monitored from the change of color from orange (~λ_{482}

$_{nm}$) to pink (~$\lambda_{515\ nm}$) with the concomitant increase in HRP-II concentration in the mixture. A linear response (R^2 = 0.995) curve was generated by plotting the ratio of absorbance (λ_{515} /λ_{482}) against the HRP-II concentrations. The method offered to detect HRP-II as low as 1 pM without any interference from some common salts and the major protein, HSA, present in the blood serum. The detection method was reproduced in a microfluidic paper based analytical device (μPAD), fabricated by printing hydrophobic alkyl ketene dimer on a chromatographic paper to create hydrophilic microchannels, test zone, and sample application zone. The device offers to use a maximum sample volume of 20 ± 0.06 μL and detects HRP-II within 5 min with LOD of 30 ± 9.6 nM in a dynamic range of 10 to 100 nM.

(B) Quantitative detection of HisRPs using silver nanoparticle-based sensitive competitive binding assay following spectroscopic approach.

In the second approach we developed a simple competitive binding assay using glutathione self-assembled silver nanoparticles (GS-AgNPS) as colorimetric probe. The divalent nickel ion (Ni^{2+}) can electrostatically form complex with both the carboxyl-functionalized GS-AgNPs and contiguous histidine moieties ($2 \geq n$) of HisRPs. However, under competing environment Ni^{2+} binds preferentially to the HisRPs leaving behind the colloidal GS-AgNPs in solution, which exhibits SPR band at $\lambda_{390\ nm}$. Whereas, in absence of HisRPs, Ni^{2+} binds to the GS-AgNPs causing their aggregation that generates an SPR band at $\lambda_{450\ nm}$. The method was validated by two poly-His tagged proteins: lactate dehydrogenase and glutamate dehydrogenase and HRP-II. The respective LOD discerned for the proteins were 3.5 nM, 5.4 nM and 30 nM (R^2 = ~0.995). The method also offered to detect HRP-II in yes/no format following visual colorimetric signal and detect HRP-II in blood serum within 30 min at a low background noise (~4.4 %).

(C) Development of specific aptamer against HRP-II and an electrochemical impedance spectroscopy based aptasensor for malaria using HRP-II as target biomarker.

In this 3rd approach we report a novel ssDNA aptamer of 90 mer sequence developed by SELEX process against HRP-II. High stability of the secondary structure of the isolated aptamer was discerned from its free energy of folding of – 20.40 kcal.mole^{-1}. The binding constant (K_d) of the aptamer with HRP-II analysed by isothermal titration calorimetry was ~ 1.32 µM. Circular dichroism studies indicated B form of the aptamer DNA. The aptamer was chemically immobilized on a gold electrode surface through a self-assembled monolayer of dithio-bis(succinimidyl) propionate (DSP) to produce the aptasensor. The step wise modification of the layers over the gold electrode during fabrication of the aptasensor was confirmed by cyclic voltammetry. The aptasensor was then challenged with different concentration of HRP-II and analysed the interaction signals through electrochemical impedance spectroscopy. The impedance signal behaved reciprocally with the increasing concentrations of the target in the sample from which a dynamic range of 1 pM - 500 pM (R^2 = 0.99) and LOD of ~3.15 pM were discerned. The applicability of the developed aptasensor to detect HRP-II in mimicked real sample was also validated.

Finally, we critically evaluated our works and forwarded our views on the future scopes of translating these proofs of concept to commercially viable products.

List of abbreviations

AFM	Atomic force microscopy
AgNP	Silver nanoparticle
AKD	Alkyl Ketene Dimer
ANG	Angipoietin
AO	Acridine orange
APAD	3-Acety pyridine adenine dinucleotide
APADH	3-Acety pyridine adenine dinucleotide hydrate
ATP	Adenosine triphosphate
Au	Gold
AuNP	Gold nanoparticle
BSA	Bovine serum albumin
CD	Circular dichroism
CDC	Centers for disease control and prevention
CM	Cerebral malaria
COE	Centre for instrument facility
CPE	Constant phase element
CSF	Cerebrospinal fluid
CV	Cyclic voltammetry

CXCL	Chemokine interferon inducible protein
DBT	Department of biotechnology
DNA	Deoxyribonucleic acid
DSP	Dithiobis(succinimidyl propionate)
EDTA	Ethylenediaminetetraacetic acid
EIS	Electrochemical impedance spectroscopy
ELISA	Enzyme linked immunosorbent assay
EPO	Erythropoietin
FACS	Fluorescence activated cell sorting
FCM	Flow cytometry
FTIR	Fourier transform infrared spectroscopy
G6PD	Glucose 6-phosphate dehydrogenase
GO	Graphene oxide
GS	Glutathione
GSAgNPs	Glutathione coated silver nanoparticles
GSK	GlaxoSmithKline
GTS	Giemsa thick smear
GTTS	Giemsa thick and thin smear
HEPES	(4-(2-hydroxyethyl)-1-piperazineethanesulfonic acid)
His	Histidine

HisRPs	Histidine rich proteins
HPLC	High performance liquid chromatography
HRP-II	Histidine rich protein II
HSA	Human serum albumin
ICAM	Intracellular adhesion molecule
ICT	Immunochromatography tests
IFA	Immunofluorescence antibody testing
IHEC	Institute human ethics committee
IL	Interleukin
IPTG	Isopropyl β-D-1-thiogalactopyranoside
IgM	Mouse monoclonal antibody
ITC	Isothermal titration calorimetry
LAMP	Loop mediated isothermal amplification
LB	Luria Bertani
LDH	Lactate dehydrogenase
LDMS	Laser desorption mass spectrometry
LOD	Limit of detection
LSPR	Localized surface plasmon resonance
mAb	Monoclonal antibody
MM	Mild malaria

MP	Microparticle
MQ	Milli-Q
MVI	Malaria Vaccine Initiative
MWCNT	Multiwalled carbon nanotube
NAD	Nicotinamide adenine dinucleotide
NADH	Nicotinamide adenine dinucleotide reduced
Ni-NTA	Nickel Nitrilotriacetic acid
OD	Optical density
ORF	Open reading frame
PAGE	Polyacrylamide gel electrophoresis
PBS	Phosphate buffered saline
PCR	Polymerase chain reaction
PDB	Protein data bank
*Pf*EMP1	*P. falciparum* erythrocyte membrane protein 1
*Pf*GDH	*Plasmodium falciparum* glutamate dehydrogenase
*Pf*LDH	*Plasmodium falciparum* lactate dehydrogenase
PmLDH	*Plasmodium malariae* lactate dehydrogenase
POC	Point of care
PVDF	Polyvinylidene fluoride
QBC	Quantitative buffy coat

RBC	Red blood cell
RDT	Rapid diagnostic test
RMSD	Root mean square deviation
RNA	Ribonucleic acid
RSD	Relative standard deviation
RT	Room temperature
SAM	Self assembled monolayer
SD	Standard deviation
SDS	Sodium dodecyl sulfate
SELEX	Systematic evolution of ligands by exponential enrichment
SERS	Surface enhanced raman spectroscopy
SAHRP	Small histidine-alanine-rich protein
sFas	Soluble Fas ligand
SM	Severe malaria
SPR	Surface plasmon resonance
ssDNA	Single stranded DNA
sTNF-R	Soluble tumour necrosis factor receptor
TAE	Tris acetate EDTA
TBE	Tris borate EDTA
TEM	Transmission electron microscopy

TSS	Transformation and storage solution
USD	United States dollars
UV	Ultra violet
WB	Western blot
WHO	World health organization
µPAD	Microfluidic paper based analytical device

List of symbols

%	Percent
~	Approximately
<	Lesser than
=	Equal to
>	Greater than
≥	Greater than equal to
°C	Degree Celsius
µA	Microampere
µcal	Microcalorie
µg	Micrograms
µl	Microliter
µM	Micromolar
µmole	Micromole
2D	Two dimensional
3D	Three dimensional
A	Ampere
Å	Angstrom
a.u.	Arbitrary units

bp	Basepair
cal	Calorie
cm	Centimeter
Da	Dalton
g	Grams
h	Hour
Hz	Hertz
Ka	Association constant
kb	Kilobasepair
kcal	Kilocalorie
Kd	Dissociation constant
kDa	Kilodalton
kHz	Kilohertz
kV	Kilovolt
L	Liter
M	Molarity
mA	Milliampere
mdeg	Millidegree
mg	Milligrams
min	Minute

ml	Milliliter
mM	Millimolar
mm	Millimeter
mV	Millivolt
mV	Millivolt
Mw	Molecular weight
MΩ	Mega ohm
N	Normality
n	No. of binding sites
ng	Nanograms
nM	Nanomolar
nm	Nanometer
Nmole	Nanomole
Pg	Picograms
Pm	Picomolar
pmole	Picomole
R^2	Regression coefficient
R_{ct}	Charge transfer resistance
Rpm	Revolutions per minute
Rs	Solution resistance

S	Second
T	Temperature
V	Volt
v/v	Volume/volume
w/v	Weight/volume
Wt	Weight
X	Times concentrated
g	Centrifugation speed in RCF
Zw	Warburg impedance
ΔG	Change in free energy
ΔH	Change in enthalpy
ΔS	Change in entropy
λ	Lambda (unit of wavelength)
Ω	Ohm

List of figures

Figure 3.4: (A) Change of UV−Vis spectra of murexide dye upon addition of increasing concentration of Ni^{2+} and (B) absorbance ratio of $A_{515/482}$ for the reaction of murexide dye with the increasing concentration of Ni^{2+} in 20 mM HEPES buffer pH 7.4.

Figure 3.5: Plot of absorbance ratio of $A_{515/482}$ for a fixed amount of murexide-Ni^{2+} (1:1) against increasing concentration of HRP-II in 20 mM HEPES buffer pH 7.4. The linear region of the data (shown in the inset of part A) was fit to a linear equation. The cluster of data in the picomolar range was expanded (shown in the inset of part B) for clarity. Panel below the graph is a real representative image of HRP-II detection in solution.

Figure 3.6: Effect of different pH on the detection system: (A) UV−Vis spectra of murexide-Ni^{2+} in the presence of 500 nM HRP-II at pH (a) 5, (b) 6, (c) 7, (d) 8, (e) 9, and (f) 10. (B) Plot of ratio of absorbance of $A_{515/482}$ at pH 7, 8, and 9 against increasing concentration of HRP-II at an equimolar mixture of 50 µM murexide and Ni^{2+}.

Figure 3.7: (A) Plot of ratio of absorbance of $A_{515/A482}$ against concentration of protein (HSA and HRP-II) titrated to equimolar concentration of 50 µM murexide-Ni^{2+} complex in 20 mM HEPES buffer at pH 7.4. (B) Graph showing detection of 1 µM HRP II in the presence of serum (diluted 1:2) and 50 µM of different species of monovalent and diavalent salts in 20 mM HEPES at pH 7.5 and equimolar murexide – Ni^{2+} (50 µM) reaction mixture

Figure 3.8: Schematic showing the fabrication of paper based platform for detection of HRP-II

Figure 3.9: (A) Image of the paper platform showing the dimensions of six test zones connected to a central sample zone. For visibility of the channels and zones, blue ink was applied. SEM images of (B) nonprinted and (C) AKD printed on Whatman filter paper 1. AFM of (D) 2-D image and (E) height profile of selected region of nonprinted paper

surface. AFM of (F) 2-D image and (G) height profile of the AKD printed part of the paper platform.

Figure 3.10: Top panel shows representative real images of HRP-II detection on µPAD. The graph showing optical response in pixel intensity against concentrations of HRP-II in µPAD with the linear region of the data (shown in inset) fitted to linear equation (Y= mx + c, where m is the slope, c is the intercept on the y axis). Each datum is the mean of six assays and the error bars represent the relative standard deviations.

Figure 4.1: Simplified representation of the competitive binding assay format for detection of HisRPs using GS-AgNPs and Ni^{2+} ions

Figure 4.2: (A) Schematic showing synthesis of GS-AgNPs (B) UV-Vis spectra of AgNPs and GSH coated AgNPs. (C) Histogram showing the GS-AgNPs size distribution derived from TEM image (Inset) using Image J software. The TEM was operated at accelerating voltage of 200 kV (D) FTIR Spectra of GSH and GS-AgNPs

Figure 4.3: (A) Detection scheme of HisRPs following competitive binding assay. Inset (a) TEM image of disaggregation of nickel conjugated GS-AgNPs in the presence of HisRPs (in this case HRP-II) and (b) aggregation of GS-AgNPs in presence of only Ni^{2+}ions. (B) UV-Vis spectra of GS-AgNPs under different conditions as shown in the inset legend.

Figure 4.4: Optical response of GS-AgNPs (150 µl) versus concentration of Ni^{2+} ions. Each datum point is an average of at least three independent experiments, error bars represent the SD. Experiment was performed in 20 mM HEPES pH 7.4, at RT for 15 mins

Figure 4.5: Competitive binding assay for the detection of (A) *Pf*GDH, (B) *Pf*LDH, and (C) HRP-II, HSA and free histidine. Insets show the linear region of the response. Bottom

List of tables

Introduction

Introduction

Malaria is a life-threatening disease occurring mostly in the tropical regions of developing and underdeveloped countries. There were 91 countries and areas including the risk regions of sub-Saharan Africa, South-East Asia, Eastern Mediterranean, Western Pacific, and the Americas had malaria transmission in 2016 (WHO report, 2017). Malaria is caused by the protozoan parasites of the genus *Plasmodium* that are transmitted to people through the bites of infected female *Anopheles* mosquitoes. Five different *Plasmodium* species are known to affect humans namely *P.falciparum*, *P.vivax*, *P.malariae*, *P.ovale*, *P.knowlesi*. Infection caused by *P.falciparum* species is the most dreaded one and it is responsible for most malaria-related deaths globally. Even though there has been a continuous effort to eradicate malaria from the world for the last several decades, it still remains a threat to the masses particularly, to the malaria endemic countries. One of the major issues that stands as hurdle in effective malaria management is the emergence of drug resistant *P. falciparum* strain. The drug-resistant strain emerged for the first time in Southeast Asia, Oceania, and South America between late 1950s and early 1960 and since then it has been spreading in other risk regions of the globe. There has also been a growing concern on the asymptomatic malaria, which occurrs due to

partial immunity against the parasite. It is generally referred to infection with low malarial parasitaemia density that does not show any acute symptoms (Lindblade *et al*., 2013). Such low parasitaemia cases can be detected mostly by highly sensitive molecular biology techniques such as, PCR. Asymptomatic malaria do not pose immediate threat to the patients as compared to severe malaria however, if ignored it can contribute to inflammatory responses, anaemia, cognitive impairment and delayed physical development (Chen *et al.,* 2016). Moreover, the group of people with these asymptomatic infections in endemic areas contribute to the human infectious reservoir. Efforts to develop malaria vaccines have been made by many organizations. One such vaccine termed RTS was developed during the year 2015 by PATH Malaria Vaccine Initiative (MVI) and GlaxoSmithKline (GSK) with support from the Bill and Melinda Gates Foundation. However, the vaccine showed poor results as the efficacy of the vaccine declined rapidly over time and hence needs to be improved for complete protection against malaria. Till then we need to have constant surveillance of malaria transmission by early diagnosis and treatment. This brings us back to the discussion of urgent requirement for an efficient and sensitive detection system which can also help malaria management to limit the recurrence of the drug resistance malaria by detecting the parasite at an early stage and at low parasite density. Several analytical techniques for malaria diagnosis are known, which will be elaborated under chapter 1. However, these techniques are associated with certain limitations such as requirement of skilled personnel and expensive equipment facility. Hence, deployment of these techniques in point of care (POC) settings is difficult. Currently, lateral flow based Rapid diagnostic tests (RDT)s are widely used in resource limiting situations and POC settings. Since most of the RDTs are antibody based, they are non-reusable, sensitive to high temperature and humidity, give highly variable results including batch to batch variations and most

importantly are unable to quantify infection. Various antibody based electrochemical immunosensors have also been developed. Nonetheless, stability and cost of these sensors are affected due to the inclusion of antibodies as recognition element. Many other malaria detection methods that rely on the chemical recognition principle though reported these techniques are in a preliminary stage of development and awaiting thorough validation for practical applications. Thus, in spite of the vast array of tests reported so far for POC settings, we are still in a hunt for a test that is quantitative, specific, sensitive, affordable and most importantly stable in harsh conditions for its successful use in malaria endemic countries with poor economic status.

Considering the above facts and gaps in the field of malaria diagnosis we focussed on developing non-antibody based malaria recognition systems that are stable, quantitative, sensitive and specific in nature. For this study we find that histidine rich protein II (HRP-II) is a suitable biomarker since it is a unique protein (37% histidine and 40% alanine) and is secreted specifically by *P.falciparum*. It is a stable, low molecular (~30 kDa) weight protein which is secreted in abundance during parasite growth and development. Due to its many attributes it is considered as an apt biomarker for *P.falciparum* malaria diagnosis. Initially, we concentrated on chemical detection systems exploring Nickel-histidine interactions as viable recognition option in optical platforms since the target biomarker constitutes high level of His residues. We also developed a new generation biorecognition molecule i.e aptamers against HRP-II by the SELEX (Systematic evolution of ligands by exponential enrichment) method. Aptamers are mostly single stranded DNA or RNA sequences that can bind to their target efficiently as antibodies. Moreover aptamers are thermally stable, cost effective due to availability of rapid mass scale synthesis protocol and can be easily modified as per the need. Further, we tried to incorporate low cost platforms such as, paper based microfluidics and screen printed

electrodes as the sensing platform to make our systems portable and low cost. The specific objectives of the work are.

- Expression, purification and characterization of HRP-II.
- Development of stable chemical recognition systems for optical detection of HRP-II
- Development of aptamer based recognition system

This thesis has been subdivided into 5 chapters as briefly described below. At the end of the chapters, a section describing the overall conclusion from the experimental works including a critical evaluation on the work and its future scope has been included.

Chapter 1: Literature review.

The objective of this chapter is to report the recent progress and status of malaria detection methods, with special emphasis on *P.falciparum* HRP-II targeted detection. This chapter reviews in detailed about the most reliable malaria biomarkers, its advantages and discusses the reasons of choosing HRP-II over other biomarker. Various conventional malaria detection methods are mentioned and compared to the more recent detection platforms to identify the important gaps to be bridged for developing efficient products of practical use.

Chapter 2: Expression, purification and characterization of *Plasmodium falciparum* Histidine Rich Protein II.

As a starting step towards the objective of developing malaria sensors, this chapter outlines the sub-cloning, expression and purification of the target protein in pure form following molecular techniques. The integrity of the purified protein was confirmed by

MALDI and CD analysis. Further characterization of protein was performed by Zeta potential and heme titration studies.

Chapter 3: Development of an indicator displacement based detection of malaria targeting HRP-II as biomarker for application in point-of-care settings.

This chapter describes a simple colorimetric method free from any labile biorecognition element to quantitatively detect specific malarial biomarker HRP-II in solution as well as on a paper based platform. The method involves the displacement of murexide dye from its coordinating Ni^{2+}complex by the target HRP-II protein through competitive binding events and then quantifying the target by measuring the colour intensity in a shift in the wavelength. A detail characterization of performance parameters, interference studies and its applicability in real serum were studied. This system was further upgraded into microfluidic paper based platform for cost effective, stable and easy detection followed by detailed characterization and studies on its performance.

Chapter 4: Quantitative detection of histidine-rich proteins using silver nanoparticle-based sensitive competitive binding assay.

This chapter discusses the method of synthesis of glutathione coated silver nanoparticles (GS-AgNPs), its characterization and application for quantitative detection of HRP-II following a principle of competitive binding assay. We also performed a detailed comparison of performance parameters with other histidine rich proteins such as poly his tagged proteins. Application of the method for real serum samples and interference studies were also studied and discussed.

Chapter 5: **Development of electrochemical impedance spectroscopy based aptasensor for malaria using HRP-II as target biomarker.**

The content in this chapter describes the development of specific DNA aptamers against HRP-II by the process of SELEX. The primary and secondary structures of the evolved aptamer candidates were determined. The specificity of the aptamer was investigated by using techniques such as, CD and ITC. The selected aptamer was further used to fabricate electrochemical aptasensor to detect HRP-II. The performance parameters of the modified electrode were examined.

Conclusion and future directions of research.

This section summarizes the work to reach a logical conclusion. Along with the concluding statements a critical evaluation on the works embodied in this thesis has been included in this section. Additionally, the scope of augmenting the work for translating the proposed proof of concepts to technologically viable products has been discussed at the end.

Chapter 1

Review of literature

Chapter 1

Review of literature

1.1 Overview

In the year 2015, World Health Organization (WHO) reported a staggering number of around 212 million cases of malaria out of which 429,000 deaths occurred worldwide. The African region was affected the most with 92 % deaths occurring due to malaria (WHO Report, 2016). The remaining 8 % deaths were detected in South East Asian countries and Mediterranean region. India is highly affected by malaria as statistics say that 75 % of all malaria cases in South-East Asia are from India. Out of all the malaria cases reported in the country, around 80 % is confined to the areas where population resides - in hilly, hard-to-reach or inaccessible regions. Malaria in India is particularly deep-rooted in low-income rural areas of eastern and north-eastern states, but also occurs in the central and more arid western parts of the country (National framework for malaria elimination Report 2016). Since the year 2010 the malaria incidence rates though fell by 21% globally, it still poses a great threat as it affects the developing nations socioeconomically.

Malaria is caused by parasites that are transmitted to people through the bites of infected female anopheles mosquitoes. With proper intervention this disease can be totally preventable and curable however when left untreated it can lead to several complications and can be a life-threatening disease. The causative agent of malaria is a protozoan parasite of the genus *Plasmodium*. There are around 5 species, *P. falciparum*, *P. vivax*, *P. malariae*, *P. ovale*, and *P. knowlesi* that can infect humans. After the bite the infective plasmodial stage enters liver parenchimal cells or hepatocytes aproximately in 45 minutes of the bite. Inside the hepatocytes, each sporozoite begins a phase of asexual reproduction resulting in the formation of a schizont, which contains thousands of merozoites. The hepatic schizogony is asymptomatic in nature, as only a few number of liver cells are infected (Bartoloni and Zammarchi, 2012). The hepatic phase of parasite development (hepatic schizogony) lasts on an average between 5.5 (*P. falciparum*) and 15 days (*P. malariae*). In case of *P. vivax* and *P. ovale* infections, a proportion of parasites may remain dormant in hepatocytes as hypnozoites for several months or up to five years which can later lead to malaria recurrence. With the rupture of mature schizonts large number of merozoites are released into the bloodstream that invade red cells rapidly to start a process of asexual multiplication (erythrocytic schizogony). Within the red blood cell, merozoites develop to trophozoites and schizonts as can be observed in different stages of infection (figure 1.1). At the time of schizont rupture, the release of malaria parasites and erythrocytic material into the circulation induce the pathophysiology process of malaria and the onset of symptoms that includes episodes of high fever which is followed by chills and rigors repeatedly in every 48 h in case of *falciparum*, *ovale* or *vivax*, every 72 h in *malariae*, and 24 h in *knowlesi* infections (https://www.cdc.gov/malaria/about /disease.html). The activation of the cytokine cascade is responsible for many of the symptoms and signs of malaria.

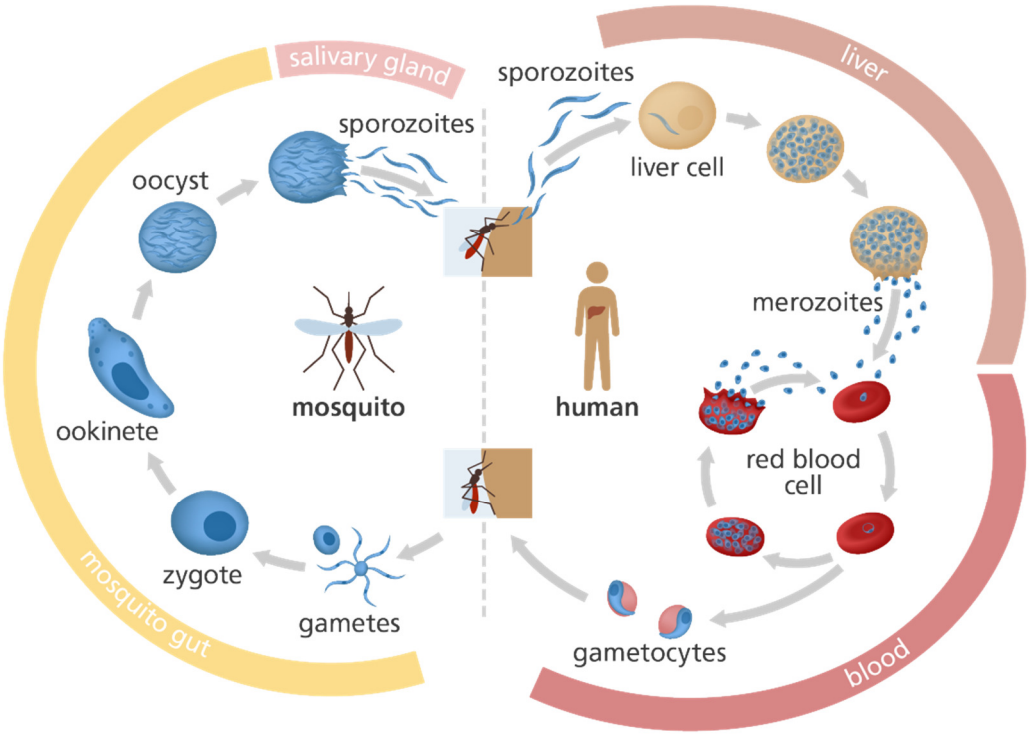

Figure 1.1: Life cycle of malaria parasite (https://www.malariagen.net/about/what-is malaria)

P. falciparum is known to be the deadliest species responsible for the highest mortality caused by malaria. Two main reasons that makes this species so dangerous: i) it replicates very fast and fever occurs within few days of the infection after which clinical deterioration takes place in 3-7 days (Trampuz *et al*., 2003), ii) Secondly, the parasite causes the Red Blood Cells (RBCs) to change shape and adhere to the endothelial lining of blood microvessels as well get sequestered into various organs thereby avoiding clearance by the spleen. This phenomenon is known as cytoadherence and is mediated by the members of the highly variable protein family known as *P. falciparum* erythrocyte membrane protein 1 (*Pf*EMP1). The sequesteration of the infected RBCs lead to blocking

of the blood vessels causing tissue hypoxia and when it occurs in the brain, the outcome is known as cerebral malaria, which is associated with most cases of severe malaria. All these information bring us to a point that there is an extreme urgency to detect malaria caused by *P.falciparum*. For specific and sensitive detection of malaria caused by *P.falciparum* we need to have an extensive knowledge about the biomarkers released that are characteristic to this *plasmodium* species. Malaria is detected by thin and thick smear microscopy, quantitative buffy coat (QBC), polymerase chain reaction (PCR), rapid diagnostic tests (RDTs) and other non-conventional methods which however, suffer from many limitations. In the following sections we shall discuss elaborately about the different biomarkers of *P.falciparum* and the detection methods developed till now.

1.2 Biomarkers of *P.falciparum*

Biomarkers are cellular, biochemical or molecular alterations that are measurable in biological samples which indicate any biological, pathogenic, or therapeutic responses (Hulka, 1991) and therefore are helpful for diagnosis as well as prognosis in many diseases. A good biomarker should have the following characteristics: (i) Suitable to diagnose a disease; (ii) identify patients at risk; (iii) stratify patients depending on disease severity; (iv) provide prognosis; (v) provide guidance in treatment; and, (vi) identify the risk for long-term complications (Stauga *et al*., 2013). *P.falciparum* synthesizes a panel of biomolecules such as, Lactate dehydrogenase, Hemozoin, Aldolase, Glutamate dehydrogenase and HRP-II which are considered as antigenic biomarkers. We also have host biomarkers that are released in response to the infection and considered as biomarkers against malaria in several cases. However these are not as specific as the antigenic biomarkers but they are still important to estimate severity of malaria.

1.2.1 Serological Biomarkers

Cerebral malaria (CM) is a life-threatening complication of malaria and is defined as an unarousable coma with a *P. falciparum* infection in the absence of other causes of encephalopathy. It is fatal within 24–72 h if left untreated (Lucchi *et al.,* 2011). The advantage of an early immunologically relevant serological biomarker for cerebral malaria CM would be helpful to distinguish febrile patients into groups: those who are likely to develop CM and those who are likely to develop severe malaria (SM) or mild malaria (MM). Although no clear biomarkers have yet been identified for CM, studies show a conspicuous relationship between host proteins such as, chemokine interferon inducible protein (CXCL10 and CXCL4) and severity of CM (Armah *et al*., 2007; Olszewski and Llinás, 2011). It was observed that patients with CM have significantly elevated levels of CXCL-10 and CXCL-4. Several other serological biomarkers for CM have also been identified. For example, CM neuropathy can be identified by observing elevated levels of soluble tumor necrosis factor receptor (sTNF-R) and soluble Fas ligand (sFas), (Armah *et al*., 2007). Cerebrospinal fluid (CSF) and serum levels of twelve cytokines and chemokines were monitored and it was found that elevated levels of interleukin 8 (IL-8), interleukin 1 receptor antagonist (IL-1ra), and TNFα were present in children infected with CM as compared to healthy controls (John *et al*., 2008). The levels of endothelial regulators such as, angiopoietin I (ANG I) and ANG II are also affected during CM. It was found that ANG II and ratio of ANG II: ANG I could be used to accurately distinguish between CM and MM patients (Lovegrove *et al*., 2009; Conroy *et al*., 2009). Potency of a neuroprotective factor, erythropoietin (EPO), was assessed to predict the risk of developing neurological sequelae after recovery to CM (Casals-Pascual *et al.*, 2008). Complement system components like C1q, C3, C4, and C5a are affected in malaria patients. Depressed levels of C3 were found in severe and

uncomplicated malaria as compared to 23 healthy controls (Wenish *et al.,* 1997; Olszewski and Llinás, 2011). Microparticles (MPs), also known as microvesicles, are fragments of plasma membrane shed by various cell types under physiological stress conditions (Freyssinet, 2003) and have also been linked with pathophysiology related to malaria (Haest, 1982). There is a dramatic difference in the plasma levels of MP of endothelial origin among Malawian children suffering from CM, severe malarial anaemia, and uncomplicated malaria caused by *P. falciparum* (Conners *et al.,* 2004). Mfonkeu and their group (Mfonkeu *et al.,* 2010) demonstrated by using fluorescence activated cell sorting (FACS) that MP of platelet origin may be a relevant marker in the routine follow up since the levels of MP dramatically increased during CM and decreased when the patient was cured.

Immunofluorescence antibody testing (IFA) is commonly used to detect any serological biomarkers but they are difficult to use reliably in diagnosing malaria. For instance, CXCR3 and its ligands have been implicated in case of several neurological diseases like West Nile virus (Klein *et al*., 2005; Zhang *et al*., 2008), *Toxoplasma gondii* (Olszewski and Llinás, 2011), and HIV infections (Sui *et al*., 2004). However, detection of these markers holds great significance to detect CM, once malaria diagnosis is confirmed by using an antigenic biomarker.

1.2.2 Antigenic malaria biomarkers

1.2.2.1 *Lactate Dehydrogenase*: During the intraerythrocytic stages, the parasite principally relies on anaerobic respiration for ATP generation from glucose, and the NAD^+ is regenerated by conversion of pyruvate to lactate while the mitochondria contribute minimally to the ATP pool (Fry *et al.,* 1990). Due to the dependence on the glycolytic cycle for energy generation, enzymes such as lactate dehydrogenase (LDH),

involved in this pathway are overexpressed (Roth, 1990). It has been found that *P. falciparum* LDH (*Pf*LDH) RNA expression level gradually increases, with the peak expression being at 24 to 30 h in the intraerythrocytic cycle and declines to zero in the schizont stage. *Pf*LDH is a tetramer where each monomer consists of two domains, the larger domain comprises the Rossmann fold that binds the cofactor NADH while the catalytic residues are located in the other domain. Protozoal LDHs display some major structural and kinetic differences compared to their mammalian counterparts that may be exploited to develop selective drugs and detection systems for malaria. Structurally the parasite enzyme differs in having a five-residue insertion "DKEWN" (D-Aspartic acid, E-Glutamic acid, K-Lysin, W-Tryptophan, and N-Asparagine) which was used as a common diagnostic epitope by Hurdayal and his group (Hurdayal *et al.,* 2010) to selectively detect parasite LDH from human LDH isoforms. Kinetically, the parasite enzyme differs by not being inhibited by excess of the substrate pyruvate, a feature not shared by mammalian enzymes (Sessions *et al.,* 1997). Another kinetic difference is the ability of the parasite LDH to efficiently use the synthetic cofactor $APAD^+$ (3-acetylpyridine adenine dinucleotide) (Dunn *et al.,* 1996; Chaikuad *et al.,* 2005). The findings underline the fact that there are structural differences between the two enzymes that may be exploited for selective detection of pLDH for malaria diagnosis.

1.2.2.2 *Glutamate dehydrogenases*: Glutamate dehydrogenases (GDHs) are ubiquitous enzymes that occupy an important branch point between carbon and nitrogen metabolism. The enzyme is implemented in the reversible interconversion of NADP linked oxidative deamination of L-glutamate to alpha ketoglutaric acid and ammonia. *P. falciparum* GDH (*Pf*GDH) is a NADP-dependent GDH which is a homohexamer with a subunit of Mw 49,500 and has three isozymes. It expressed episomally in *P. falciparum* and localizes exclusively to the parasite's cytosol (Storm *et al.,* 1997). It has been

postulated to play a role in the parasite's redox metabolism (Roth, 1990). GDHs possess a unique N terminal residue extension not found in the mature human enzyme and are present throughout the intraerythrocytic cycle of the parasite. Furthermore, GDHs are absent in the host RBC making them a potent biomarker (Wagner *et al.,* 1998). *Pf*GDH was used to detect the presence of *P. falciparum* using western blotting as well (Rodríguez-Acosta *et al*., 1998). Monoclonal antibodies in combination with colloidal gold were used in an immunochromatographic assay for diagnosis of *P. falciparum*. This assay showed a sensitivity and specificity of 86.6 % and 96.4 %, respectively (Li *et al*., 2005). These characteristics of *Pf*GDH make it an ideal candidate for the diagnosis of malaria with high sensitivity and specificity

1.2.2.3 *Hemozoin*: Hemozoin is an insoluble microcrystalline product formed from the digestion of blood by *Plasmodium* spp. and few other species of blood-feeding parasites (Oliveira *et al*., 1999; Chen *et al*., 2001; Pisciotta *et al*., 2005). Originally, Giovanni Maria Lancisi (1717) had observed that internal organs of malaria victims are decolorized; the biochemical reason of it was, however, not known. Later on the cause was attributed to hemozoin. Hemozoin plays a role as visible marker in identifying malarial parasites and hence, it is popularly termed as malaria pigment. The parasites infect the RBCs and digest hemoglobin resulting in release of amino acids and toxic-free heme (ferriprotoporphyrin IX) which is polymerized to hemozoin. The crystal structure of hemozoin consists of an unusual polymer of hemes linked between the central ferric ion of one heme and a carboxylate side-group oxygen of another heme (Slater *et al*., 1991). Later on its crystal structure was confirmed to be similar to synthetic β-hematin using X-ray diffraction powder pattern (Pagola *et al.,* 2000). Though there has been extensive study on the structure and characterization of hemozoin crystals, the process of its nucleation is not yet clearly known. There are reports about initiation of hemozoin

formation occuring autocatalytically, while other reports suggest that it requires external aids (Adams *et al.,* 1996). However, there are other mechanisms that support the view that it is promoted by polar membrane lipids (Bendrat *et al.,* 1995) and neutral lipid bodies (Fitch *et al.,* 1999; Jackson *et al.,* 2004; Pisciotta *et al.,* 2007). Since it is a survival tactic of the parasite from the heme toxicity, it has been targeted for malaria drug study for many years (Solomonov *et al.,* 2007).

1.2.2.4 *Aldolase*: The Aldolase enzyme holds a key role in the glycolytic pathway of the parasite as its function is to catalyse fructose- 1,6-bisphosphate into glyceraldehyde-3-phosphate and dihydroxyacetone phosphate (Srivastava *et al*., 1990). The enzyme is homotetrameric protein with each subunit of approximately 40 kDa (Döbeli *et al*., 1990). The enzyme has high degree of sequence diversity from the host and thus has the potential as a drug target. There have been studies on inhibition of recombinant *P. falciparum* aldolase by several candidates like rabbit antibodies, a 19- residue synthetic peptide, and phosphorothioate and antisense oligodeoxynucleotides (Döbeli *et al*., 1990; Shear *et al.,* 1999). Many reports have shown poor sensitivity of aldolase RDTs which encouraged studying more its genetic diversity. Lee *et al*. (2006a) studied the diversity in *P. falciparum* and *P. vivax* aldolase and showed that the aldolase gene was highly conserved, indicating that antigenic diversity is not a cause of variable RDT sensitivity, and the reason for the poor performance of aldolase based RDT tests thus remains to be investigated.

1.2.2.5 *Histidine-Rich Protein (HRP)-II*: Histidine rich proteins were detected when numerous cytoplasmic granules were isolated and studied for the first time in the avian malarial parasite *P. lophure*. The proteins showed an unusual amino acid composition with 73 % histidine, 7.5 % proline, 7 % alanine, 6 % glutamic acid, and 2.1 % aspartic acid that gave its name and raised interest in the structure of the protein and its function

(Kilejian, 1974). *P. falciparum* is known to synthesize unique set of soluble HRPs during the asexual erythrocytic development which are denoted as HRPs I, II, and III in the order of their discovery (Howard *et al*., 1986). HRP-I protein, also known as knob-associated protein (KAHRP-I), is found in Knob+ strain which means phenotypically it expresses knob-like protrusion on the cell surface and is suggested to help in the cytoadherence of infected erythrocytes to the venular endothelium (Pologe *et al.,* 1987) which partially contributes to the high parasitemia and hypoxia associated with *P. falciparum* as shown in figure 1.2. HRP-II, which is exclusive to *P. falciparum*, is found in both Knob+ and Knob− strains and is reported to have many functions such as, cytoadherence by forming knob like protrusions as HRP-I as well as heme binding and heme detoxification by forming hemozoin (Leech *et al.,* 1984; Lynn *et al.,* 1999). Lastly, HRP-III, also known as small histidine-alanine-rich protein (SAHRP), is a smaller protein which is not found as abundant as the other two proteins. It shares high homology with HRP-II (Wellems and Howard *et al.,* 1986). Due to its homology, varying degrees of cross-reactivity between HRP-II and HRP-III have been reported for HRP-II MAbs: 2G12, MAb87, and 1D6 (Rock *et al.,* 1987). However, there are reports of HRP-III sequence of FC27 strain, a *Plasmodium* isolate FCQ27/PNG from Papua New Guinea, shown to have polymorphisms in the gene's repeats (Stahl *et al.,* 1985). Out of the three proteins HRP-II is the most widely studied biomarker of choice since it is expressed on the membrane surface and is found in abundance than the other two proteins.

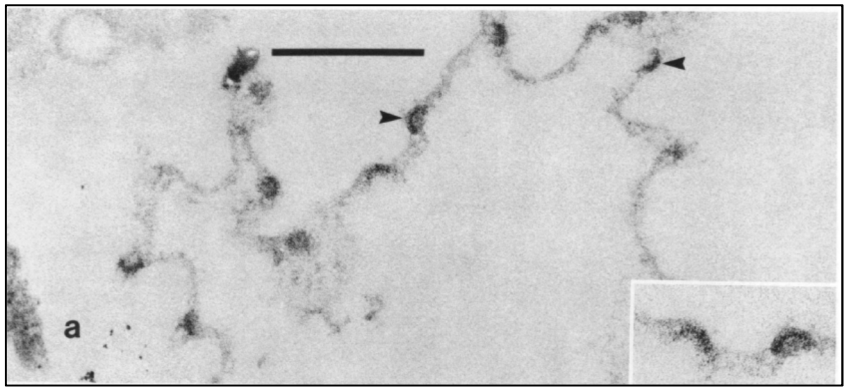

Figure 1.2: Electron micrograph of detergent-insoluble residues of infected RBC showing electron dense cups (▶) that act as focal points for knob like protrusions by HRPs (Leech *et al*, 1984).

The genomic sequence of HRP-II contains a hydrophobic signal peptide, an intervening intron and an extensive region of tandem repeats that encodes a 35 kDa polypeptide consisting mostly of histidine, alanine, and aspartic acid. There are 18 tripeptides (Ala-His-His), 3 pentapeptides (Ala-His-His-Ala-Ala), and 33 hexapeptides (Ala-His-His-Ala-Ala-Asp. There is about 85–90 % homology between the tandem repeat domains and the regions flanking the repeats of HRP-II and HRP-III genes which imply that both have originated in the duplication of an ancestral sequence. Both HRPs-II and -III share many similarities, but it is still unclear how these genes function and why HRP-II is released in large quantities than HRP-III.

Studies were performed to observe HRP-II synthesis and location during the parasite's intracellular growth. IgM mouse monoclonal antibody (mAb 87) specific to HRP-II was used to study the molecular form of the protein in the infected RBCs by immune-precipitation and immunoblotting. To find the subcellular location of the protein, immunofluorescence and cryothin-section immunoelectron microscopy were performed

where the location of bound mAb 87 was identified by conjugated colloidal gold particles that were observed as clusters within the cytoplasm of the intracellular malaria parasite, within the cytoplasm of the host cell, and periphery of the infected RBC. The authors reported that HRP-II synthesis begins with immature parasites and continued throughout the trophozoite stage as a water soluble extracellular protein which is exported through the erythrocyte cytoplasm, surface membrane to accumulate in the extracellular culture supernatant at the end. They further confirmed that HRP-II is released from RBCs containing growing parasites as they recovered the protein from 2 and 8 h culture supernatants (Howard *et al*., 1986). HRP-II is found in other places too such as cerebrospinal fluid and urine of infected patients (Parra *et al*., 1991; Valle *et al*., 1991) as well as food vacuole (Desakorn *et al.,* 2005) and digestive vacuole (Sullivan *et al.,* 1996) of the infected RBCs (Rock *et al.,* 1987). In short, HRP-II is found everywhere and released in abundance which is the reason for its importance as a biomarker of malaria.

The actual function of the HRP-II is not yet adequately known but many reports have demonstrated that its main function is heme binding that may link its role in the heme detoxification in malaria parasites. Spectroscopic studies showed that a single HRP-II molecule can bind to multiple 15-18 heme molecules (Choi *et al.,* 1999; Sullivan *et al.,* 1996; Schneider and Marletta, 2005; Pandey *et al.,* 2001). The K_d values for heme binding were calculated to be 0.34 μM and 0.94 μM. Further, it was confirmed that the heme-HRP-II complex binds in low spin, six coordinated, and bis-imidazole fashion. The crystal structure of HRP-II is not determined yet but the CD spectrum of HRP-II in aqueous medium indicates the secondary structure as random coil. However, the spectrum changes dramatically from random coil to 3_{10}-helix conformation as soon as heme molecules are titrated in the solution. It is interesting to note that the 3_{10}-helix

conformation is commonly observed in proteins as short sequences of three to four residues, mostly associated with N- or C-termini of α-helices (Barlow and Thornton., 1988; Karpen *et al*., 1992). Nonetheless, the length of 3_{10}-helix is found to be unusually long in case of HRP-II. Hence, based on these studies authors predicted three model structures of HRP-II as 3_{10}-helix and α-helices which are shown in the figure 1.3. Another interesting observation was that at saturating heme concentration, HRP-II was found to form dimers which are attributed to the structural changes that takes place upon heme binding and brings two HRP-II monomers within close proximity thus facilitating disulphide bond formation.

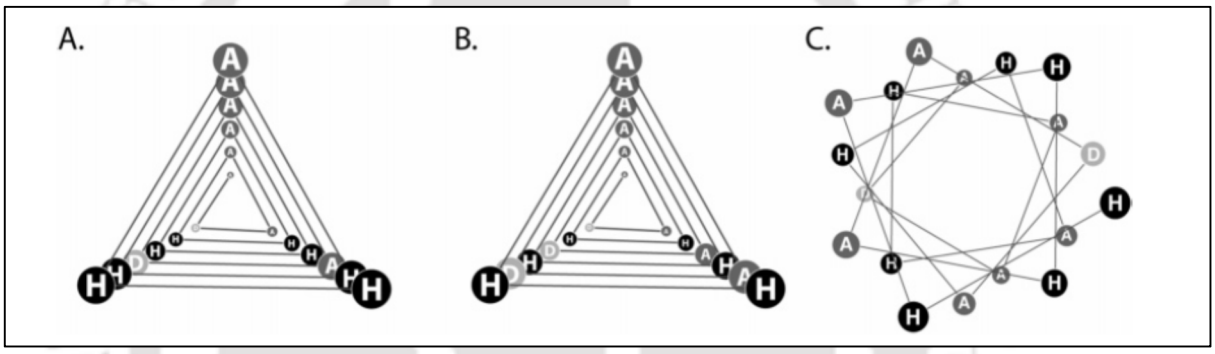

Figure 1.3: Predicted models of HRP-II repeats as 3_{10}- and α-helices. (A) Two repeats of HHAHHAADA modeled as a 3_{10}-helix. (B) Three repeats of HHAADA modeled as a 3_{10}-helix. (C) Two repeats of HHAHHAADA modeled as α-helix. For all models, histidine is in black (**H**), alanine is in dark gray (**A**), and aspartate is in light gray (**D**). (Adapted from Schneider and Marletta, 2005).

A popular belief is that HRP-II helps in the initiation of hemozoin formation as it binds firmly to heme molecule in aqueous environment. It was proved by *in vitro* heme polymerization assay performed at the optimum pH 4.0 with native and recombinant HRP-II that promoted the formation of hemozoin. Polymerization increased with time, protein concentration, and initial concentration of heme (Sullivan *et al*., 1996). A study

conducted on biomineralized dendrimeric templates that mimicked HRP-II tandem repeats showed potential of heme binding to metal moieties and initiated hemozoin formation (Ziegler *et al.,* 1999). Due to its alleged association in the formation of hemozoin, HRP-II was also projected as a model candidate for vaccine development against malaria (Kilejian, 1974). The formation of hemozoin is, however, a complex phenomenon and needs further investigation to be understood adequately.

Few other theories suggested the function of HRP-II which are as follows. Apart from heme HRP-II binds to metal moieties which was later utilized to extract and purify the protein by metal affinity chromatography. There were also reports on binding with Artemisinin, an antimalarial drug with much higher affinity (Accardo *et al.,* 2007). HRP-II interacts with negative groups on actin and phosphatidylinositol 4,5-biphosphate (PIP2) of host cells suggesting it acts as a buffering protein that helps the parasite to stabilize the changes of the cytoskeleton induced by other released parasitic proteins (Benedetti *et al.,* 2003). Another function of HRP-II is the neutralization of bacterial toxin LPS (Bosshart and Heinzelmann 2003). The observed LPS-neutralizing effect of HRPs has probably resulted from the electrostatic interactions between histidines and the negatively charged phosphate groups of LPS. HRP-II is also considered as a virulence factor that contributes to cerebral malaria by compromising the integrity of the blood-brain barrier as it activates the endothelial cell inflammasome, resulting in decreased integrity of tight junctions and increased endothelial barrier permeability (Pal *et al.,* 2016).

Hence to conclude from the above findings, HRP-II is an attractive target for malaria diagnosis as well as an anti-malarial drug design target because of these attributes (i) It is produced in large quantities, (ii) it is released extracellularly, (iii) present in other sources apart from blood, (iv) binds to heme and other metal ions (v) its tandem repeats

were targeted to develop antibodies and at last but not the least (vi) it is unique protein synthesized only by *P.falciparum*. Due to these attractive features, it was the first antigen exploited to develop a rapid diagnostic test for malaria detection.

1.3 Diagnosis of Malaria

1.3.1 Conventional Techniques.

Microscopy for malaria diagnosis has been used since 1904 (Fleischer, 2004). It is time consuming, labour intensive and requires expert skills. To enhance the sensitivity of microscopic detection, fluorescent microscopy using fluorophores such as, acridine orange (AO) and benzothiocarboxypurine has been frequently used in quantitative buffy coat technique. Although microscopy was considered as "gold standard" for malaria diagnosis, recent reports suggest otherwise. The Bayesian latent class models were used to estimate sensitivities and specificities of various diagnostic tests and revealed that microscopy is a poor reference test (Goncalves *et al*., 2012). Apart from microscopy, nucleic acid techniques such as PCR, nested PCR (Lee *et al*., 2012; Morassin *et al.,* 2002) and LAMP (Loop-mediated Isothermal Amplification) have also been used for malaria detection. LAMP can be conducted under isothermal conditions and does not need expensive thermocyclers (Lee *et al*., 2012). However, this method may pose danger of cross-contamination during addition of dye for visualization of results. Also this method is not suitable for target DNA greater than 500 bp, as this causes a hindrance to strand displacement (Lau *et al.*, 2011)

Flow cytometry (FCM) and automated blood cell counting techniques can be used to detect hemozoin or *Plasmodium* dsDNA in infected erythrocytes; however, the use of *Plasmodium* dsDNA as a marker in flow cytometry can result in false positives because pathological conditions are characterized by an efflux of normoblasts and erythroblasts

in blood (Malleret *et al*., 2011). Hemozoin strongly absorbs UV light resulting in vaporization of individual heme molecules. LDMS (Laser Desorption Mass Spectrometry) only detects small molecules (<1.5 kDa) and favours phospholipids and porphyrins; hence, it is ideally suited for heme detection; however, the detection is only semi-quantitative and cannot differentiate between species (Feldman, 2006). A unified sandwich ELISA (Enzyme-Linked Immunosorbent Assay) targeting *Pf*LDH and HRP-II was reported that allowed concurrent measurement of the biomolecules (Martin *et al*., 2009). ELISA is an efficient method to detect malaria in a short time frame. Despite the advantages such as, high sensitivity, the application of ELISA remains restricted to research settings and blood bank screening where large number of samples have to be screened every day, since there are no commercial species-specific ELISA tests kits for all species (Noedl *et al*., 2006). T of these conventional methods have been summarised in Table 1.1.

Table 1.1: Comparison on critical performance parameters among different conventional techniques. Part of the table adapted with permission from Tangpukdee *et al.,*(2009).

Types of test	Principle of the method	Instrument used	Sensitivity and specificity	Detection limit *	Response time (min)
Peripheral blood smears (PBS)	Morphological changes in the stages of parasite by thick and thin blood smears	Optical microscope	Depends on the instrument quality and the skill of the handler	50-100	30-60

(continued)

Quantitative buffy coat (QBC)	Blood staining by acridine orange (AO)	Epi-fluorescent microscope	Non-specific: AO stains DNA from all cell types. High variation in sensitivity at lower parasitaemia	>5	<15
RDTs	Detection based on antigen-antibody interactions and enzyme assay	Disposable dipsticks	Moderate at Higher parasitaemia (>100 parasite.μl^{-1})	50-100	10-15
PCR	Specific amplification of malaria DNA	Thermocycler	High	≥1	45-360 depending on the methods
Serological tests	Detection of malaria antigen or anti-parasite antibodies in blood	Microplate reader (for ELISA)	Relatively high	Not mentioned	30-60
LAMP	Detection of turbidity after amplifying DNA sequences	Turbidity meter	High	>5	<6

(continued)

Microarrays	Hybrization of DNA and quantification by fluorescent based detection	DNA chip	High	Not mentioned	<60
Flow cytometry	Detection of hemozoin	Flow cytometer	Variable sensitivity, high specificity	Poor correlation with parasitaemia	<1
Automated blood cell counters	Detection of hemozoin in activated monocyte	Hematology analyzers	Variable sensitivity and specificity	5-20	<1
Mass spectrometry	Identification of heme	Laser desorption mass spectrometry	Undetermined	100 for whole blood	<1

1.3.2 Rapid Detection Approaches

Rapid Diagnostic Tests (RDTs) are quick and portable immunochromatographic dipsticks whose sensitivity generally reaches > 95% (Bjorkman and Martensson, 2010). They rely on capture of parasite antigen from peripheral blood using monoclonal antibodies conjugated to either a liposome containing selenium dye or gold particles. A second monoclonal antibody applied to a strip of nitrocellulose acts as the immobile phase. The antigen-antibody complex in the mobile phase migrates along the strip and is captured by the monoclonal antibody of the immobile phase, thus producing a visible coloured line (Moody, 2002). The dipsticks can be divided into two classes based on their target antigenic biomarkers, namely, HRP-II (only for *P. falciparum*) and pLDH. Most

commercial RDTs that detect *P. falciparum* target HRP-II and few others target pLDH. To enhance the efficiency of malaria detection, RDTs targeting many biomarkers at the same time were prepared (Tjitra *et al*., 1999; Eisen and Saul, 2000). In many ways ICTs (Immunochromatography test) appear ideal: they are rapid (< 30mins) and can be easily used by healthcare workers or semiskilled volunteers and results are usually obtained in 5 to 15 minutes (Wongsrichanalai *et al*., 2001). However variations in RDT performance have been seen with season, year, age of patient, and presence or absence of fever during consultation (Abeku *et al*., 2008). The most common cause of poor performance of RDTs on the tropics is exposure to high temperature/humidity (Jorgensen *et al*., 2006). The loss in activity is attributed to damage to monoclonal antibodies or the nitrocellulose membrane. This was further confirmed by Chiodini who tested five RDTs from the same lot but stored at different temperatures of 35 ˚C, 45 ˚C, and 60 ˚C (Chiodini *et al*., 2007). Although dipsticks are widely used, they have certain limitations such as poor species and stage differentiation and quantification, false positive results due to persistent HRP-II antigenemia (Mayxay *et al*., 2001, Kyabayinze *et al*., 2008) and rheumatoid factors in some patients (Laferi *et al*., 1997; Iqbal *et al*., 2000), and false negative results due to excess antigen in case of high parasitaemia (Jelinek *et al*., 1999) or HRP-II gene deletion (Palmer *et al.,*1998; Iqbal *et al*., 2004; Lee *et al*., 2006b). The sensitivity of Parascreen (Zephyr Biomedical Systems) was found low for *P. falciparum* infections. This RDT was not acceptable for malaria diagnosis under the field conditions in the Peruvian Amazon due to HRP-II and HRP-III gene deletions in the malaria parasite genome (Gamboa *et al*., 2010; Maltha *et al*., 2012; Bendezu *et al.*, 2010). However reports suggest otherwise in case of south east Asian countries such as, India where HRP-II and HRP-III deletion phenomenon is found very low (Bharti *et al.,* 2016). Plasma HRP-II has prognostic significance and provides a tool to assess the risk of "true" severe malaria as compared

to other severe illnesses in parasitaemic African children (Hendriksen *et al*., 2012). This justifies the development of plasma HRP-II concentration as a method for assessing severe falciparum malaria in African children. Several reviews outline various RDTs (Baker *et al.*, 2005) and their evaluation reports (Wongsrichanalai *et al*., 2001). In spite of over 100 such reports their comparative assessment is, however, difficult due to difference in population sizes, their clinical and epidemiological characteristics, different trial guidelines, and so forth (Wongsrichanalai *et al*., 2007). A comparison of sensitivity and specificity of few of the field evaluations done during the last decade is shown in Table 1.2. It can be observed from the table that the sensitivity and selectivity of RDTs significantly vary over different studies and thus there is a need for more sensitive, selective, and reliable methods for rapid detection of malaria. One such effort was made by Peng *et al.* (2012) by developing the Wondfo rapid diagnostic test which is a nanogold based immunochromatography assay that uses monoclonal antibodies. It is a more rapid and sensitive parasite detection method and results showed very good concordance with microscopy examination with a sensitivity and specificity of 95.49 % and 99.53 %, respectively.

Table 1.2: Comparison on the performance factors of different dipstick RDTs as evaluated in some prominent reports.

Dipstick	**Standard**	**Population**	**Sensitivity (%)**	**Selectivity (%)**	**Reference**
Carestart AccessBio, (Princeton, NJ, USA)	GTTS*	South-western Uganda	95.6	91.5	Fogg *et al*., 2008

(continued)

Vistapan Mitra, (New Delhi, India)	GTTS*	South-western Uganda	91.9	89.6	Fogg *et al*., 2008
Parabank Orchid/Zephyr, (Goa, India)	GTTS*	South-western Uganda	84.7	94.3	Fogg *et al*., 2008
Paracheck pf, Orchid/Zephyr, (Goa, India)	GTTS*	South-western Uganda	94	87.3	Fogg *et al*., 2008
Optimal-IT, DiaMed, (Cressier, Switzerland)	GTS	Gabon Children under 11 years	94	97	Mawili-Mboumba *et al*., 2010
Acon, Acon Labs, (San Diego, CA)	GTS	Gabon Children under 11 years	94	90	Mawili-Mboumba *et al*., 2010
PALUTOP+4 ALL.DIAG, (Strasbourg, France)	GTTS* and PCR	Madagascar	95.4	97.1	Rakotonirina *et al*., 2008
Optimal-IT, DiaMed, (Cressier, Switzerland)	GTTS* and PCR	Madagascar	75.8	99.0	Rakotonirina *et al*., 2008
ParaHIT Pf Test, Span Diagnostic Ltd., (Surat, India)	GTTS* and PCR	Tanzania	69.2	100	Nicastri *et al*., 2009
Malaria Pf™, ICT Diagnostics, (South Africa)	GTTS*	Uganda	98	72	Kyabayinze *et al*., 2008

(continued)

Paracheck Pf, Orchid Biomedical Systems, (Goa, India)	GTTS*	Kenya	91.7	96.7	de Oliveira *et al*., 2009
Malar-Check_Pf test, Cumberland Diagnostics, (USA)	GTS**	Brazil	97.4	88.5	Avila *et al*., 2002
Makromed Dipstick Assay, Makro medical, (South Africa)	PCR	Cananda	97.0	96.0	Richardson *et al*., 2002
ParaSight®-F, Becton Dickinson, (USA)	Thin blood smears and QBC	France	94	99	Uguen *et al*., 1995
ParaSight®-F, Becton Dickinson, (USA)	Microscopy	Iquitos, Peru,and Maesod, Thailand	95	86	Forney *et al*., 2001
Paracheck Pf, Orchid Biomedical Systems, (Goa, India)	Microscopy	India	93	84	Singh *et al*., 2005
ParaHIT-Pf, Span Diagnostics, (Surat, India)	GTS**	Tanzania	90.7	73.5	McMorrow *et al*., 2010
ParaHIT-Pf , Span Diagnostics, (Surat, India)	Microscopy	India	87.5	97	Singh *et al*., 2005

GTTS*-Giemsa thick and thin smear, GTS**-Giemsa thick smear

1.3.3. Advanced Techniques and Platforms

A biosensor is a self-contained integrated device that is capable of providing specific quantitative or semi-quantitative analytical information using a biological recognition element that is retained in direct spatial contact with a transduction element. The biorecognition elements commonly reported for developing biosensors are enzyme, antibody, aptamer, DNA, and cells. The transduction principles widely used to develop biosensors are electrochemistry, piezoelectricity, and optical behaviours. Biosensor research holds promise for developing stable portable devices for rapid, sensitive, selective, reproducible, and economical detection of many analytes of clinical importance. It has the advantage of being used by semiskilled operators in point of care testing and by patients themselves. However, research on biosensors for detecting malaria is in nascent stage as evident from the limited number of the publications in this area. The biorecognition systems reported so far for developing malaria biosensors using HRP-II as a target are mostly confined to antibody which will be discussed shortly.

Most popular platform developed for malaria biosensors are electrochemical immunosensors which are based on antibodies raised against HRP-II and pLDH. The principle on which electrochemical immunosensors are constructed is the specificity of the molecular recognition of antigens by antibodies to form a stable complex which gives response as a signal change of either current (Amperometric), voltage (potentiometric) resistance or impedance (conductimetric and impedance spectroscopy). Electrochemical immunosensors serve some great advantages such as easy miniaturization, fast response time, low detection limits, easy surface modification and can be used to study vast array of analytes.

Another popular platform which was employed to detect malaria using antibodies are optical and colorimetric based systems. The optical and colorimetric based systems reported till date are based on ELISA and lateral flow immunoassays respectively. ELISA based detection sensitivity is high and comparable to electrochemical immunosensors whereas colorimetric immunoassays suffer from lower sensitivity due to coffee ring effect which can lead to non-homogenous colour development (Kakoti *et al.,* 2015). However, colorimetric methods considered better from the point of care (POC) viewpoint as they provide equipment-free readout with naked eye detection which is useful in resource-limited settings. The introduction of microfluidic channels on cellulose-based materials such as chromatography paper and filter paper have emerged into attractive platforms for developing colorimetric tests (Martinez *et al.,* 2010). Also known as Microfluidic paper based analytical device (μPAD) , these have garnered extreme popularity in the recent years as they qualify ASSURED (accurate, sensitive, specific, user-friendly, rapid, and robust, equipment free, and deliverable to end users) criteria prescribed by WHO (Peeling *et al .,* 2006). Table 1.3 enlists the major HRP-II based immunosensors reported till date. Antibody based immunosensors suffer from severe disadvantages such as high cost production, poor reusability and the most importantly instability at higher temperatures. Keeping in mind that malaria is a tropical disease, availability of stable detection platforms that can withstand humidity and high temperatures, with no significant loss of functionality, is imperative. Due to this reason, the research on malaria detection systems is growingly shifting focus towards development platforms that use DNA or other chemical recognition elements that can eliminate these issues (Chakma *et al*., 2016).

Table 1.3: Comparison on the performance factors of different HRP-II and LDH based electrochemical (yellow) and Optical/Colorimetric (green) immunosensors.

Assay name	Sensor platform	Biomarker	Range	Detection limit	References
Amperometric immunosensor	MWCNTs and Au nanoparticles mdified SPE	HRP-II	-	8 $ng.ml^{-1}$	Sharma, *et al* 2008
Amperometric immunosensor	Gold nanoparticles /alumina sol-gel modified SPE	HRP-II	-		Sharma, *et al* 2010
Piezoelectric sensor	Quartz crystal	HRP-II	15-60 $ng.ml^{-1}$	12 $ng.ml^{-1}$	Sharma, *et al* 2011
Magneto immunosensor	Graphite-Epoxy Composite Magneto Electrodes	HRP-II	-	0.36 $ng.ml^{-1}$	Castilho, *et al* 2011
Electrochemical phone based immunosensors	Polydimethylsiloxn e microfluidic chips	HRP-II	-	16 $ng.ml^{-1}$	Lillehoj, *et al* 2013
Carbon Nanofibers immunosensors	Carbon nanofiber forest grown on glass microballons	HRP-II	0.01–10 $ng.ml^{-1}$	0.025 $ng.ml^{-1}$	Gikunoo, *et al* 2014
Self-assembled nanofiber immunosensor	Mercaptopropylpho sphonic acid Functionalized copper doped zinc oxide nanofibers	HRP-II	10 $ag.ml^{-1}$-10 $\mu g.ml^{-1}$	6.8 $ag.ml^{-1}$	Brince , *et al* 2016

(continued)

Enzyme-free electrochemical immunosensor	MB, hydrazine and platinum nanoparticles (Pt NPs) on Low electrocatalytic ITO modified glass electrodes	HRP-II	1 $pg.ml^{-1}$-100$ng.ml^{-1}$	2.2 $pg.ml^{-1}$	Dutta, *et al* 2017
Enzyme-free electrochemical immunosensor	Electrochemical-chemical-chemical (ECC) redox cycling signal amplification on (ITO) modified glass electrodes;		10 $fg.ml^{-1}$ –100 $ng.mL^{-1}$	10 $fg.ml^{-1}$	Dutta, *et al* 2017
Electrochemical immunosensors	Gold nanoparticles modified gold SPE	HRP-II	-	36 $pg.ml^{-1}$	Hemben, *et al* 2017
Electrochemical aptasensor	PvLDH aptamer functionalized gold electrode	*Pf*LDH	-	120.1 fM	Lee *et al*., 2012a
Magneto-ELISA	Magnetic nanoparticles/ Magnetic beads	HRP-II	0.35-7.81 1.31-62.5 $ng.ml^{-1}$	0.35 and 1.31 $ng.ml^{-1}$ for Magnetic nanoparticles/ beads respectively	Castilho, *et al* 2011

(continued)

Immuno-fluorescence chromatographic assay	Fluorescent nanoparticle labelled immune-chromatographic strips	HRP-II	-	25 parasites.μl^{-1}	Kang, *et al* 2015
Colorimetric Enzyme amplification immunoassay	Cellulose paper Functionalized by enzyme/metal/polymer conjugated antibody	HRP-II	-	0.32, 0.15, 6.9 , 6.2 nM for paper Functionalized by enzyme / metal/ polymer respectively	Lathwal, *et al* 2016
Signal amplification with porphyrin nanoparticles immunoassay	Antibody conjugated TCPP NPs in sandwich Assay	HRP-II	10-1000 pM	2.05±0.003 pM	Gibson, *et al* 2016
Bead-based immunoassay	Antibody functionalized polystyrene beads in ELISA format	HRP-II		1 pg.ml^{-1}	Rogier, *et al* 2017
Fluorescent immunochromat-ographic test	Coumarin derived dendrimer	*Pv*LDH		0.1 ng	Song *et al*., 2012

(continued)

Colorimetric aptasensor	Gold nanoparticle-Aptamer-Salt	*Pf*LDH	57 pg.µl^{-1}	Cheung *et al*., 2013
Colorimetric aptasensor	AuNP-Aptamer-Cationic polymer PDDA2 and PAH3	*Pv*LDH	8.7 pM and 8.3 pM for PDDA2 and PAH3, respectively	Jeon *et al*., 2013
Fluorescence-linked immunosorbent assay	Coumarin-derived dendrimer	*Pv*LDH	0.01ng.ml^{-1}	Yeo *et al*., 2014.
Colorimetric aptasensor	AuNP-Aptamer-Cationic surfactant	*Pv*LDH	1.25 pM	Lee *et al*., 2014
Magnetic beads and coloured dye based enzyme assay	Magnetic microparticle	*Pf*LDH	2parasites.ml^{-1}	Markwalter et al., 2016
Fluorescence aptasensor	FAM4-aptamer-MoS_2 nanosheets	*Pf*LDH	550 pM	Geldert *et al*., 2016

1.3.4 Potential non- antibody based bio-recognition molecules

The bio-recognition systems reported so far for developing malaria biosensors are mostly confined to antibody based detection that can detect HRP-II and pLDH. Nucleic acid aptamers, a group of oligonucleotide ligands comprising of single stranded DNA or RNA sequences with abilities to bind to vast targets with great specificity and affinity often

rivalling those of antibodies have gained a lot of attention (Yang *et al*., 1998; Stoltenburg *et al*., 2012; Marangoni *et al*., 2015; Radom *et al*., 2013). The word "aptamer" was derived from the Latin words "aptus" meaning "to fit", and Greek "meros" meaning "region" . They are generated by an *in vitro* selection process called SELEX (systematic evolution of ligands by exponential enrichment) which involves the screening of large combinatorial libraries (10^{12}-10^{-15} molecules) of oligonucleotides by an iterative process of *in vitro* selection and amplification as shown in fig 1.4 (Cho et al., 2009). The screened aptamers have the ability to fold into distinct three-dimensional (3D) structures and bind to their targets in a manner similar to antigen-antibody interactions. Aptamer-target recognition is dominated by intermolecular interactions such as, aromatic rings, π-π stacking, van der Waals and electrostatic interactions between charged groups and hydrogen bonding. The dissociation constants are usually comparable or even smaller than that of antibodies which usually lie in the pico- to nano-molar range (Kimoto *et al*., 2013; Kraemer *et al*, 2011; Parekh *et al*., 2013). Aptamers offer several advantages over the conventional antibodies. They are known to discriminate targets even on the basis of subtle structural differences (Xiong *et al*., 2014; Cho *et al*., 2009; Ng *et al*., 2006). For example, the theophylline binding aptamer shows a 10,000 fold higher affinity for its ligand than caffeine, which differs from theophylline by only a single methyl group at nitrogen atom N7. They are nonimmunogenic and nontoxic (Ireson *et al*., 2006), can be absorbed and penetrated more efficiently through tissues, exhibit fast renal filtration and short circulating halftime (Martinez *et al*., 2014; Melancon *et al*., 2014). Moreover Aptamers addresses the practical issues of its commercial viability with promising characteristics like thermal stability, low cost production, rapid mass scale synthesis and chemical modification capability (Sun *et al*., 2015; Potyrailo *et al*., 2015). Due to these

advantages aptamers are great candidates that can replace thermally unstable and expensive antibodies.

Besides aptamers scientists have reported other chemical based alternatives for detecting HRP-II such as, using Ni(II)NTA (Nickel-nitrilotriacetic acid) chelation chemistry. It is a well-known fact that Ni(II)NTA chelation has high affinity towards histidine and have been used to probe poly-histidine tagged proteins by using conjugated gold nanoparticles. The Ni(II)NTA conjugated particles utilizes 1:1 association between the target and the surface ligand. However, targets containing multiple binding sites are expected to bind and localize multiple nanoparticles thereby inducing visibly detectable plasmon shifts.

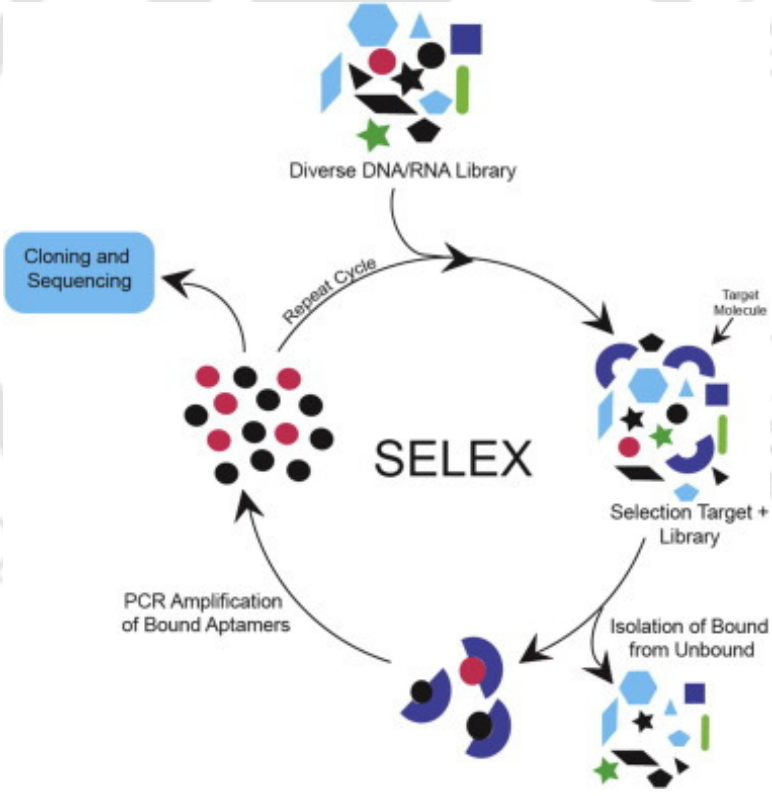

Figure 1.4: Schematic showing *in vitro* selection by SELEX. (Adapted from Wu, *et al* 2016)

Based on this Ni(II)NTA functionalized gold, silver and magnetic nanoparticles have been frequently used to detect HRP-II (Swatrz *et al* 2011). The platforms using this

principle so far are optical based and have been designed to work in a low research settings. The same authors improved the assay sensitivity and platform stability by using negatively charged Peg4-thiol as spacer ligand to obtain low nanomolar limits of HRP-II concentration and maintain excellent stability at 37 ˚C when stored for four weeks (Gulka *et al* 2015). Another detection system was inspired by the coffee ring phenomenon using Ni(II)nitrilotriacetic acid (NTA) gold plated polystyrene microspheres (AuPS) and Ni(II)NTA-functionalized glass. HRP-II was reacted with Ni(II)NTA-functionalized particles and dropped on a Ni(II)NTA-functionalized glass surface and then allowed to dry (Gulka, *et al* 2014). As the drop of the reaction mix evaporates due to radial diffusion of the particle–protein conjugates, rings of aggregated Ni(II)NTA AuPSs becomes visible which gets prominent with higher concentration of analyte as shown in fig 1.5. Metal-based phosphorescent probes such as the cyclometalated Ir(III) complexes were synthesized that can selectively bind to histidine moiety of HRP-II to give stabile and efficient emission (Davis, *et al*. 2015). However, the aforementioned systems suffered from sensitivity and specificity issues.

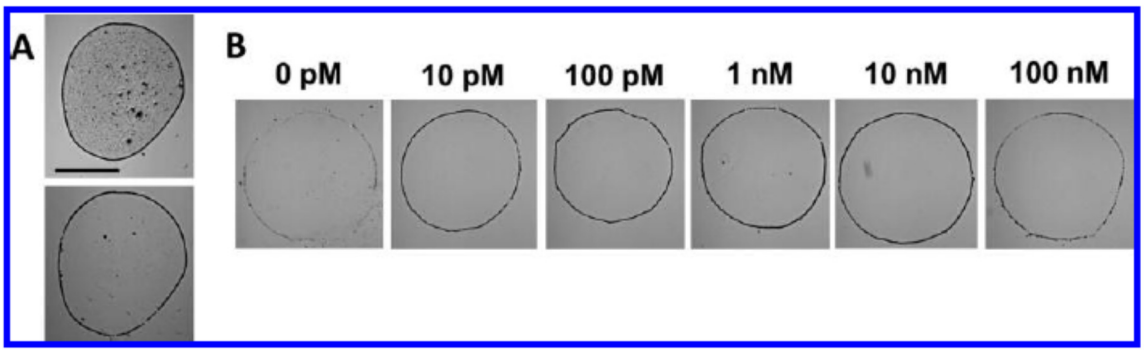

Figure 1.5: Ni(II)NTA AuPS ring assay for detection of HRP-II. (A) The top image shows the drop before washing, while the bottom image shows the drop after washing in the presence of the HRP-II biomarker. The ring retains its structure due to the presence

of the analyte which is sandwiched between the Ni(II)NTA-functionalized glass and Ni(II)NTA AuPS. (B) Images on the progression of the ring formation due to logarithmic titration of HRP-II. (Gulka, *et al* 2014).

Chapter 2

Expression, purification and characterization of *Plasmodium falciparum* HRP-II

Chapter 2

Expression, purification and characterization of *Plasmodium falciparum* HRP-II

2.1 Overview

The malarial parasite, *P. falciparum* synthesizes a unique set of soluble histidine rich proteins during the asexual erythrocytic development which are denoted as HRP I, II, and III in order of their discovery. Out of the three, HRP-II is the most widely studied protein and has been established as a promising malaria biomarker. It is a small 30 kDa protein which consists of many tandem repeats of -Ala-His-His-Ala-Ala-Asp-. It is exclusive to *P.falciparum* and is reported to have many functions such as, heme binding and heme detoxification by forming hemozoin. Spectroscopic studies showed that a single HRP-II molecule may bind to multiple heme molecules (Choi et al., 1999). Due to its unusual amount of histidine residues it also has the property to bind to Ni^{2+} ions strongly. HRP-II is ubiquitously found in large quantities everywhere in the bodily fluid of the infected patients. It is present in the serum of plasma, cerebrospinal fluid and urine of infected patients as well as in food vacuole, digestive vacuole (Jain *et al*., 2014) and membrane surface of the infected RBCs. The CD spectrum of HRP-II in aqueous medium

was indicative of random coil and the spectrum changes dramatically from random coil to 3_{10}-helix conformation as soon as heme molecules are titrated in the solution (Schneider and Marletta, 2005).

Our aim is to develop an efficient malaria detection system that can detect specifically HRP-II, the biomarker for the most dreaded malaria parasite, *P. falciparum*. To fulfil the aim we prepared the pure recombinant HRP-II using the clone of *hrp-II* following its transformation into BL21 (DE3) cells. This chapter describes transformation, expression and purification steps of HRP-II protein as well characterization of the expressed recombinant protein.

2.2 Experimental Approaches

2.2.1 Materials

Recombinant expression vector MRA-67, which is PET 3D vector containing *hrp-II* (834 bp) insert (Sullivan, D.J et al., 1996), was obtained from **BEI Resources** (Biodefense and Emerging Infections Research Resources Repository, USA). The BioMix^{TM} Red PCR kit was purchased from Bioline (UK). NcoI Restriction enzyme and Quick ligation^{TM} kit were obtained from NEB (UK). GEL extraction kit was obtained from Sigma Aldrich (USA). All other chemicals were of analytical or molecular biology grade and their sources have been cited in the methodology, wherever necessary.

2.2.2 Bacterial cell culture

The *E.coli* bacteria strain was cultured and maintained in the Luria Bertani broth (Himedia, India). The culture was grown in the presence of ampicillin at 37 °C for overnight in a shaker incubator at 180 rpm. The *E.coli* strains and composition of the culture media used in this work have been mentioned in table A1, and A2, respectively

in the appendix. Glycerol stocks of *E.coli* cultures were maintained at -80 °C for further use.

2.2.3 Quantification of DNA

The concentration and purity of DNA samples were estimated spectrophotometrically. Samples were diluted in nuclease free water at a ratio of DNA: water of 1:1000 and the ratio of optical density (O.D) at $\lambda_{260\ nm}$ to $\lambda_{280\ nm}$ were calculated. A value of this ratio ranging from 1.8 to 2.0 indicates pure DNA. An O.D value of one at $\lambda_{260\ nm}$ was considered to represent a concentration of 50 $\mu g.ml^{-1}$ or 33 $\mu g.ml^{-1}$, respectively for double stranded DNA and single stranded DNA (Barbas III et al., 2001). The DNA concentration was calculated using the equation:

$$\text{DNA concentration } (\mu g.ml^{-1}) = O.D_{260} \text{ X dilution factor X } 50 \text{ or } 33$$

2.2.4 Plasmid isolation

The plasmid DNA isolation was carried out by alkaline lysis method (Green and Sambrook, 2012). All the composition of reagents used in this process are listed in table A3 in the appendix. A single *E.coli* colony carrying the recombinant plasmid was selected and inoculated in a 5 ml LB broth where 5 µl of 100 $mg.ml^{-1}$ of ampicillin was added. The culture was incubated in an incubator shaker overnight at 37 °C under constant shaking at 180 rpm. Next day the culture was pelleted at 12,000 x g for one min at 4 °C and the pellet obtained was resuspended in 100 µl of ice-cold solution I. Cell lysis was performed by addition of 200 µl of freshly prepared solution II. The cell suspension was inverted gently 5-6 times, followed by an incubation on ice for 3-5 min. Precipitation of bacterial genomic DNA and bacterial cell debris was performed by adding 150 µl of ice cold solution III and incubation on ice for 5 min followed by centrifugation at 12,000 x g for 10 min at 4 °C. The supernatant was transferred to a fresh tube and an equal

volume of Tris saturated (pH 8.0) phenol: chloroform: iso-amyl alcohol (25:24:1 v/v) (Sigma Aldrich, USA) was added. The organic and aqueous phases were separated by centrifugation at 12,000 x g for 10 min at 4 °C. The aqueous phase was collected by aspiration into a fresh tube and 2 volumes 100 % ethanol was added to precipitate the plasmid DNA by incubating at - 20 °C overnight. The next day precipitated plasmid DNA was collected by centrifugation at 12,000 x g for 10 min at 4 °C. The supernatant was removed gently and the DNA pellet was washed with 70 % ethanol. The precipitated plasmid DNA was incubated at 25 ^{0}C (room temperature, RT) for 10 min, and then pelleted by centrifugation at 12,000 x g for 15 min, at 4 °C. The supernatant was gently aspirated, and the tube was allowed to dry in an inverted position on a paper towel. After a second wash with 70 % ethanol, the plasmid DNA pellet was air dried and dissolved in suitable volume of nuclease free water.

2.2.5 Agarose gel electrophoresis

Agarose gel (0.8 - 2 % w/v) was prepared in 50 ml volume of 1X TAE buffer (appendix table A3) with the addition of 0.5 µg.ml^{-1} of ethidium bromide. The DNA samples were prepared by adding 0.20 volume of 6 X gel loading buffer and then MQ water (resistivity >18 MΩ.cm) was added to make up the volume. Electrophoresis was carried out in 1X TAE at 75 V until the desired resolution was achieved. A wide range DNA marker (DirectLoadTM) was run along with DNA samples, wherever necessary. The DNA fragments were visualized on a UV-Trans-illuminator and then imaged using a gel documentation system (ChemiDoc XRS+ Imaging System, BIO RAD)

2.2.6 Gel elution of DNA

The enzyme digested plasmids and inserts were eluted out of agarose gels using GenEluteTM Gel Extraction kit (Sigma Aldrich, USA) following the manufacturer's

protocol. After running the agarose gel with the sample DNA, the gel was visualised under a UV trans-illuminator. The DNA band of interest was excised using a sterile scalpel precisely. The piece of agarose gel was weighed and then dissolved completely by adding 300 µl of gel solubilization solution for every 100 mg of gel, heated at 50 - 60 °C for 10 min and mixed with intermittent vortexing. At first, the binding column was prepared by placing in a 2 ml collection tube and washing with 500 µl of column preparation solution followed by centrifugation at 12,000 x g, for 1 min. The solubilized gel was mixed with equal volume of 100 % isopropanol. The solution was then loaded on to the prepared binding column and subjected to 12,000 x g, for 1 min. The flow through was disposed and the column was washed with 700 µl of wash solution which was provided in the kit. It was again subjected to 12,000 x g, for 1 min. To remove the residual ethanol another centrifugation step was performed. DNA was eluted by adding a suitable volume of pre heated (65 °C) nuclease free water and incubating at RT for 2 min followed by centrifugation at 12,000 x g, for 1 min, in a fresh sterile collection tube.

2.2.7 Digestion of DNA by Restriction enzyme

MRA-67 was subjected to single digestion using Nco I restriction endonuclease obtained from NEB, UK. The typical composition of a digestion mixture was as follows:

Components of digestion mixture	**Amount**
10 x Buffer 4 or 10 x Buffer 3	2.5 µl
NcoI Restriction endonuclease (20 units.μl^{-1})	1 µl
DNA template	8 µl (~1 µg)
Nuclease free water	to make final volume to 25 µl

Digestion mixture was incubated at 37 °C and digestion was carried out for 6 h, according to the manufacturer's instructions. Digested products were resolved on 0.8 % agarose gel for analysis.

2.2.8 Preparation of competent cells

Competent *E.coli* DH5α/BL21 (DE3) cells were prepared as described by Chung *et al.* (1989). A single colony of *E.coli* was inoculated aseptically in 5 ml of LB media as a primary culture and allowed to incubate overnight at 37 °C under constant shaking at 180 rpm. Around 1 % primary culture was charged aseptically to obtain secondary culture in a 25 ml LB broth and grown till early exponential phase until the optical density (O.D) at $\lambda_{660\ nm}$ reads 0.4 - 0.5. The culture was then pelleted at 3000 x g for 10 min at 4 °C. The media supernatant was discarded and the bacterial pellet was resuspended aseptically in 2.5 ml of sterile ice-cold transformation and storage solution (TSS solution) (Table A3, appendix). The competent cells were frozen and stored in aliquots immediately at -80 °C until further use.

2.2.9 Transformation of competent *E.coli* cells

Competent *E. coli* cells were transformed with the expression vector by adding 10 µl of pure plasmid (MRA67) to a 100 µl volume of competent cells, and gently mixed by a pipette. The cell mixture were then incubated for 30 min. It was then subjected to a heat shock of 90 s by incubating it in a water bath which was maintained at 42 °C. Around 800 µl of pre-warmed LB broth was added to the mixture and was incubated at 37 °C for 1 h, in a shaker incubator maintained at 180 rpm. The cells were pelleted by centrifugation at 3000 x g for 10 min at 4 °C and the pellet was resuspended in100 µl of fresh LB media. The resuspended cells were mixed gently and then plated on LB agar plates containing appropriate concentration of antibiotic corresponding to the antibiotic

resistance gene present in the recombinant plasmid. Transformed colonies were selected following an overnight incubation at 37 °C, and further screened by restriction digestion.

2.2.10 Sequencing of cloned insert

Sequencing was performed at a DBT-supported DNA sequencing facility at Delhi University, south campus, India, using 96 capillary high throughput sequencer, ABI 3730 XL following Sanger sequencing protocol.

2.2.11 Expression of HRP-II

An *E.coli* BL21 (DE3) colony carrying the recombinant vector MRA67 (pET 3d*_hrp-II)*, was grown in 5 ml of sterile LB broth containing ampicillin (100 $mg.l^{-1}$) at 37 °C overnight, in a shaking incubator at 180 rpm. The primary culture was sub cultured in 300 ml of LB broth with the same concentration of antibiotic till the O.D. at $\lambda_{660\ nm}$ reached 0.5-0.6. Protein expression was induced by adding isopropyl *β*-D thiogalactopyranoside (IPTG) at a concentration of 0.5 mM IPTG, at 28 °C for 12 h in a shaker incubator maintained at 180 rpm. Cells were pelleted at 8000 x g and resuspended in 20 mM Tris, pH 8 containing 0.5 M NaCl. The cells were then subjected to sonication using an ultrasonic processor (Hielscher) at 25 % amplitude with 0.5 cycle at 4 °C till the lysate appeared clearer. The sonicated sample was subjected to 12,000 x g for 25 min at 4 °C. The supernatant was collected and stored at 4 °C for further downstream processes.

2.2.12 Purification of HRP-II

Purification of HRP-II was performed using Ni affinity chromatography using Ni NTA HisTrap™ column (GE Healthcare) as reported (Sullivan et al., 1996) . The column was briefly washed with 10 volumes of MQ water to remove alcohol which was used for storage. Then it was equilibrated with 10 column volumes of equilibration buffer (20 mM Tris, 0.5 M NaCl pH 8). The supernatant after sonication of the recombinant clones was

passed through the pre-equilibrated column at a rate of 0.5 ml.min^{-1}. The column was then washed with 20 column volumes of washing buffer (20 mM Tris, 0.5 M NaCl pH 8). A step gradient of 50 and 100 mM imidazole was used to remove unbound proteins. The target protein was then eluted using 350 mM imidazole at a rate of 2 ml.min^{-1}. The residual imidazole was removed from the purified protein by dialysis against an appropriate buffer as required. The purified proteins were quantified using the Biuret assay. The composition of solutions used for protein purification have been listed in table A3, appendix.

2.2.13 Sodium dodecyl sulphate polyacrylamide gel electrophoresis (SDS PAGE) of protein

The proteins purified through Ni affinity chromatography were analyzed on SDS PAGE following the protocol of Laemmli, (1970). An appropriate amount of purified recombinant proteins and unpurified crude cell lysate was mixed with 4 x SDS-PAGE gel loading buffer with reducing agent (2-mercaptoethanol) and heated in a boiling water bath for 5 min to denature the proteins. Pre stained protein marker for SDS PAGE were obtained from New England Biolabs (USA) and processed according to manufacturer's instruction. Electrophoresis was carried out on a discontinuous buffer system with a 5 % stacking on top of a 12 % separating gel, with a thickness of 0.75 mm at a constant voltage of 120 V in a MiniVE vertical electrophoresis unit (GE Healthcare). Visualization of resolved protein bands on the gel was carried out using "Blue silver staining" protocol of Candiano *et al.*, (2004), where colloidal Coomassie G-250 (Sigma Aldrich, USA) (Table A3, appendix) was the staining dye.

2.2.14 Quantification of protein

To quantitate the recombinant protein, biuret protein assay was performed spectrophotometrically at $\lambda_{550\ nm}$ and compared against a BSA standard. The biuret test was used for detecting the presence of peptide bonds. Copper (II) ion forms violet-coloured coordination complexes in an alkaline solution with the peptide bonds of the proteins. The composition of the biuret reagent is mentioned in table A3.

2.2.15 Circular Dichroism study

Circular dichroism (CD) spectra of purified HRP-II (~ 0.3 $mg.ml^{-1}$) were recorded using a spectropolarimeter (J-815, Jasco, Japan.) after calibrating the instrument with (+)-10-camphorsulfonic acid for optical rotation. The spectra were recorded from $\lambda_{190\ nm}$ to $\lambda_{240\ nm}$, using a 1 mm path length suprasil quartz cuvette at a scan rate of 100 $nm.min^{-1}$, interval of 0.5 nm, time constant of 1 s, and taking an accumulation of 4 scans. The spectrum was corrected for baseline and smoothed by Savitsky–Golay filter using Jasco spectral analysis software. The secondary structure analysis was performed using the Jasco SSE-protein secondary structure estimation program supplied with the instrument.

2.2.16 Matrix- assisted laser desorption ionization- mass spectroscopy

Intact mass analysis of HRP-II was determined by performing matrix- assisted laser desorption ionization-Mass Spectrometry (MALDI-MS) (4800 plus MALDI TOF/TOF Analyzer, AB SCIEX, USA). Sinapinic acid was used as the matrix for MALDI and the spectra were collected in a positive mode and averaged for 100 shots.

2.2.17 Determination of isoelectric point (p*I*)

The isoelectric point (p*I*) of HRP-II was determined by using Zetasizer Nano Instrument system (Malvern Instruments Limited, UK). Around 0.5 $mg.ml^{-1}$ of the protein was

incubated in 20 mM of different buffers of pH ranging from 4-10 with increment of 1 for at least half an hour prior to analysis in the instrument. All solutions were filtered through 0.22-micron syringe filter. The samples were injected into a specially designed folded capillary cell with gold plated copper electrode (Malvern Instruments Limited, UK). Data were acquired at 20 °C, repeated 20 times and averaged. The viscosity was set to 1 cP at a scattering angle of 90° and resulting autocorrelation function was analyzed by the integrated control software to obtain the p*I* value.

2.2.18 Heme binding studies

A stock of 1 mM heme solution was prepared by dissolving an appropriate amount of hemin chloride in 100 mM NaOH. The number of heme-binding sites was determined by using an established method (Choi et al., 1999; Schneider and Marletta, 2005). The heme solution was titrated, in 1 µM increment to a 0.2 µM HRP-II protein solution in 100 mM HEPES (pH 7.0). The experiments were performed at RT and absorption spectra were recorded after each addition. The spectra had a maximum at 416 nm. The heme binding curve was constructed by plotting ΔA_{416nm} versus the heme equivalents.

2.3 Results and discussion

2.3.1 Transformation, expression and purification of HRP-II

The strategy used for transformation and expression of the HRP-II protein is depicted in figure 2.1. The vector provided was 0.05 µg.µl^{-1} in RNase free water at – 20 °C. Transformation of *hrp-II* gene into DH5α and BL21 (DE3) cells was performed by adding 0.2 µg of expression vector to the respective competent cells which was proceeded by heat shock method. The transformed cells were selected on the basis of ampicillin resistance and confirmed through restriction enzyme digestion by using NcoI.

The release of an insert of ~834 bp by the digestion confirmed successful transformation of *hrp-II* (Figure 2.2). DNA sequencing of the insert in the selected clone was performed by using forward T7 promoter primer (universal). The sequence obtained was compared with the complete coding sequence of HRP-II (GenBank: U69551.1) through pairwise sequence alignment. It showed 99 % sequence similarity with an Expect (E) value of 0.0 which is a significant result. Subsequently, transformed BL21-DE3 cells with the HRP-II expression vector were induced with optimized IPTG concentration (0.5 mM) for 4, 6, 8 and 12 h at 28 °C and then protein expression profile was studied in the soluble cytoplasmic fractions (Figure 2.3 A). Since the recombinant HRP-II protein has a large number of histidine residues, which allow the protein to be purified by Ni-NTA columns. For a single round of protein purification, 300 ml recombinant culture was lysed and the protein was purified using Ni affinity chromatography (HisTrap-5ml by GE healthcare). The fractions containing the protein were pooled and dialyzed against appropriate buffer. Protein purification was confirmed by SDS-PAGE gel and concentration of the purified protein was determined to be 0.6 $mg.ml^{-1}$ by using biuret assay. Purified protein band was observed at ~ 55 kDa even though the weight of single monomer of HRP-II is ~30 kDa (Figure 2.3 B). The anomalous movement of protein has been reported by Schneider et al (Schneider and Marletta, 2005). The reason is attributed to the high histidine residues which interfere in the SDS loading on the protein (Rath et al., 2009).

2.3.2 Characterization of HRP-II

As mentioned earlier the unique nature of HRP-II leads to the anomalous migration in SDS-PAGE. Therefore, to confirm the molecular weight of the protein intact mass analysis by mass spectrometry was performed. The mass spectra (Figure 2.4 A) showed one single peak at 29.4 kDa confirming successful expression and purification of HRP-II. The structural integrity of HRP-II was also validated by CD studies (Figure 2.4 B) and

found to be in agreement with previous reports (Schneider and Marletta, 2005). We analysed secondary structure of the protein using yang's database which showed a predominant negative ellipticity at ~200 nm confirming that the protein belongs to mostly random coiled protein. Zeta potential studies of HRP-II at various pH revealed a p*I* of ~ 6.5 (Figure 2.4 C). The result was in agreement to the p*I* calculated by computing p*I*/Mw tool available on ExPASy server (https://web.expasy.org/protparam/).

2.3.3 Heme binding study

The electronic absorption spectrum of the HRP-II-heme complex gives a peak at ~ 416 nm. We performed spectrophotometric heme titration experiments to determine the number of heme-binding sites on HRP-II. Absorption spectra were recorded at varying heme concentrations and heme-binding curve was generated by plotting change in absorbance at 416 nm (ΔA_{416}) against heme equivalents as shown in Figure 2.5. The linear portion of the binding curve represents complete binding of added heme, whereas the curved portion indicates the presence of unbound heme. The intersection of the initial slope of the binding curve and complete binding of heme leads us to the saturation point of the heme-binding sites. We find 18 heme molecules bind per HRP-II molecule which is in agreement with the previous reports (Schneider and Marletta, 2005).

2.4 Conclusion

As a starting step towards the objective of developing malaria sensor, the target HRP-II protein was prepared in pure form following standard molecular techniques. Briefly, the expression vector MRA67 was successfully transformed into BL21 (DE3) cells. The recombinant protein was purified by Ni-NTA affinity chromatography. The purity of the protein was confirmed by SDS PAGE and quantified by biuret assay. Further characterization of the protein was done using CD, MALDI-M and Zeta potential studies.

Heme binding studies were performed and confirmed that ~18 molecules of heme can bind to a molecule of HRP-II.

Figures

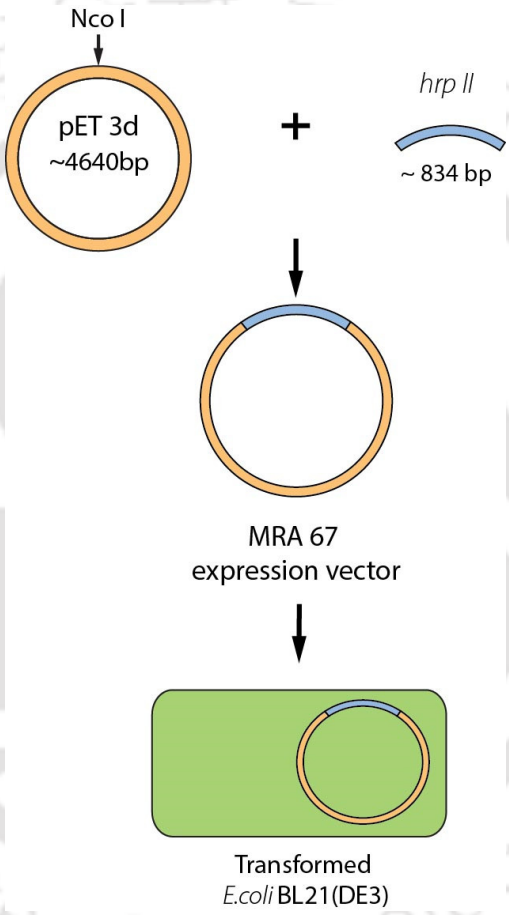

Figure 2.1: Schematic representation on the cloning strategy for *hrp-II* used in the present work.

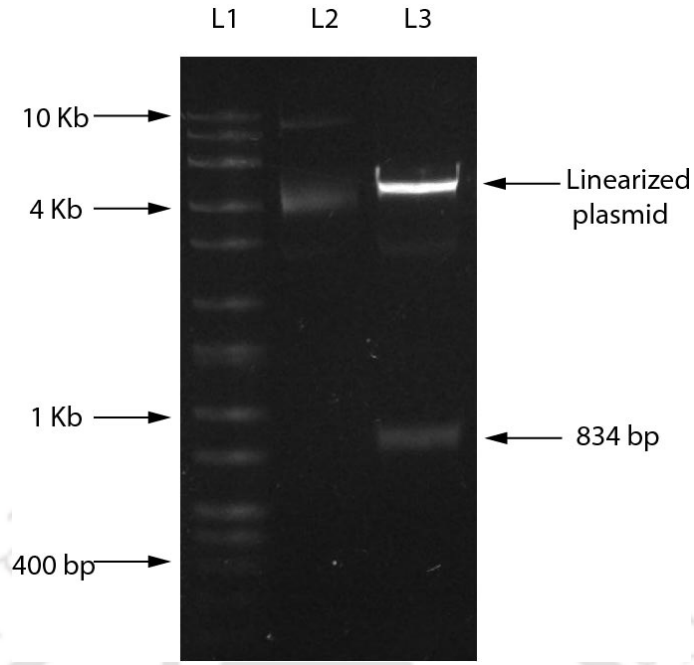

Figure 2.2: Restriction enzyme digestion of the expression vector MRA 67. Lane L1: DNA marker, lane L2: pET 3d plasmid containing *hrp-II* gene and lane L3: digested plasmid releasing the insert.

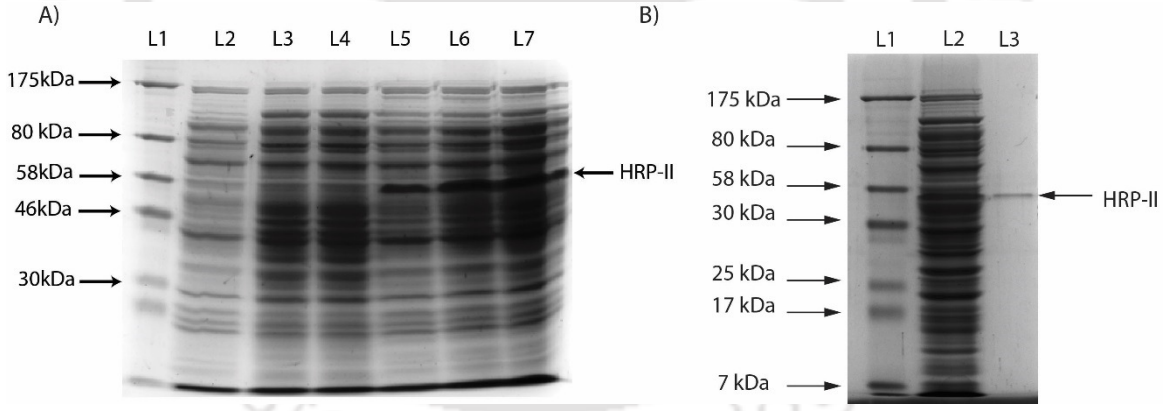

Figure 2.3: SDS PAGE (12 % gel) analysis of (A) Expressed recombinant HRP-II protein and expression was performed at an IPTG concentration of 0.5 mM and incubated at 28 °C for different time period. Lane L1: protein molecular marker, lane L2: BL21 (DE3) uninduced, lane L3: supernatant fraction of uninduced clone and lanes L4, L5, L6 and L7: supernatant fraction of clone induced at 0, 4, 8 and 12 h, respectively. (B) Purified recombinant HRP-II. Lane L1: protein molecular marker, lane L2: crude cell lysate and lane L3: purified protein.

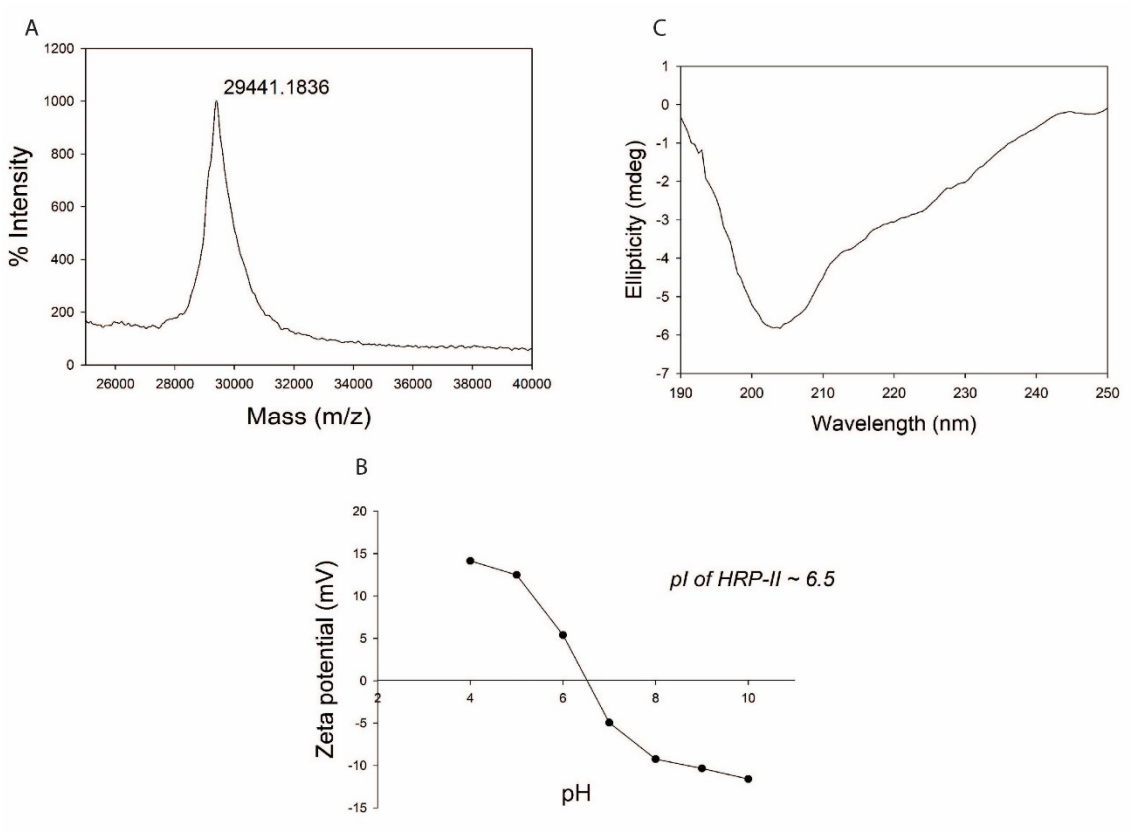

Figure 2.4: (A) MALDI- MS spectrum of HRP-II. (B) Zeta potential of HRP-II at varying pH (C) CD spectrum of HRP-II.

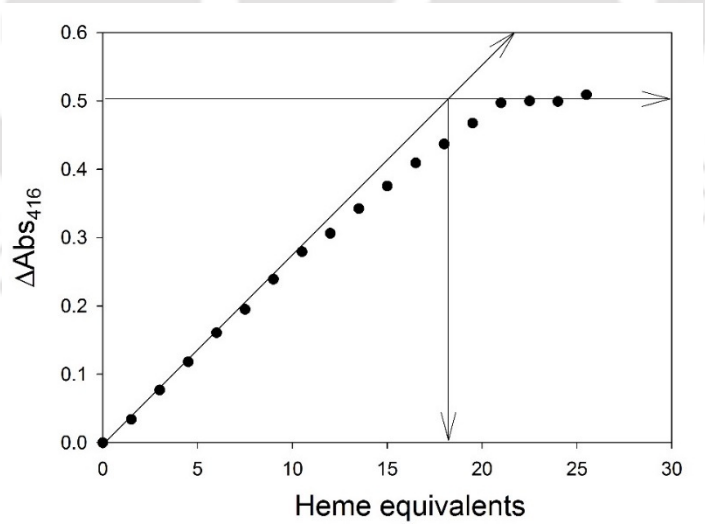

Figure 2.5: Heme binding curve generated from the difference absorption spectra by plotting ΔA_{416} vs the heme equivalents.

Chapter 3

Indicator displacement based assay to detect HRP-II in point-of-care settings

Chapter 3

Indicator displacement based assay to detect HRP-II in point-of-care settings

3.1 Overview

Accurate and timely diagnosis of malaria in malaria endemic countries is important for its effective remedial treatment which demands an affordable, stable, simple, sensitive, and fast malaria diagnostic tool or technique. Presently, rapid diagnostic tests (RDT), which are based on antibody as recognition element, have been widely used in these malaria prevalent regions owing to their many positive qualities such as, simple to operate, fast, and inexpensive.(Maltha *et al*., 2013). However, there are reports indicating several issues on these antibody based RDTs such as, cross reactivity with autoantibodies (Lee *et al*., 2014), low stability in hot and humid climate which leads to test failures (Albertini *et al*., 2012; Chiodini *et al*., 2007; Murray *et al*., 2008), false negative results during severe malaria due to Prozone effect (Gillet *et al*., 2009; Luchavez *et al*., 2011; Lynn *et al*., 1999), and are non-quantitative in nature. Efforts have been made to overcome these problems by replacing antibody with other recognition elements

targeting HRP-II. Histidine targeted spectrophotometric sensor using Ni(II) NTA (nickel nitrilotriacetic acid)-functionalized Au and Ag nanoparticles has been reported (Swartz *et al*., 2011; Swartz *et al*., 2011). Later on following the same principle, a detection system for low resource setting was developed where Ni-NTA functionalized glass slides and magnetic nanoparticles were used. Following addition of the HRP-II protein a visible coffee ring like structure was developed (Gulka *et al*., 2014). Later on, Ni-NTA gold nanoparticles with different spacer molecules to enhance the sensitivity of HRP-II detection were studied (Gulka *et al*., 2015). An iridium (III) complex, (Minami *et al*., 2014; Nguyen and Anslyn, 2006) luminescent probe which selectively binds to the histidine residues of HRP-II and gives a phosphorescent signal was also proposed (Davis *et al*., 2015). The sensitivity and specificity of these methods, however, needs to be adequately addressed to realize their practical applicability. Additionally, these detection systems are complex and expensive due to their use of nanomaterials that require functionalization and coating for stabilization. All the aforementioned alternative methods are in conceptual stage and are yet to be validated for practical utility.

Here, we developed a sensitive, simple, and stable method for quantification of HRP-II using indicator displacement assay (IDA). The assay is expected to offer many advantages over the conventional assays as the IDA does not require the indicator to be covalently attached to the receptor, it works well in aqueous and organic medium as well, and can easily be tailored to different receptors and ligands (Minami *et al*., 2014; Nguyen and Anslyn, 2006). A commonly available complexometric indicator dye murexide, also known as ammonium purpurate, has been used in this assay. The dye has high affinity toward nickel ions and gives an orange color upon binding to the ions. It is a hydrophilic tridentate ligand which binds to Ni^{2+} with three coordination bonds as shown in figure 3.1. Earlier this dye was used for spectrophotometric detection of free histidine in urine

samples (Sun *et al*., 2012). Based on this concept of binding affinity of the dye for both histidine and Ni^{2+} we formulated this IDA assay. HRP-II competes with the dye due to its large number of histidine moieties, displacing Ni^{2+} from the murexide-Ni^{2+}complex thus regenerating the original color of the dye as shown in figure 3.2. To make this sensing method economical and viable for low resource settings we replicated the detection in a microfluidic paper based analytical device (μPAD), which complies with the ASSURED (accurate, sensitive, specific, user-friendly, rapid, and robust, equipment free, and deliverable to end users) criteria prescribed by WHO (Peeling and Mabey, 2010). The microfluidic channels on the paper surface were created by forming hydrophobic barriers in a very hassle free and cost-effective manner (Kakoti *et al*., 2015; Martinez *et al*., 2010). The performance of the developed μPAD was evaluated for detection of HRP-II. A detailed account on the experiment, results and conclusion are described in this chapter.

3.2 Experimental approaches

3.2.1 Chemicals and Reagents

Murexide, nickel (II) sulphate heptahydrate, and HEPES were obtained from HIMEDIA. Whatman filter paper grade 1 (7 mm × 10 mm) and human serum albumin (HSA) were purchased from Sigma. Recombinant HRP-II was expressed in the laboratory. Alkyl ketene dimer 1840 (AKD) purchased from Flourish Paper and Chemicals Limited (Mumbai, India). All the other reagents used were of analytical grade. All solutions were prepared in ultrapure water with resistivity >18 MΩ.cm. The experiments were performed at 25 ^{0}C (room temperature; RT) unless stated specifically.

3.2.2 Spectrophotometric Studies

The IDA reactions were performed in 20 mM HEPES buffer at pH 7.4. The reaction mixtures were allowed to incubate at RT for 10 min, absorbance was taken at λ_{515nm} and $\lambda_{482\ nm}$ in a flat bottom 96 well microtiter plate in a microtiter plate reader (TECAN M200 Pro, Switzerland). Spectral characterization was performed by UV–Vis spectrophotometer (Cary 200 Bio, Agilent). Graphs were plotted using Sigma Plot software, and the data points plotted in the graph were the mean of three measurements, while the error bars represent the relative standard deviation.

3.2.3 Preparation of real serum

Real serum samples were collected from healthy volunteers following an established protocol and ethical guidelines. In an anticoagulant free collection tube, 12 mL of blood was collected and allowed to settle for 15–30 min to clot. The samples were then centrifuged at 2000 g for 10 min in a refrigerated tube to remove the clot. The supernatant collected was designated as serum and was used for experiments.

3.2.4 Fabrication of μPAD

μPAD was developed on Whatman filter paper 1. The design patterns were created by using Adobe illustrator CS6. The pattern consisted of a circular sample zone of 8 mm (diameter) and 6 test zones of 4 mm (diameter) for enabling the repeat of six measurements. The sample zone and the test zones were connected by channels which had dimensions of 2 mm (width) × 4 mm (length) and a thickness of 180 μm. The AKD printing was done in a HP deskjet-100 printer. The cartridge of the printer was modified by replacing the hydrophobic foam with hydrophilic chromatography paper and absorbent cotton. The ink cartridge was filled with 0.5 % (w/v) AKD solution in n-heptane. After the printing, the paper was heated on a hot plate at 100 °C for 10 min and

then allowed to cure for few hours before use. The AKD printed paper was characterized by scanning electron microscopy (SEM) (LEO 1430 VP, ZEISS, Germany). The samples were gold coated for 120 s at 5 mA and were mounted on the sample holder using carbon tape. The samples were examined under low beam energies (5−8 kV EHT) at RT. Atomic force microscopy (AFM) using an ambient air scanning probe microscope (Agilent Technologies, 5500) was also used to check the topography and roughness of the paper substrate before and after the printing. The images were taken with tapping mode using PicosScan 5 software.

3.2.5 Detection of HRP-II on μPAD.

The samples migrated to the test zone were allowed to react with the reagents at ambient conditions. After the reaction the paper platforms were allowed to dry for 15 min. The images of the color developed on the paper platform following the sample applications were acquired by using the HP scanner. The images taken by HP Laser jet pro M1132 MFP were transferred to a computer, converting them to a CMYK mode to quantify the response using Adobe Photoshop (CS6). The magenta filter was considered to determine the pixel intensities (Martinez *et al*., 2008). The mean pixel intensity corresponding to the analyte concentration was calculated by the histogram feature. All data points presented here are the mean intensities of six measurements against each concentration using independent devices, while the error bars represent the relative standard deviation.

3.3 Results and Discussion

3.3.1 Spectrophotometric detection of HRP-II

Free murexide solution exhibited an intense peak at $\sim\lambda_{515nm}$. The peak shifted to $\sim\lambda_{482nm}$ when Ni^{2+} solution was added to it (Figure 3.4 A). For optimization of the reaction, 50 μM of murexide was titrated with increasing concentrations of Ni^{2+}. The saturation was

reached at ~50 μM of Ni^{2+} (Figure 3.4 B), indicating 1:1 stoichiometry of the reaction. From the plot, the binding constant (K_d) of 1.4×10^{-6} M^{-1} was discerned for the dye from the equation $Y = B_{max}X/K_d + X$, where B_{max} is the maximum available concentration of receptors, X is concentration of ligand, and Y is concentration of receptor. The ratio metric ($\lambda_{515\ nm}/\lambda_{482\ nm}$) response was considered to improve the reliability of the assay (Sun *et al*., 2012). When an equimolar (50 μM) mixture of murexide and Ni^{2+} were titrated with HRP-II, the orange color ($\sim\lambda_{482nm}$) of the solution gradually changes to pink ($\sim\lambda_{515nm}$) with the corresponding increase in protein concentration (bottom panel in Figure 3.5). Using the said concentrations of dye and $Ni^{2+,}$ a dynamic detection range of 1 nM – 3 μM and a limit of detection (LOD) of 53 ± 7.1 nM for HRP-II ($R^2 = 0.995$) were discerned using LOD = 3 × Sy/b, where Sy is the standard deviation (SD) of y-intercept, and b is the slope of the linear curve. The method could detect as low as 1 pM of HRP-II in the solution. The K_d value calculated for HRP-II-Ni^{2+} was 6.8×10^{-9} M^{-1}. This higher K_d value of HRP-II than the murexide dye for Ni^{2+} validates the ability of HRP-II to displace Ni^{2+} easily from the dye complex. Notably, the high affinity binding of Ni^{2+} to His amino acid is commonly exploited to purify His-tag proteins and HRP-II through the column chromatographic technique. However, this displacement based reaction is not known to utilize for detection of HRP-II and other proteins. The method offers a fast, sensitive, and label free detection of HRP-II. Moreover, the analysis does not involve any expensive reagents, hence it has great potential to use in a resource limiting platform.

3.3.2 Effect of pH on spectrophotometric detection of HRP-II

The effect of pH on the displacement reaction was investigated (Figure 3.6 A). The response was conspicuous in alkaline conditions and drastically increased with increasing the pH value from 7 to 9 (inset in Figure 3.6 A). At lower pH (< 6.5)

conditions, both the dye (pK_1 = 9.2 and pK_2 = 10.5) and HRP-II protein (pI ~ 6.5) exist in protonated forms, hence are not amenable to bind to Ni^{2+}. A previous study on the binding of Ni (II) ions to hexa-histidine as a model system of His-tagged proteins indicated that deprotonation takes place with increasing pH value in the alkaline side. The octahedral 2N Ni (His6) H species releases a H^+ from an imidazole group resulting in the formation of square planar 3N Ni(His6) that upon aggregation produces the 4N Ni(His6)n stabilized by hydrogen bonds (Valenti *et al*., 2006). It is assumed that HRP-II also functions in a similar manner due to which it binds with Ni^{2+} strongly and quickly at higher pH conditions. The limit of detection (LOD) calculated from the response curves (Figure 3.6 B) for pH 7, 8, and 9 were 330.26 nM, 41.67 nM, and 7.62 nM, respectively, using LOD = 3 × Sy/b, where Sy is the SD of y-intercept, and b is the slope of the linear curve. The results clearly demonstrated that higher alkaline pH is conducive to yield higher sensitivity for the detection, which offers an opportunity to enhance the sensitivity of the assay on demand.

3.3.3 Interference studies and analysis in serum sample

The specificity of the assay was also investigated by challenging the reaction with a major serum protein, HSA that accounts for ~55 % (~0.6 – 0.7 mM) of the blood proteins. The response for the concentration of 1 μM HSA was negligible (~0.7 ± 0.005 %) as can be seen from surface (Figure 3.7A). The effect of some common serum metal ions, namely, Na^+, K^+, Mg^{2+}, Ca^{2+}, and Fe^{2+} on the assay was investigated. An equal concentration of the ion and Ni^{2+} (50 μM) were added to the reaction mixture and absorbance was recorded by adding 1 μM of HRP-II to each of the reactions. Selectivity coefficient (SC) for each of the potential interfering agents was calculated using the formula, $SC = A_{c+i}/A_c$ where A_{c+i} and A_c are the response for Ni^{2+} in the presence and absence of each interfering agents, respectively. The results indicate that response of the reaction did not get affected

by the presence of these ions as the SC of ~1 was obtained for each of the cases (figure 3.7 B). To understand any interference by other unknown potential interfering agents present in human serum, the assay was performed in serum samples spiked with different concentrations of HRP-II. The SC calculated for serum sample in the presence of 1 µM HRP-II was ~1.09 which is a maximum of 15.4 ± 0.012 % increase in response as compared to the control experiments (without serum) indicating minor interference from the blood serum.

Notably, the endogenous interference originates from the substances found naturally in the patient sample, such as blood serum is known (Dimeski, 2008) To avoid such interference, adequate dilution of the serum samples is commonly performed for clinical samples (Fakanya and Tothill, 2014; Toedter *et al*., 2008).

3.3.4 Characterization of fabricated microfluidic platform

A µPAD with test zone and sample zone was fabricated as shown in the schematic figure 3.8. The capacities of the test and sample zones were 1 µl and 20 µl, respectively. As evident from the SEM images (Figure 3.9 B, C), the non-printed hydrophilic part of the paper surface retained the fibrous and porous structure, whereas in the printed hydrophobic part the porosity was substantially reduced. AFM images of the AKD printed surface (Figure 3.9 F) showed a rough surface with an uneven morphology whereas the unmodified appeared to be smoother with periodic ridges which were formed by the printer head while printing. The root-mean-square (RMS) roughness factors for the nonprinted and printed regions were 44.6 ± 1.35 nm and 20 ± 0.22 nm, respectively. The surface height of the nonprinted and AKD printed (Figure 3.9 E,G) regions were 25 ± 0.81 nm and 120 ± 6.23 nm, respectively, indicating an increase in paper height after the printing.

3.3.5 Detection of HRP-II in μPAD platform

The reagents, murexide and Ni^{2+} (each of 1 μl from 1 mM stocks) (Ni^{2+}-murexide: 1:1) was deposited on the test zone and then dried at RT to make the μPAD ready for the test. The sample containing HRP-II, when applied to the sample zone, travelled through the microchannels to the test zone where it reacted with the reagents and then produced a color image. Application of the μPAD limited the sample volume to 20 ± 06 μl. The mean pixels of the images were calculated and plotted against applied HRP-II concentrations (Figure 3.10). A dynamic detection range of 10 – 100 nM and LOD of 30 ± 9.6 nM were discerned from the linear regression equation (Figure 3.10, inset). The method presented here with non-biological recognition system targeting HRP-II has some clear advantages in addition to the other general positive traits mentioned elsewhere over the antibody based detection methods. There have been cases where patients with complicated malaria failed to show positive results in RDTs. The LOD value offered by the sensor indicating that the developed μPAD is applicable to both uncomplicated and complicated malaria. The concentration of HRP-II in cases of complicated malaria may be as high as ~80 nM (Rubach *et al*., 2012). The false negative results due to Prozone effect at high concentration of HRP-II,(Luchavez *et al*., 2011; Santos *et al*., 2015) and cross contamination with other antibodies (Lee *et al*., 2014; Meatherall *et al*., 2014) as reported for antibody based lateral flow methods may be avoided. Therefore, there is a great scope of using the present detection system as an additional test along with the current RDTs to eliminate false negative results in the case of patients with high parasitaemia and auto immune diseases.

3.4 Conclusion

A simple spectroscopic method free from any labile bio-recognition element to quantitatively detect specific malarial biomarker HRP-II directly in the serum sample is reported here for the first time. The method involves the displacement of a dye (murexide) from its coordinating Ni^{2+}complex by the target HRP-II protein through competitive binding events and then quantifying the target by measuring the color intensity in a shifted wavelength occurring concurrently with the progress of the displacement reaction. The method offers a scope to enhance the detection sensitivity on demand such as, for early detection of malaria by simply increasing the pH of the reaction mixture from physiological state up to ~9. The detection method is cost-effective as it does not involve any expensive biological recognition compound and is sensitive with are reasonably wide dynamic detection range. The assay has been reproduced in a μPAD and thereby made the detection system more cost-effective due to the requirement of only fewer amounts of reagents and free from any external equipment.

Each paper platform cost was ~0.07 U.S. dollars that includes the cost of the reagents. Additionally, the reagents did not produce any interfering color on the paper platform and thus made the pixel image free from any background noise. The developed μPAD sensor has application potential in resource-limited situations following its coupling with a simple device of common use, such as a mobile phone with a camera, to quickly capture and process the pixel image for generating specific information on the status and progression of malaria in the patients.

Figures

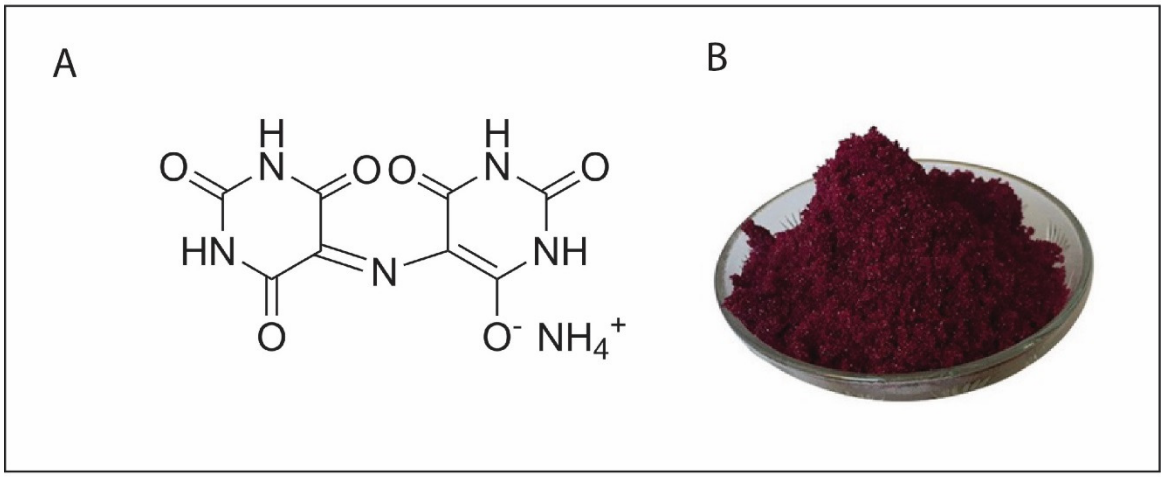

Figure 3.1: (A) Chemical structure of murexide (B) Murexide powder in its free solid state (Image obtained from Wikipedia and https://www.alibaba.com/product-detail/Murexide-C8H8N6O6-CAS-3051-09-0_60562555406.html, respectively).

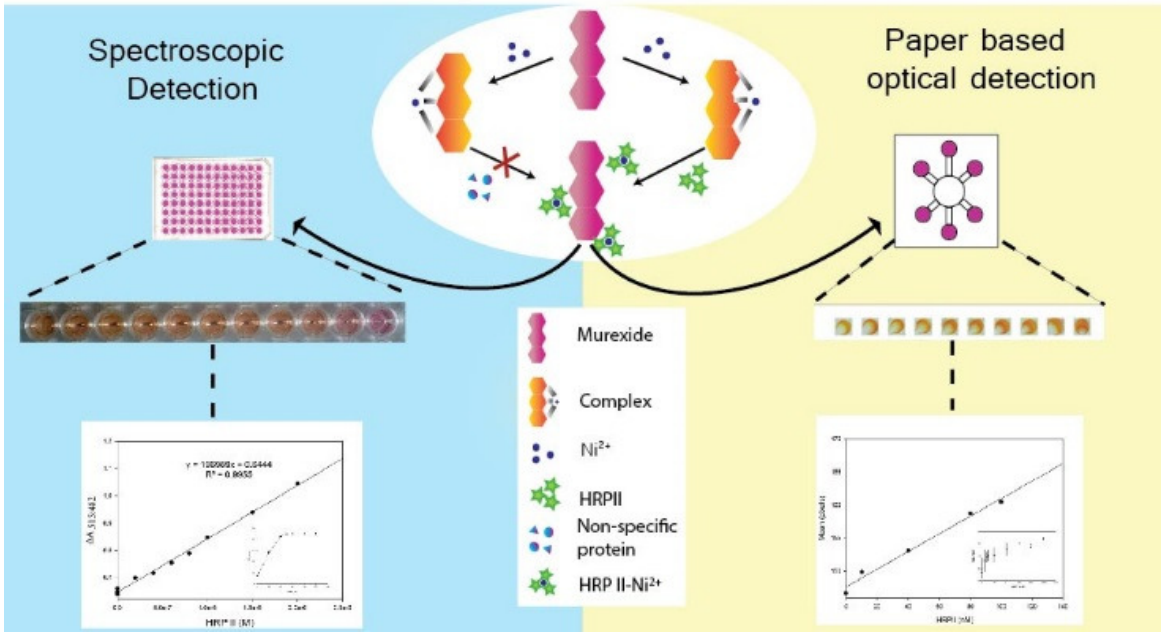

Figure 3.2: Graphical representation of indicator based assay using murexide dye and Ni^{2+} ions to optically detect HRP-II in solution and paper based platform.

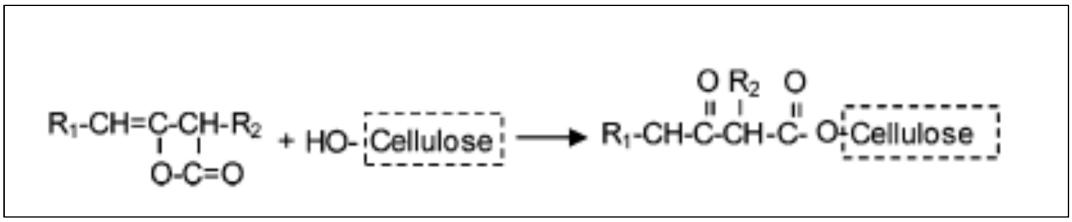

Figure 3.3: The reaction of alkyl and alkenyl ketene dimers with cellulose. Adapted From Li *et al.,* (2009).

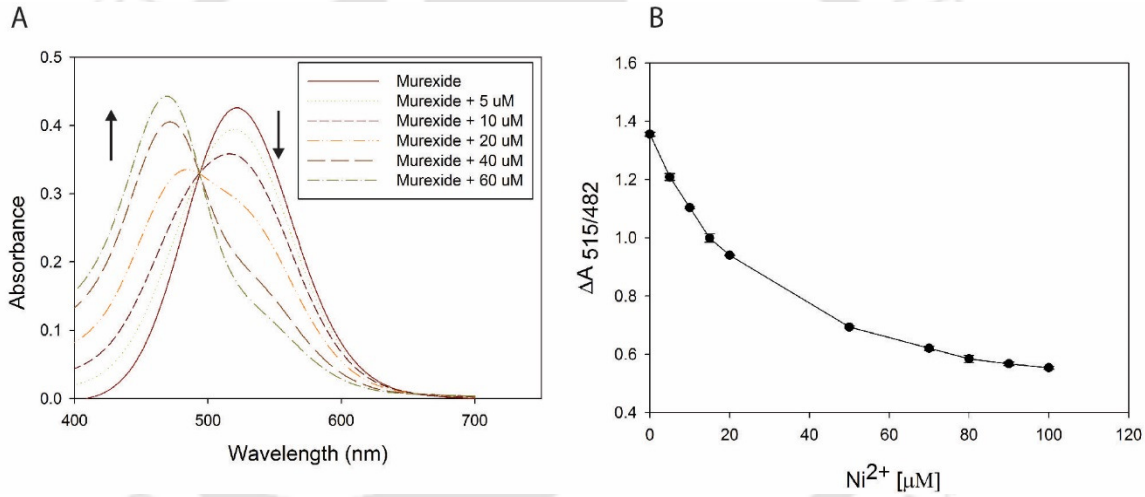

Figure 3.4: (A) Change of UV−Vis spectra of murexide dye upon addition of increasing concentration of Ni^{2+} and (B) absorbance ratio of $A_{515/482}$ for the reaction of murexide dye with the increasing concentration of Ni^{2+} in 20 mM HEPES buffer pH 7.4.

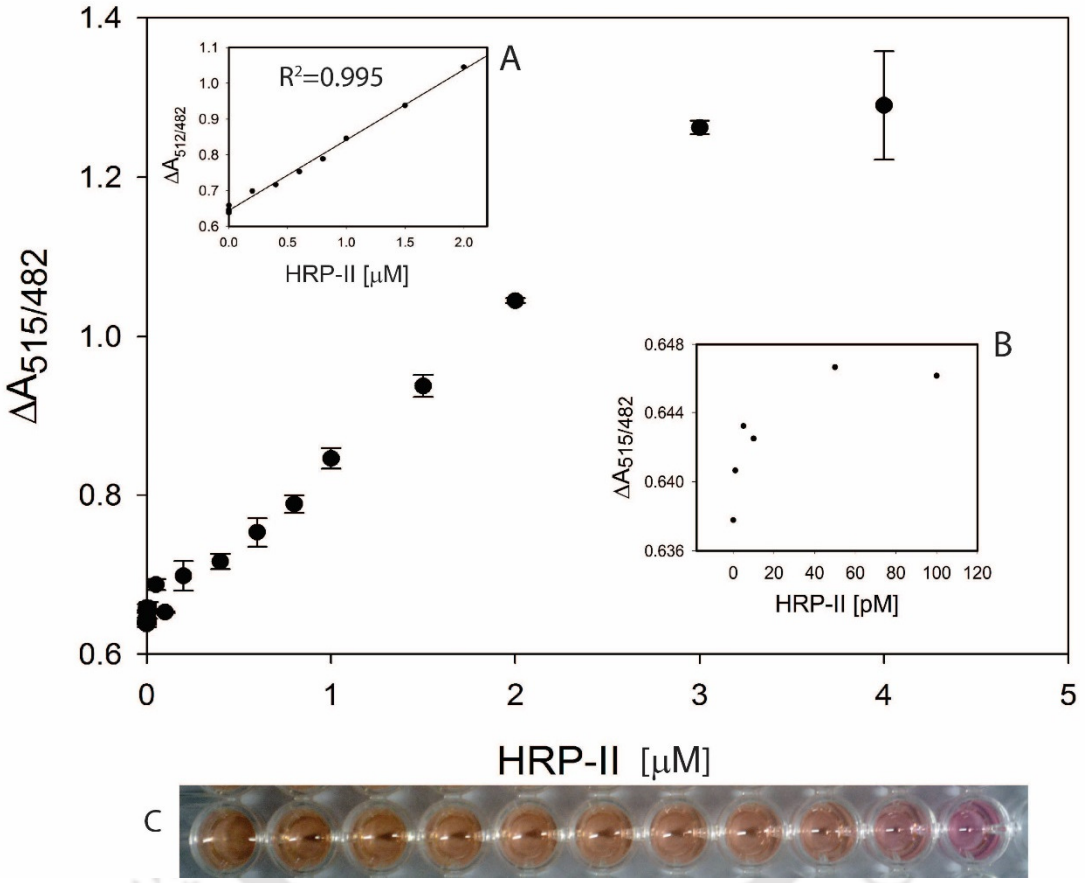

Figure 3.5: Plot of absorbance ratio of $A_{515/482}$ for a fixed amount of murexide-Ni^{2+} (1:1) against increasing concentration of HRP-II in 20 mM HEPES buffer pH 7.4. The linear region of the data (shown in the inset of part A) was fit to a linear equation. The cluster of data in the picomolar range was expanded (shown in the inset of part B) for clarity. Panel below (C) the graph is a real representative image of HRP-II detection in solution.

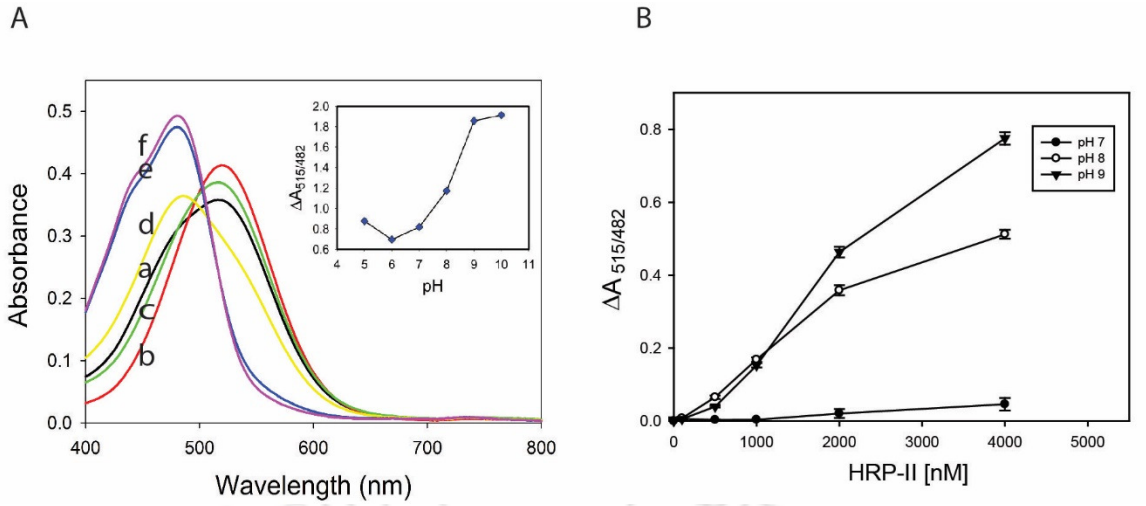

Figure 3.6: Effect of different pH on the detection system: (A) UV−Vis spectra of murexide-Ni^{2+} in the presence of 500 nM HRP-II at pH (a) 5, (b) 6, (c) 7, (d) 8, (e) 9, and (f) 10. (B) Plot of ratio of absorbance of $A_{515/482}$ at pH 7, 8, and 9 against increasing concentration of HRP-II at an equimolar mixture of 50 µM murexide and Ni^{2+}.

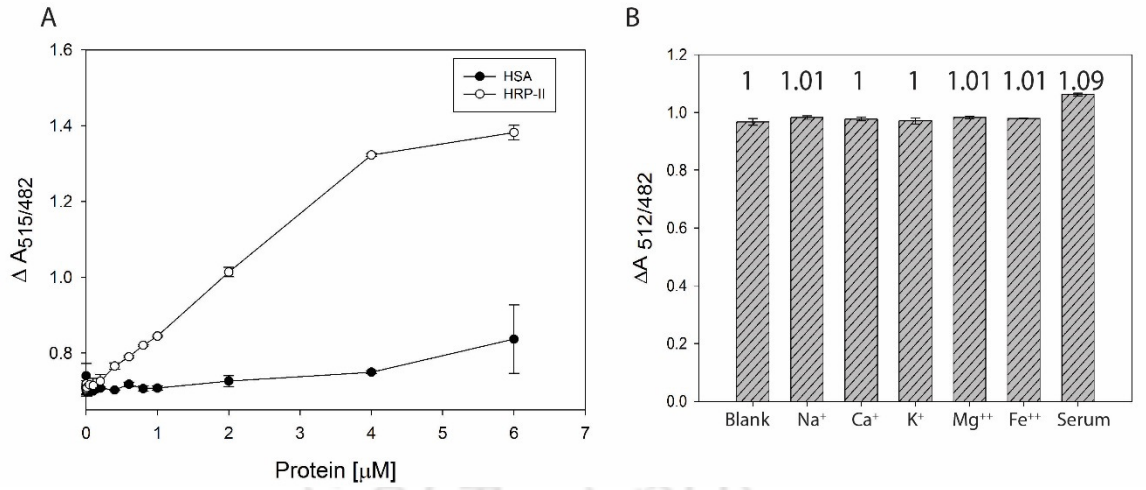

Figure 3.7: (A) Plot of ratio of absorbance of $A_{515/A482}$ against concentration of protein (HSA and HRP-II) titrated to equimolar concentration of 50 µM murexide-Ni^{2+} complex in 20 mM HEPES buffer at pH 7.4. (B) Graph showing detection of 1 µM HRP II in the presence of serum (diluted 1:2) and 50 µM of different species of monovalent and diavalent salts in 20 mM HEPES at pH 7.5 and equimolar murexide – Ni^{2+} (50 µM) reaction mixture.

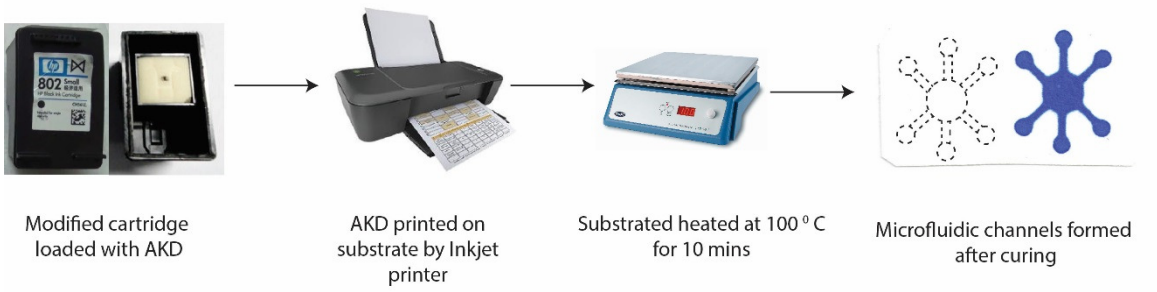

Figure 3.8: Schematic showing the fabrication of paper based platform for detection of HRP-II

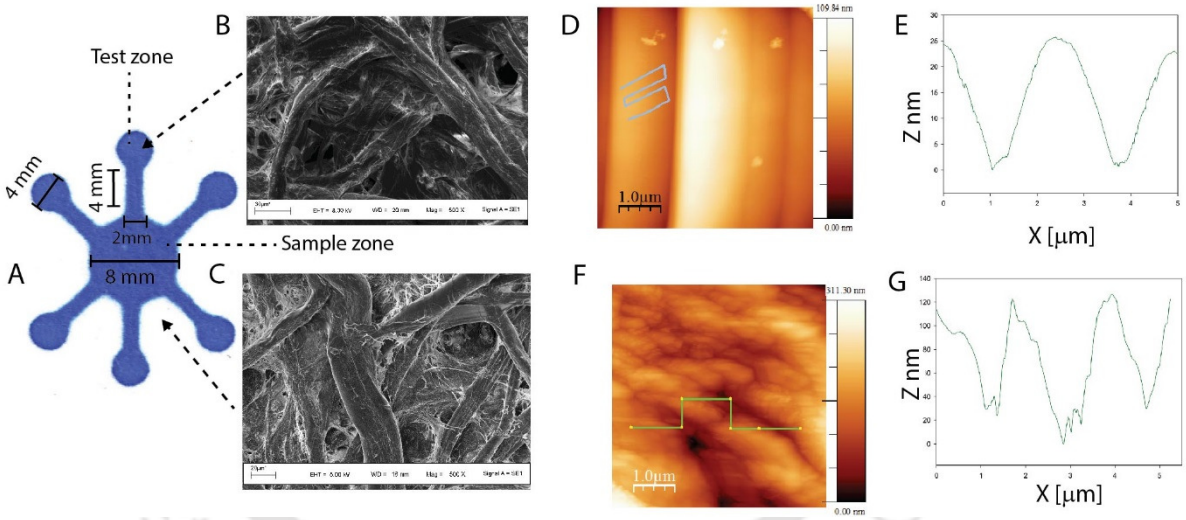

Figure 3.9: (A) Image of the paper platform showing the dimensions of six test zones connected to a central sample zone. For visibility of the channels and zones, blue ink was applied. SEM images of (B) nonprinted and (C) AKD printed on Whatman filter paper 1. AFM of (D) 2-D image and (E) height profile of selected region of nonprinted paper surface. AFM of (F) 2-D image and (G) height profile of the AKD printed part of the paper platform.

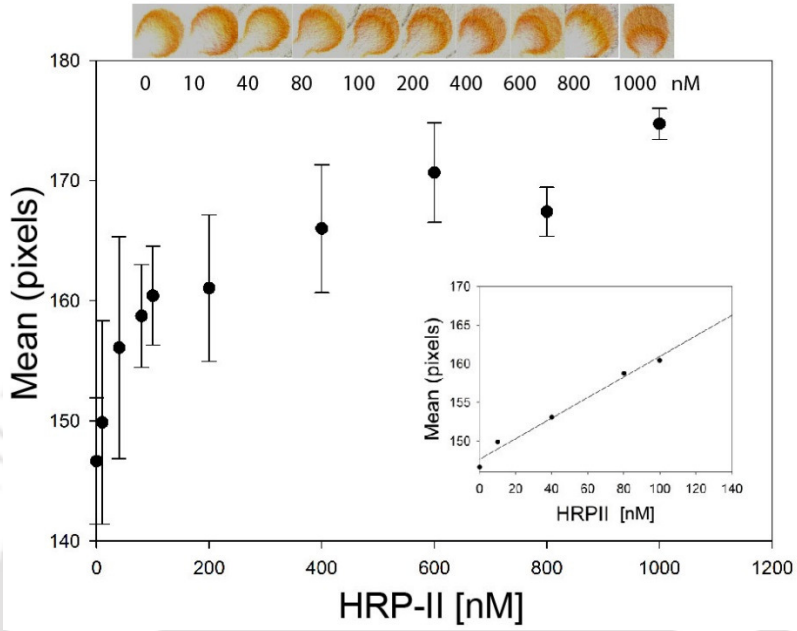

Figure 3.10: Top panel shows representative real images of HRP-II detection on μPAD. The graph showing optical response in pixel intensity against concentrations of HRP-II in μPAD with the linear region of the data (shown in inset) fitted to linear equation (Y= mx + c, where m is the slope, c is the intercept on the y axis). Each datum is the mean of six assays and the error bars represent the relative standard deviations.

Chapter 4

Quantitative detection of histidine-rich proteins using silver nanoparticle-based sensitive competitive binding assay

Chapter 4

Quantitative detection of histidine-rich proteins using silver nanoparticle-based sensitive competitive binding assay

4.1 Overview

Noble metal nanoparticles have been growingly used to detect of a wide range of analytes via colorimetric approach as they possess unique tuneable optical properties conferred by their shape and size dependant localized surface plasmon resonance (LSPR) phenomena. They are easy to synthesize, use and functionalize according to the target analyte of interest (Chinnadayyala *et al*., 2015; Oh *et al*., 2015; Jain *et al*., 2016). Silver nanoparticles (AgNPs) are growingly used in colorimetric assays owing to their higher surface enhanced Raman spectroscopic (SERS) efficiency and comparatively low cost of production. The sharp and intense resonance peaks of the AgNPs are considered as attractive traits for their efficient sensor applications (Lee and El-Sayed, 2006). These AgNPs exhibit characteristic LSPR band in a wide spectral range ($\lambda_{350-800nm}$) (Willets and Duyne 2006). LSPR occurs when light interacts with the nanoparticles that lead to a plasmon oscillation around the nanoparticles. It is sensitive to changes of local dielectric

environment caused by the changes of surface or size of the metal nanoparticles. With these foundations, AgNps have been exploited to monitor bimolecular interactions for diverse applications (Ravindran *et al*., 2013; Tnag and Li 2017).

AgNPs can be easily functionalized by using thiolated compounds that stabilize the nanoparticles. There are three common strategies that are used to functionalize nanoparticles: 1) preparing the nanoparticles directly in the presence of ω-functionalized thiols, 2) exchanging an existing ligand for a ω-functionalized thiol, and 3) modifying the original thiol covalently by an interfacial reaction (Love *et al*., 2005). In this chapter we functionalized AgNPs by glutathione (GSH) using the first strategy. GSH is a short oligopeptide (γ-Glu-Cys-Gly) that contains a –SH group that can be easily adsorbed onto the surface of metal nanoparticles. It is quite sturdy and can tolerate the reductive conditions that are used to prepare nanoparticles which also help to stabilize and protect the nanoparticles. The GSH functionalized nanoparticles have been used to detect many metal ions. (Lim *et al*., 2008; Kiatkumjom *et al*., 2014; Yu *et al*., 2016)

There is an enormous importance of quantitative detection of histidine rich proteins (HisRPs) not only for detection of HRP-II in malarial diagnostic applications, but also in generic molecular biological works (Chakma *et al*., 2016; Swartz *et al*., 2011). The methods and techniques developed so far for the detection of the HisRPs have utilized mostly antibodies as biorecognition elements (Darain *et al*., 2004; Wasowicz *et al*., 2008; Wasowicz *et al*., 2010). These antibody based methods are however, complex, time consuming and expensive and in many cases are encountered with variable results, as described in the previous chapters. We propose here a chemical approach exploiting the sensitive optical property of the functionalized metal nanoparticles for quantitative detection of the target. Our main motivation to consider these plasmonic nanoparticles as signal transduction platform is to improve further the sensitivity and dynamic detection

range for the target biomarker than the work described in the previous chapter. Notably, the sensitivity has been considered as one of the major performance factors of the detection systems in the context of current global malaria management programmes owing to its tremendous importance in detecting asymptomatic malaria infections (Bousema *et al.,* 2014). The high surface to volume ratio of the nanoparticles is known to increase the surface area for reactions leading to enhance detection range (Biener *et al.,* 2009). We exploited GS-AgNPs as a colorimetric probe to develop a simple competitive reaction-based assay to detect HisRPs using two types of histidine rich proteins as targets- one with poly-his tagged proteins, while the second one HRP-II that contains naturally abundant histidine residues and is specifically secreted by *Plasmodium falciparum.* The method involves preferential binding of nickel ions with the target protein through coordination complex that causes blue-shift of the SPR band of GS-AgNPs-Ni^{2+} complex as a consequence of its disaggregation as shown in figure 4.1. Till now report on quantitative detection of HisRPs using non biological recognition elements is not available in open literature. A detailed account on the method has been described in this chapter.

4.2 Materials and Methods

4.2.1 Materials and reagents

HEPES ($C_8H_{18}N_2O_4S$), Glutathione ($C_{10}H_{17}N_3O_6S$), Tris buffer ($C_4H_{11}NO_3$), Imidazole ($C_3H_4N_2$), Ampicillin ($C_{16}H_{19}N_3O_4S$), IPTG($C_9H_{18}O_5S$), L-Histidine were procured from Himedia (India). Silver nitrate ($AgNO_3$) (> 99.9 % pure) and Sodium borohydride ($NaBH_4$) were purchased from SRL (India) and Spectrochem (India), respectively. Poly-his tagged *P. falciparum* - lactate dehydrogenase (*Pf*LDH) and glutamate dehydrogenase (*Pf*GDH) protein were cloned and expressed following standard or partially modified

molecular protocol. *P. falciparum* HRP-II was expressed without the poly-his-tag as described in chapter 2. The recombinant proteins were purified using Ni^{2+} affinity chromatography and then dialyzed in appropriate buffers as described in chapter 2. All the other reagents used were of analytical grade. Real serum was collected from healthy volunteers following an established protocol and ethical guidelines of IIT Guwahati. All the solutions were prepared in MQ water with resistivity > 18 MΩ.cm.

4.2.2 Preparation of glutathione stabilized silver nanoparticle (GS-AgNPs)

Silver nanoparticles (AgNPs) were synthesised by $NaBH_4$ (3 mM) based reduction of $AgNO_3$ (0.2 M) (Li *et al*., 2009). The pale yellow silver colloidal solution so formed was stirred for five minutes at RT and then added glutathione to it to a final concentration of 1mM that turned the colour of the solution from pale to dark yellow. To ensure complete assembly of GSH on the AgNPs, the dark yellow solution was incubated for 2 h at RT with constant stirring. The prepared GS-AgNPs could be used for a week.

4.2.3 Spectroscopic analysis

The UV-Vis absorption spectra were taken in a flat bottom 96 microtiter plate reader (TECAN M200 Pro, Switzerland). To perform the colorimetric detection, protein samples (*Pf*GDH, *Pf*LDH, HRP-II, HSA and free histidine) in increasing amount ranging from 10 pM to 2 µM were added to an optimized Ni^{2+} solution of 100 µM in 20 mM HEPES buffer pH 7.4. The solution was incubated for 15 min to ensure proper binding of Ni^{2+} to the samples. A total of 150 µl of 0.2 M GS-AgNPs was then added to the solution and incubated for 10 min. Absorbance was taken at a wavelength of λ_{390nm} and λ_{450nm}. All the experiments were performed in triplicates and graphs were plotted in sigma plot.

FTIR spectra of the sample were recorded at a resolution of 4 cm^{-1}in aqueous medium using IR grade KBr. A pellet of finely grinded KBr was prepared to which one µl of the sample was added and allowed to dry at RT prior taking the spectra.

4.3 Results and Discussion

4.3.1. Synthesis and characterization of GS-AgNPs

AgNPs were synthesized by following a simple method involving reduction of silver nitrate with sodium borohydride. The synthesised AgNPs were then coated with glutathione to produce stable GS-AgNPs (Figure 4.2 A). The formation of AgNPs and GS-AgNPs was confirmed by UV-Vis spectroscopy (Figure 4.2 B). AgNPs exhibited strong surface plasmon resonance (SPR) band at $\lambda_{390\ nm}$. When GSH was coated on the AgNPs, the band was marginally shifted to $\lambda_{400\ nm}$ due to change in refractive index of the surrounding medium that changes the plasma oscillation frequency around the nanoparticles (Ameer *et al*., 2016). The average size of the GS-AgNPs was ~5 nm as discerned from the histogram distributions derived from the TEM image (Figure 4.2 C). The binding of GSH to the AgNPs was further confirmed from the IR spectra (Figure 4.2 D). The spectra of pure GSH and GS-AgNPs were compared to confirm that GSH was attached to AgNPs successfully. As observed from the spectrum, the peak at 2526 cm^{-1} corresponding to -SH bond disappeared when GSH was self-assembled on AgNPs indicating the formation of thiol bond between the cysteine group of GSH and AgNPs. The minor but clear peaks at 1761 cm^{-1} and 1530 cm^{-1}corresponding to C=O stretching and N-H bending vibration observed in pure GSH were disappeared following incubation with AgNPs. The probable reason has been attributed to the electrostatic interactions between these two interacting entities that arrest the vibrational freedom of these functional moieties.

Moreover, the peak intensities in the range of 1630 cm^{-1} to 1000 cm^{-1} for the AgNPs were substantially decreased following the glutathione coating due to decrease in the dipole moment of the bonds after binding to AgNPs.

4.3.2 Detection of HisRPs following competitive binding assay

The principle we propose here for the detection of HisRPs has been portrayed in the figure 4.3 A. GS-AgNPs were aggregated in the presence of Ni^{2+} ions as evident from the TEM image (Figure 4.3 2A inset b). With the addition of HisRPs to the system, as exemplified here with HRP-II, the aggregation process was hindered as evident from the TEM image (Figure 4.3 A inset a). The HisRP mediated disaggregation process could also be monitored visually from the corresponding reversal of the solution color from orange to pale yellow. A blue-shift of ~60 nm of the SPR peak of the Ni^{2+} conjugated GS-AgNPs upon addition of HRP-II with corresponding changes in absorption maxima from $\lambda_{450\ nm}$ to $\lambda_{390\ nm}$ is evident (Figure 4.3 B).

The glutathione peptide has –COOH, $-NH_2$ and –SH functional groups. The -SH bond participates in the thiol binding with the AgNPs as confirmed and discussed above. The remaining -COOH and NH_2 groups are likely to participate in the complex formation with Ni^{2+}ions. Zeta-potential studies revealed that the surface charge potentials of AgNPs, GS-AgNPs and Ni^{2+} ions treated GS-AgNPs were -24.4 ± 4.78 mV, -34.9 ± 6.6 mV and -28.2 ± 5.1 mV, respectively. The magnitude of –ve charge on the bare AgNP was increased further by ~ 43 % when it was coated with GSH at physiological pH 7.4. The Ni^{2+} ions when introduced, form complex with –COOH groups leading to the decrease in the surface charge of GS-AgNPs by neutralizing the –ve charge through electrostatic binding. This coordination complex of GSH and Ni^{2+} ions can be hypothesized to be tetra or penta-coordinated, interacting with oxygen atoms of the

carboxylic group (Liu *et al*., 2014). We suggest that the intermolecular co-ordination complex initiated by the electrostatic binding of the Ni^{2+} ions with the glutathione carboxylic groups on the surface of the GS-AgNPs moiety promotes rapid aggregation of the nanoparticles.

The optimum concentration of Ni^{2+} ions involved in the binding of GS-AgNPs (150 µl) was ~100 µM (Figure 4.4). Since there was a peak shift from ~$\lambda_{390\ nm}$ to ~$\lambda_{450\ nm}$ with the increasing concentration of Ni^{2+}, a plot of absorbance ratio of $\lambda_{390\ nm}$ to $\lambda_{450\ nm}$ versus Ni^{2+} concentration was considered for a reliable detection of the Ni^{2+}concentration. The binding affinity (K_d) of the interaction of Ni^{2+} with the GS-AgNPs and HisRP (HRP-II) was calculated using the equation: $f = B_{max}*abs(x)/ (K_d + abs(x))$, where, f and B_{max} were specific binding and maximum number of binding sites, respectively. The K_d values for the interaction of Ni^{2+} with GS-AgNPs was calculated to be ~ 1.36 X 10^{-4} M. The K_d for interaction of Ni^{2+} with histidine tag was calculated to be10^{-6} M at neutral pH using SPR method (Neiba *et al*., 1997). The introduction of HisRPs leads to disaggregation of the Ni^{2+} induced aggregated GS-AgNPs due to competitive binding of Ni^{2+} to HisRP as supported by the lower K_d value of Ni^{2+} for HisRP. This shift of SPR band leads to change in colour from orange ($\lambda_{450\ nm}$) to yellow ($\lambda_{390\ nm}$).

The extent of disaggregation of the Ni^{2+} conjugated GS-AgNPs was examined in the presence of different HisRPs (Figure 4.5). The response was strongly positive with all the high histidine containing proteins whereas, for free histidine and HSA, the level of aggregations was negligible (Figure 4.5 C).The dynamic detection range for different targets were in the trend of HRP-II > *Pf*LDH > *Pf*GDH (Table 4.1). The LOD was calculated from the slope using the relation, LOD = 3 *Sy/b, where Sy is the standard deviation (SD) of y-intercept, and b is the slope of the linear curve. Among all the test proteins, *Pf*GDH exhibited the lowest LOD value (Table 4. 1).

The binding affinity of poly-histidine molecules to nickel containing matrices increases with increasing the number of His residues and the highest binding was observed with 6 X His tag (Knecht *et al*., 2009). Ni^{2+} coordinates to the carboxyl group, the imidazole and the amino nitrogen atoms to histidine in an octahedral coordination. However, in the case of multiple His residue (n > 2) systems, histidines coordinates to the metal ions in a square planar geometry which is stabilized by inter/ intramolecular hydrogen bonds (Valenti *et al*., 2006). Coming back to our target proteins *Pf*LDH and *Pf*GDH, both are multimeric proteins with four and six monomers, respectively, whereas, HRP-II is monomeric in nature. *Pf*GDH showed higher signal (high slope, low LOD) since it contains more 6 X His tag per molecule of the protein, and hence binds to more $Ni^{2+}$with high affinity by the phenomenon explained earlier in comparison to *Pf*LDH and HRP-II. The HRP-II protein, which is a random coiled structure, on the other hand comprises of only two contiguous His residues spreading across 18 tripeptides (Ala-His-His), 3 pentapeptides (Ala-His-His-Ala-Ala), and 33 hexapeptides (Ala-His-His-Ala-Ala-Asp) (Jain *et al.,* 2014). Hence, due to lack of n > 2 multiple his residue systems in HRP-II the coordination complex of the nickel ions may not attained strongly favourable square planner geometry for better binding of the ions with the His and allied ligands in the protein matrix resulting in achieving slow binding with high LOD. The high dynamic range achieved with HRP-II is a manifestation of the involvement of high protein to nickel (which is fixed here as 100 µM) ratio in the binding. The important parameters for *Pf*GDH, *Pf*LDH, HRP-II, are summarized in the table 4.1.The proposed method was put into test using *Pf*GDH as the sample protein with the standardized parameters mentioned above to see whether it could detect histidine rich target proteins quantitatively in presence of other non-specific proteins (Albumin and Myoglobin). A known amount of *Pf*GDH (0.133 µg) and it's mixture with other proteins (total 0.8 µg) were taken

following Bradford assay and then the concentration of *Pf*GDH in these samples were measured by the competitive binding assay. The percentage (%) recovery was calculated using the relation: (Observed concentration/True concentration) * 100. A recovery of 0.137 µg with 103 ± 1.7 % recovery for *Pf*GDH could be achieved.We therefore, propose that this simple method has the potential to selectively and quantitatively detect recombinant His-tagged proteins in a mixture of proteins in aqueous sample. A Lysine-functionalized silver nanoparticles based colorimetric method for visual detection and separation of histidine and histidine-tagged proteins has been developed, which is however non-quantitative in nature. (Bae *et al*., 2010).

Table 4.1: Response characteristics of different histidine rich and control proteins in the GS-AgNPs based competitive binding assay. X represents other amino acids.

HisRPs	Type of His sequence	Size(kDa)	No. of amino acids	p*I*	LOD (nM)	Dynamic range (nM)
HRP-II	-XHHX-	30	309	6.43	30.0	0.10-800
***Pf*LDH**	-HHHHHH-	136	316	7.12	5.4	5.00-50
***Pf*GDH**	-HHHHHH-	318	470	7.48	3.5	0.25-25

4.3.3 Detection of malaria by measuring HRP-II

A diagnostic application of the developed method was explored using HRP-II as target biomarker for detection of malaria. As documented above, the detection system conferred a dynamic detection range of 0.10 - 800 nM and LOD of 30 ±5.6 nM for HRP-II (R^2 = 0.995). Additionally, the detection could be performed visually in a yes/no format following colorimetric signal. The developed method has also potential to detect cerebral malaria as the LOD offered by the method meets the sensitivity needed for diagnosis the

disease (Rubach *et al*., 2012). The developed assay could also discriminate the target HRP-II from the major blood protein HSA without any significant interference. There were minor signals observed for both HSA and histidine at their high concentrations (> 1 µM) which is however, negligible in comparison to the signal obtained for the HRP-II. The competitive binding assay was then performed in blood serum by spiking it with two different concentrations of HRP-II (Figure 4.6 A). The HRP-II spiked serum was incubated with 100 µM of Ni^{2+} for 15 min at RT. Following which 150 µl of GS-AgNPs was added and then reading was taken after 10 min. A background noise of nearly 4.4 % was generated, though a clear response signal corroborating to the corresponding concentration of HRP-II could be identified. This minor background noise signal from the blood serum may be subtracted from the data set to clean the signal at the time data processing. The effect of different major salt species present in the blood serum on the detection system was also examined by calculating the percentage change in signal as compared to the blank (Figure 4.6 B). Selectivity coefficient (SC) for each of the potential interfering agents was calculated using the formula, $SC = A_{c+i}/A_c$, where A_{c+I} and A_c are the response for HRP-II in the presence and absence of each interfering agents, respectively. There were marginal interferences of 10 %, 11 % and 7 % from the corresponding factors Mg^{2+} $Ca^{2+}$and Zn^{2+} observed which were attributed due to their divalent nature competing with the Nickel ions.

The influence of sample pH on the analytical performance of the competitive binding assay for the target HRP-II was investigated (Figure 4.6 C). A pH range of 5 - 9 was considered to cover away the severe aberration of blood pH values which occurred under some pathological conditions. The aggregation of GS-AgNPs in presence of Ni^{2+} increased with increasing pH value of the sample. Notably, with the increase in sample alkalinity de-protonation of the carboxylic groups ($pK_1 = 2.12$ and $pK_2 = 3.59$) from the

GSH moiety also surges that enhances the binding affinity between GS-AgNPs and $Ni^{2+}$and linked aggregation process. In the presence of HRP-II and *Pf*GDH the SPR signal intensity were significantly changed above the neutral pH value of the samples. When these HisRPs were introduced, Ni^{2+} binds effectively to the proteins (p*I*s in Table 4.1) due to increase negative charge on these proteins that leads to increased dis-aggregation of the nanoparticles. An effective pH range of 7 - 8 as evident from the plots (Figure 4.6 C) has been suggested to perform the assay as the range covers the physiological pH value for wide applications.

4.4. Conclusion

The competitive binding assay developed through this investigation using GS-AgNPS as colorimetric probe has been validated with two types of histidine rich proteins: one with poly-histidine tag, which is commonly co-expressed with the target proteins in molecular biological works for the convenience of isolating the expressed proteins, and the other is HRP-II with naturally abundant histidine residues in the peptide back-bone. In regards to the detection of poly-his tag proteins, the presented method obviates the need of preliminary concentration (e.g. using NTA magnetic beads) and separation steps (such as, gel-electrophoresis) that are commonly practised in most of the reported methods. The information on the quantitative assay of other naturally abundant HisRPs is limited and discussed in literature mostly in the context of detection of the malarial biomarker HRP-II, the level of which in the blood serum is significantly high under the pathological conditions which can reach upto 100 $\mu g.ml^{-1}$ (Pal *et al.,* 2016). The method we present here though reacts with all the HRP with contiguous minimum two His residues in the sequences, the potential applications of the method explored through this investigation are not hampered. Since, for both the types of HisRP cases pure or highly copious targets are involved. The competitive binding assay developed through this investigation has

been successfully used to detect HisRPs at nano molar level in aqueous samples. Additionally, the diagnostic potential of the developed assay for HRP-II has been confirmed in blood serum. The sensitivity of the method appears to be governed by the density and type of sequence of the histidine residues in the protein as evident from the present case. Additionally, the size of the nanoparticles needs to be properly standardized for each study due to the obvious reason of influence of the nanoparticle size on the SPR bands. The assay offers a sensitive (nanomolar level) and inexpensive detection of histidine rich proteins within a reasonable time frame (~30 min) without entailing any labile bio recognition system, such as antibody and protein-based enzymes.

Figures:

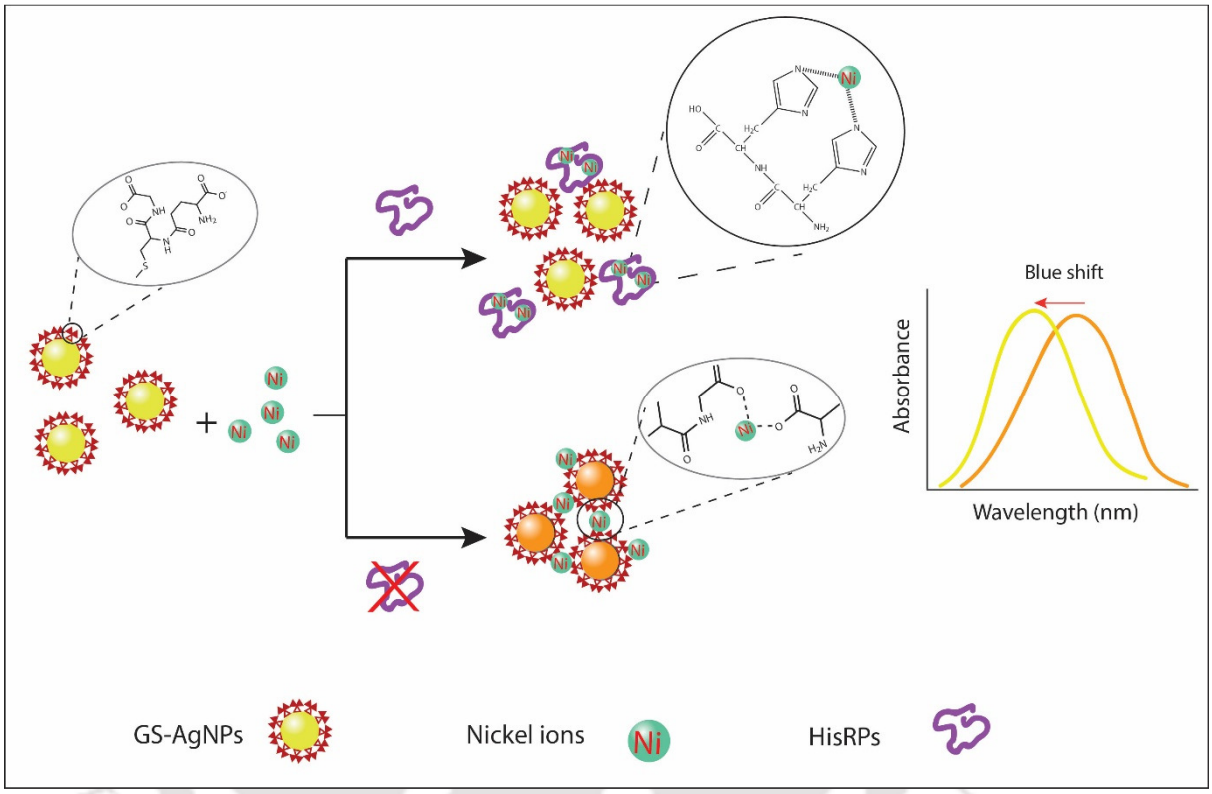

Figure 4.1: Simplified representation of the competitive binding assay format for detection of HisRPs using GS-AgNPs and Ni^{2+} ions

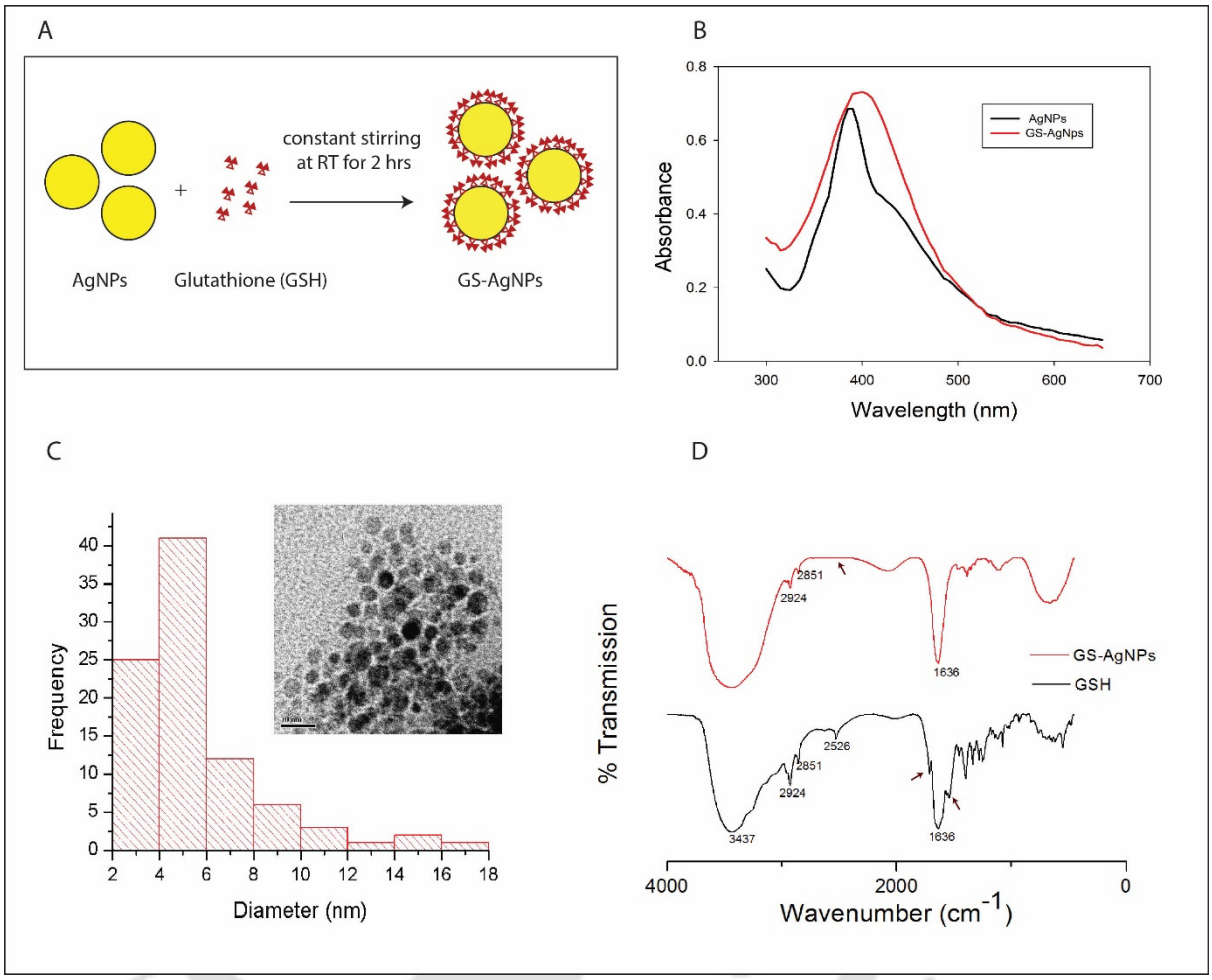

Figure 4.2: (A) Schematic showing synthesis of GS-AgNPs (B) UV-Vis spectra of AgNPs and GSH coated AgNPs. (C) Histogram showing the GS-AgNPs size distribution derived from TEM image (Inset) using Image J software. The TEM was operated at accelerating voltage of 200 kV (D) FTIR Spectra of GSH and GS-AgNPs.

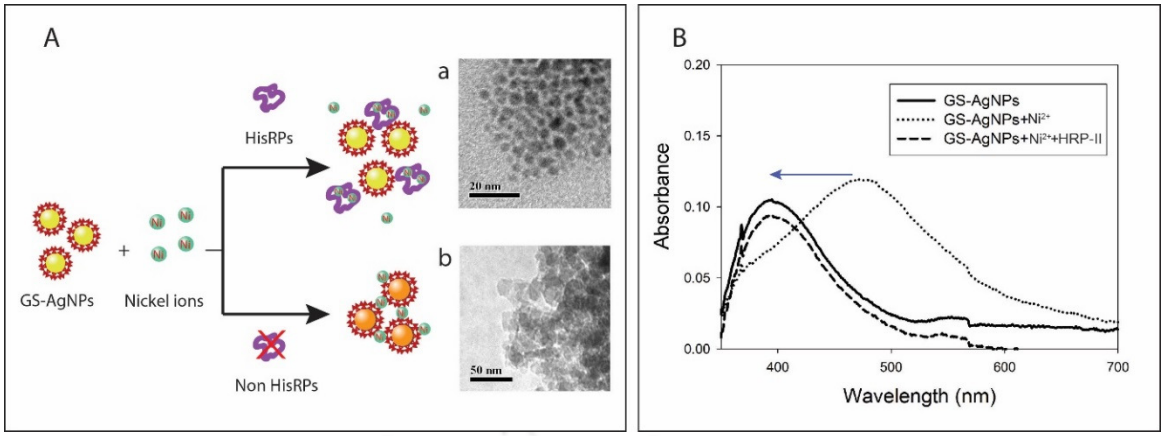

Figure 4.3: (A) Detection scheme of HisRPs following competitive binding assay. Inset (a) TEM image of disaggregation of nickel conjugated GS-AgNPs in the presence of HisRPs (in this case HRP-II) and (b) aggregation of GS-AgNPs in presence of only Ni^{2+}ions. (B) UV-Vis spectra of GS-AgNPs under different conditions as shown in the inset legend.

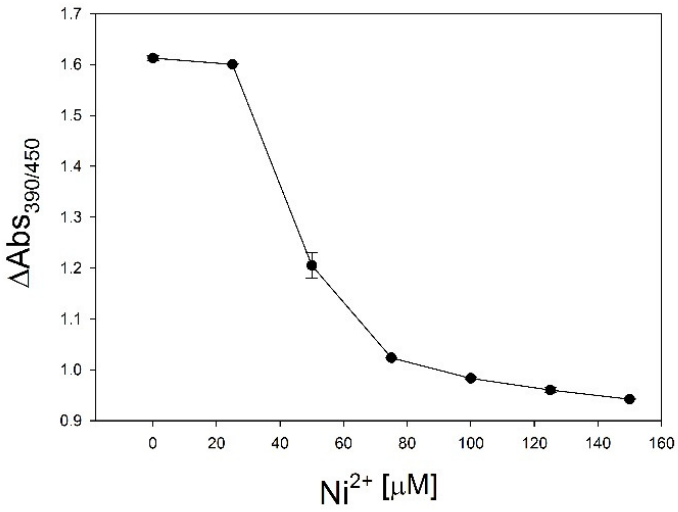

Figure 4.4: Optical response of GS-AgNPs (150 µl) versus concentration of Ni^{2+} ions. Each datum point is an average of at least three independent experiments, error bars represent the SD. Experiment was performed in 20 mM HEPES pH 7.4, at RT for 15 mins.

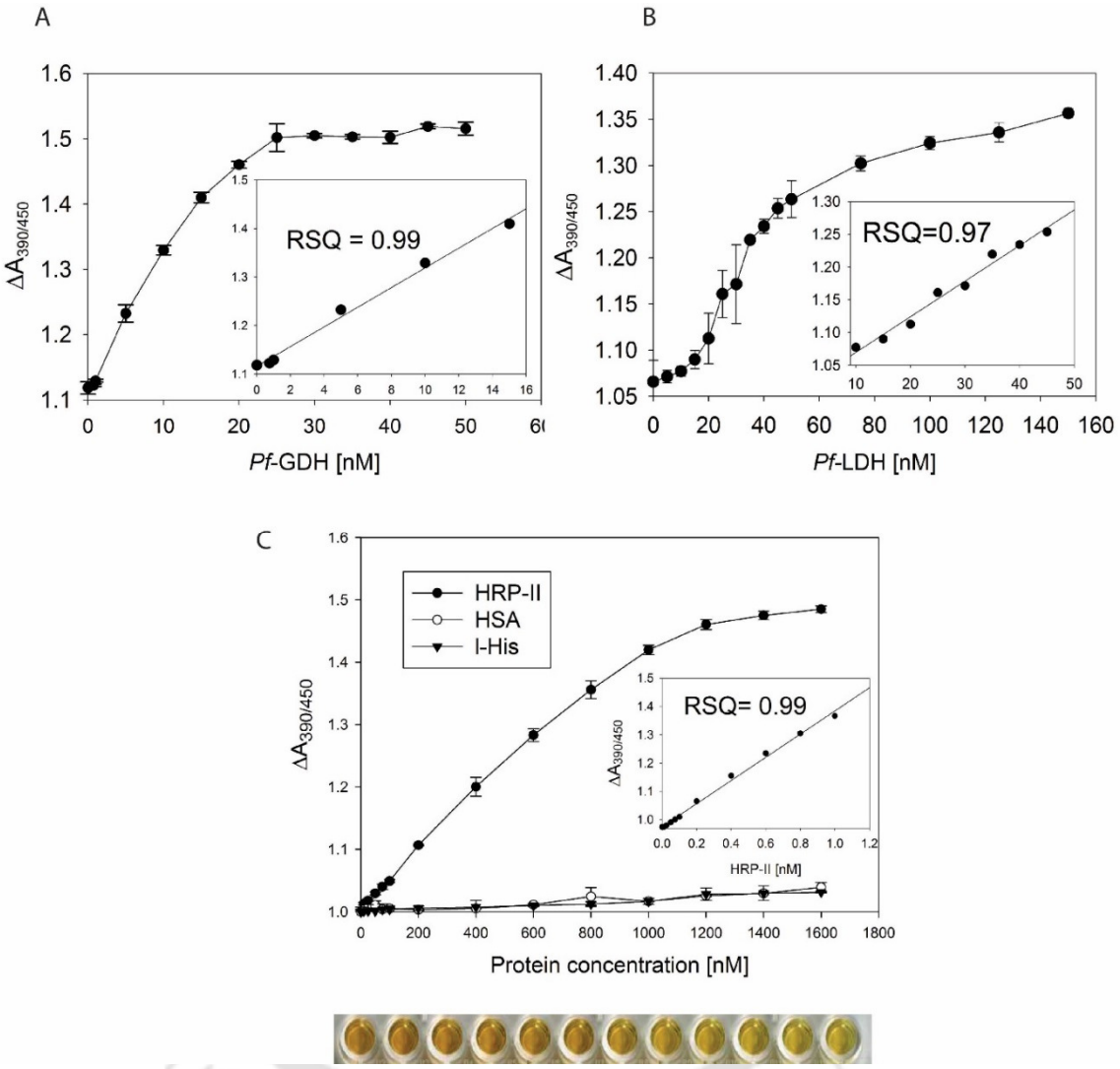

Figure 4.5: Competitive binding assay for the detection of (A) *Pf*GDH, (B) *Pf*LDH, and (C) HRP-II, HSA and free histidine. Insets show the linear region of the response. Bottom photographed panel shows the change in colour of the reaction mixture with increasing concentration of HRP-II corresponding to the x-axis values.

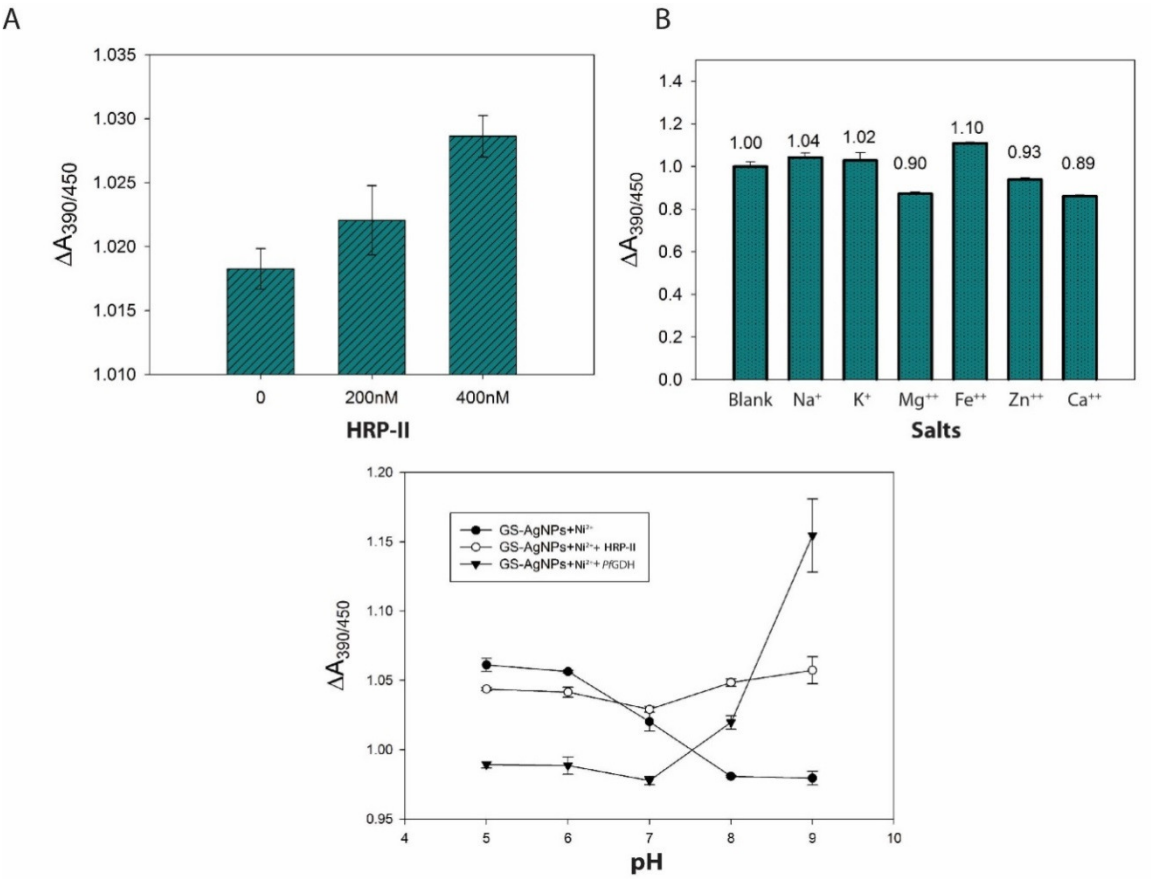

Figure 4.6: (A) Optical response for HRP-II in the presence of (A) blood serum (diluted 2X) (B) salts and (C) different pH conditions. For studies with salts, a total 100 µM of each salt solution was incubated with 100 µM Ni^{2+} and 0.5 µM HRP-II and then incubated for 15 mins before taking the absorbance. Different pH solutions were prepared in 20 mM HEPES buffers containing 100 µM of Ni^{2+} and 0.5 µM of the HisRPs (HRP-II or *Pf*GDH).

Chapter 5

Development of electrochemical impedance spectroscopy based malaria aptasensor using HRP-II as target biomarker.

Chapter 5

Development of electrochemical impedance spectroscopy based malaria aptasensor using HRP-II as target biomarker.

5.1 Overview

There has been a continuous strive to develop effective bio-recognition systems for malaria that surmount the drawbacks of the prevailing antibody-based sensors for detection of the parasites as mentioned in earlier chapters. The antibody based malaria detection systems are though empowered by the state-of-art antibody production strategies and high selectivity, the labile nature of these protein-based recognition elements stands as hurdle while their applications in point of care (POC) diagnosis is sought in countries, which are saddled with hot and humid climates with low resource settings. Notably, malaria is a tropical disease occurring largely in hot and humid climate, which is congenial for the growth and reproduction of the parasite vector, *Anopheles* mosquito. The widely used antibody based rapid malaria detection systems also suffer from cross reactivity with auto-antibodies, false negative results due to

prozone effect, batch to batch variations, and are non-quantitative in nature as discussed in the previous chapters (Kasetsirikul *et al*., 2016).

General interest on nucleic acid based aptamers as biorecognition elements for biosensors and bio-detection applications is sharply growing owing to their certain clear advantages identified over the antibodies among which high thermal stability, low cost of production and capability to synthesize in large scales may be reckoned first. Nucleic acid aptamers are short single stranded oligonucleotides (DNA or RNA) which can bind to their targets with specificity and affinity. They are screened through an *in-vitro* selection process known as SELEX (systematic evolution of ligands by exponential enrichment) from a huge random library (10^{12}–10^{15} sequences). The selected aptamers fold in to three dimensional shapes and bind to their targets via a combination of hydrogen bonding, π-π stacking, van der Waals forces, and electrostatic interactions (Kakoti *et al*., 2017). Till now, there has been no report on fabrication of bio-detection systems for malaria using aptamers as bio-recognition element against the HRP-II biomarker. Here we describe the selection of an ssDNA aptamer against HRP-II following the SELEX process. The selected aptamer was characterized for its structure, as well as assessed its specificity and binding affinity towards the target HRP-II. The developed aptamer was then immobilized on a gold electrode surface following a rationally designed chemical approach and subsequently used the fabricated aptamer electrode to detect HRP-II in blood serum sample following electrochemical impedance spectroscopy (EIS). EIS method is a very sensitive technique which is quantitative in nature and has the ability to separate the surface binding events from the solution resistance. This method was chosen for the experiments because it is less destructive to biomolecules bound to the electrode surface (Benividi *et al*., 2015). A detailed account of the encouraging performance of the aptasensor has been described in this chapter.

5.2 Experimental approaches

5.2.1 Materials

DNA oligonucleotides, primers and ssDNA library were synthesized from IDT, USA. The selected aptamers were ordered from Bioserve Biotechnologies, India Pvt. Ltd. for the work. Polyvinylidene fluoride (PVDF) membrane (Hybond P) was obtained from Amersham, UK. SYBR Gold (10,000 X) nucleic acid stain was obtained from Invitrogen (USA), restriction endonucleases, and streptavidin coated magnetic beads were procured from New England Biolabs (USA), pGEMT easy TA cloning kit was obtained from Promega (USA) and DSP (dithiobis(succinimidyl propionate)) also known as Lomant's reagent was procured from ThermoFisher Scientific. All other chemicals were of analytical grade.

5.2.2 Construction of ssDNA library

A 90 bp long ssDNA library was constructed such that a stretch of 40 randomized nucleotides was flanked by constant primer binding sites on both sides as follows.

5'-CACCTAATACGACTCACTATAGCGGATCCGA-**N40**-CTGGCTCGAACAAGCTTGC-3'

The primer sequences used for PCR amplification of the library are listed in table A4.

5.2.3 Immobilization of protein on the PVDF membrane

Protein was immobilized on a piece of PVDF membrane (0.5 cm x 0.5 cm) and placed in a 2 ml Eppendorf tube. The membrane was first activated by immersing in methanol for 10 min followed by equilibration in binding buffer for 20 min. A total of 1 ml (1 $mg.ml^{-1}$) target protein (HRP-II) in binding buffer was added to the tube followed by gentle agitation on a rocking platform for one h. The membrane was then washed twice and

stored in binding buffer at 4 °C. The amount of protein immobilized on the membrane was quantified by differential method using Biuret assay, where amount of protein in the eluate was subtracted from the original protein solution.

To check the binding of protein on the membrane, AFM on an ambient air scanning probe microscope (Agilent Technologies 5500, USA) was performed using a silicon nitride probe. Images were recorded in a non-contact mode using Picoscan 5 software. The change in morphology of the PVDF membrane with subsequent protein immobilization was studied by using WSxM data acquisition and processing software.

5.2.4 SELEX study

SELEX was performed to produce specific ssDNA aptamers against HRP-II from a random oligonucleotide library of 90 nucleotides sequence (5'-CAC CTA ATA CGA CTC ACT ATA GCG GA-N40- GCA AGC TTG TTC GAG CCA G-3') of which 40 mer sequence (N40) confers the variation. A total 2.5 nmole of ssDNA pool was reconstituted in binding buffer (Table A3) and was denatured by heating at 90 ºC for 10 mins, followed by incubation at 4 °C for 10 min then cooled to 25 ºC (room temperature, RT) before binding. The ssDNA pool was incubated with HRP-II immobilized PVDF membrane at RT for an hr, on a rocking platform to allow binding. After incubation, the unbound ssDNA oligonucleotides were removed and stored through washing and spinning whereas the bound oligonucleotides to HRP–II were eluted in 200 µl PCR grade water by heating the membrane at 90 °C for 5 min. Bound ssDNAs were amplified using BioMix Red DNA polymerase (Bioline) following the amplification protocol : initial denaturation at 95 °C for 10 min, followed by 18 cycles of 95 °C for 15 s,68 °C for 15 s, 72 °C for 3 s and final extension at 72 °C for 3 s. To separate ssDNA from the amplified dsDNA, streptavidin coated magnetic beads were used. The PCR product was incubated with 30 µl of the beads in a coupling buffer at RT for one hour. The beads were washed

with coupling buffer and ssDNA strands were separated from biotinylated strands using 100 µl of 100 mM NaOH by denaturation. The pH of the solution was then adjusted to 7.5 with addition of dihydrogen phosphate (NaH_2PO_4). The separated ssDNA strands were used for the next round of SELEX as the next set of library. A total of 11 SELEX cycles were carried out, out of which one was counter SELEX against PVDF membrane and 10 were positive SELEX against HRP-II. Buffer compositions are mentioned in table A3.

5.2.5 Cloning and sequencing of the enriched aptamers

At the end of the 10^{th} positive SELEX cycle, the PCR product was cloned into pGEMT easy vector and transformed into competent *E. coli* DH5α cells. The positive clones carrying the aptamer inserts were selected on the basis of blue-white screening, and PCR. The recombinant plasmids from positive clones were sequenced by Bioserve Biotechnologies, India Pvt. Ltd and the aptamer sequences were aligned using Clustal X2 programme, for comparison.

5.2.6 Circular dichroism (CD) studies

To study the structural integrity and effect of binding of protein to the aptamer, CD studies were performed in Jasco J-815 spectropolarimeter. A total of 5 µM aptamer was heated for 10 mins at 90 °C, cooled to RT, followed by addition of 1µM of the individual proteins. The mixture was incubated for 1 h at RT followed by recording of the CD spectra at 25 ˚C using far UV scans in continuous mode, collecting measurements every 1 nm between 200 - 340 nm. Spectra were collected with an average of 3 accumulations, scan rate of 100 $nm.min^{-1}$, band width of 1nm and response of 2 s. Buffer contributions were subtracted from spectra and smoothed by Savitsky-Golay algorithm.

5.2.7 Isothermal Titration Calorimetry (ITC).

To determine thermodynamic parameters, ITC experiments were performed on a GE Healthcare UK, ITC 200 microcalorimeter. 20 µM of aptamer and 4 µM of target (HRP-II) and control (HSA) protein solutions in 50 mM HEPES buffer, pH 7.4, were prepared to be used as ligand, and macromolecule, respectively. The protein and aptamer solutions were dialyzed in the same buffer to avoid any heat generation due to mismatch of buffer solutions. It was then filtered and spun for 20 min at 12000 rpm before their use in the ITC. Following the first injection of 0.4 µl aptamer solution, subsequent injections of 2 µl each were administered by the ITC syringe to the reaction cell in 20 titrations, at 150 s intervals, at 25 °C and a stirring speed of 150 rpm. Control experiment without HRP-II was performed to correct for heat of dilution using only buffer in the sample column. Analysis of ITC data was performed by Origin v 7.0 (Origin Lab, USA).

5.2.8 Fabrication of aptasensor

A gold disk electrode of 0.5 cm diameter was cleaned thoroughly by chemical, mechanical and electrochemical methods before fabrication of the aptasensor. It was dipped in freshly prepared piranha solution for 30 sec to remove any organic matter then it was mechanically polished using alumina powder and ultrasonicated for 5 min each in MQ water and ethanol to remove alumina particles. It was then electrochemically cleaned by performing 30 cycles of CV in 0.5 M H_2SO_4. The gold electrode was then dipped in DSP (dithiobis (succinimidyl propionate)) also known as Lomant's reagent (ThermoFisher Scientific) to form SAM layers of activated COO^- groups for 1 h at RT. The Au/DSP modified electrode was then consecutively washed with acetone, isopropanol and MQ to remove unreacted DSP molecules. 1 µM of B4 amine functionalized aptamer was heated at 90˚C and cooled in ice for 10 mins each after which

it was introduced to the Au/DSP modified gold electrode for 12 h. After aptamer binding the Au/DSP/B4 modified electrode was incubated with 1 % ethanolamine to block any unreacted COO^- groups for 15 mins at RT. The Au/DSP/B4 modified electrode was washed thoroughly to remove excess ethanolamine and then it was ready for use for following experiments.

5.2.9 Electrochemical analysis

Cyclic voltammetry (CV) and electrochemical impedance spectroscopy (EIS) measurements were performed on Zahner Zennium electrochemical workstation (Zahner-elektrik, Germany) in the potentiostat mode and a three-electrode configuration. Ag/AgCl (3 M NaCl), platinum wire (Pt) and Au/DSP/B4 modified electrode were used as reference, auxiliary and working electrodes, respectively. All the measurements were taken in the electrolyte solution containing 5 mM $K_3Fe(CN)_6/K_4Fe(CN)_6$ (1:1) and 0.1 M KCl in PBS. The EIS measurements were performed within 100 kHz to 100 mHz and the amplitude of the alternate voltage was 10 mV. All the experiments were performed at RT in a dust free condition. The current study with human samples was approved by the Institute Human Ethics Committee (IHEC) of the Indian Institute of Technology Guwahati, India.

5.3 Results and discussion

5.3.1 Selection of aptamers

A single stranded DNA library (~10^{12}–10^{15}) conferred by a 40 mer long random sequence flanked by constant primer binding regions for amplification, was used as a starting pool for SELEX (Figure 5.1). As a target binding support, PVDF membrane was used to immobilize HRP-II to perform the SELEX. The PVDF membrane is known to immobilize proteins by various combination of hydrophobic and dipole interactions

(Matsudaira 1987). Also, proteins interact with the membrane by electrostatic interactions in a non-uniform fashion (Ahmad *et al*., 2016) thus increasing the possibility of a wider array of ‘‘aptatopes’’ in the cycles as compared to using chemical linkers for binding the protein to the membrane surface. AFM study revealed that the bare PVDF membrane was uneven with average roughness factor of 0.0918. The surface morphology of the membrane was shifted to more coarse state following its interactions with the protein and ssDNA with average roughness factor of 0.1244 and 0.1449, respectively. The thickness of the membrane was increased from ~250 nm for the bare membrane to ~400-500 nm for the protein immobilized one, and finally it was reached to ~500-600 nm upon topping the immobilized proteins with the aptamers (Figure 5.2). Counter selection steps against uncoated PVDF membrane were included to eliminate the enrichment of non-specific aptamer candidates against HRP-II. The evolved pool of aptamers generated following each positive cycle was analysed by gel electrophoresis. A gradual enrichment of aptamer candidates occurring at each subsequent cycle was observed (Figure 5.3 A). A total of 33 positive clones selected from the blue white screening were then further screened by using PCR as shown in figure 5.4 to a total of 23 recombinant clones that carried the enriched aptamer inserts. The recombinant clones were picked up and cultured to acquire plasmids containing aptamer amplicons for sequencing. The sequencing results showed that out of 23 colonies only 18 colonies contained the amplicon whereas, the remaining five colonies did not carry the amplicon (Figure 5.3 B). The correct sequences were then analysed by Clustal X2 and revealed that two sequences (Table 5.1) were enriched at levels more than the other 16 sequences. Analysis of the alignment results did not display any strong conserved regions across these sequences.

Table 5.1: Sequence profile of the aptamer candidates enriched by SELEX.

Serial no.	Sequence (5'-3')	Assigned Aptamer name
1	CACCTAATACGACTCACTATAGCGGATCCGAATCAGC AGAAACAAGAATCGACTGTCTTCTCGATAGGGGGCTG GCTCGAACAAGCTTGC	B3
2	CACCTAATACGACTCACTATAGCGGATCCGAACGGCA ATTAGCCCCCTTTCCTCCTGGCCTCGGTCGGCGGCTGG CTCGAACAAGCTTGC	B4

5.3.2 Study of aptamer-protein interactions

The secondary structure prediction of the four aptamers was carried out using the Mfold web server (Zuker 2003). The free energy folding for B3 and B4 were found to be - 8.34 and - 20.40 kcal.mole^{-1}, respectively indicating higher stability of the secondary structure of B4. The ionic conditions were chosen as 50 mM NaCl and 2.5 mM $MgCl_2$ and temperature was fixed at 25 ˚C. To further study the aptamers and their conformations after binding to HRP-II, CD analyses were performed. The CD spectra of the two selected aptamers displayed a negative band at 245 nm and a positive band at around 260 - 280 nm, which is the characteristic of the B-form of DNA due to multiplicity of π-π* transitions (Figure 5.5A for B4) (Kypr*et al*., 2009). When the aptamers were allowed to bind to HRP-II, the ellipticity of only B4 was significantly perturbed as evident from the increase its peak intensity at ~ 275 nm. The peak intensity was increased with the increasing concentration of HRP-II and eventually the intensity was stabilized as evident

from figure 5.5 B (un-normalized). The intensity of the positive CD band of B-DNA at 275 nm increased as a consequence of natural modification of DNA (Chang *et al*., 2012). Unlike B4, no stark changes of CD spectral pattern of B3 were observed when it was treated with HRP-II.

The binding affinity of the aptamers were further analysed by ITC where aptamers were titrated to the protein in the same buffer. The aptamer, B4 generated a rational response to the target (Figure 5.6 A), whereas, the B3 candidate did not produce any tangible response (Data not shown). The isothermal binding curve for B4 was fitted well into the three sites sequential binding model with good statistics for parameters as shown in Figure. 5.6 A (inset). Sequential binding sites in general is a model for n ligand binding sites and can correspond to sites that might be identical or non-identical, independent or cooperative. As suggested for unstructured proteins (Majava *et al.,* 2008), HRP-II has been assumed to follow similar positive cooperative binding model. The initial binding enthalpy for K1 is not high but changes the structure of the protein and makes a second high-affinity specific binding event (K2). The third binding enthalpy is quite low which could be due to electrostatic interactions between the protein and aptamer. Therefore we consider the lowest K_d (~ 1.32 µM) as the binding constant of the aptamers (Table 5.2). The ITC data for non-specific proteins and buffer gave no significant enthalpy change suggesting the aptamer B4 is highly specific to HRP-II (Figure. 5.6 B, C). Based on the CD and ITC results generated for the aptamers candidates, B4 was carried forward for biosensing applications described in the next sections.

Table 5.2: Kinetic parameters obtained from ITC

Name	Association constants (M^{-1})	K_d (M)
K_1	3.00 X 10^5	3.33 X 10^{-6}
K_2	7.52 X 10^5	1.32 X 10^{-6}
K_3	2.75 X 10^5	3.6 X 10^{-6}

5.3.3 Fabrication and characterisation of electrochemical aptasensor

A cleaned gold electrode was dipped into DSP solution and activated by sodium borohydride to form a self-assembled monolayer (SAM) of DSP on the gold electrode surface through thiol bonds. The activated COO^- groups of SAM DSP were then conjugated to the aptamer B4 through its functionalized amine groups as shown in figure 5.7. To examine the formation of SAM layers and B4 binding, CV was performed at 100 $mV.S^{-1}$ by tracking the charge transfer of $K_3Fe(CN)_6/K_4Fe(CN)_6$ system (Figure 5.8 A). The redox peak currents for both oxidation and reduction reactions were decreased with increasing molecular layers over the electrode surface in the order Au < Au/DSP < Au/DSP/B4 owing to the parallel growth of the charge transfer resistance caused by the increasing layers on the electrode surface. There is also corresponding shift of the cathodic peak potentials towards the lower potential direction indicating that the redox species is getting harder to reduce as the layers grown (Figure 5.8 B). The reason could be attributed to the interference of charge transfer on the electrode surface caused by the negatively charged functional groups of DSP and ssDNA aptamer.

5.3.4 Response characteristics of the aptasensor

Impedimetric method was adopted for the detection of HRP-II using the aptamers modified electrode as it is one of the best sensitive techniques for studying the adsorption processes on the electrode surface. It helps to monitor charge transfer resistance which critically depends on the composition of the electrode surface. The electrochemical response against HRP-II was carried out by incubating increasing amount of HRP-II in 50 mM HEPES buffer pH 7.4. The impedance was decreased with increasing the target concentration in the electrolyte as visible from the Nyquist plots (Figure 5.9 A). A significant decrease in the impedance signal was observed between 0.5 pM to 1 nM of HRP-II. The obtained Nyquist plots were fitted to Randles–Ershler type equivalent circuit, (Figure 5.9 A, inset), where R_s is the solution resistance, Q1 is the constant phase element (CPE) which is a non-ideal capacitance to reflect the double layer capacitance and Q2 is the Warburg impedance. The results of the fitting when plotted generated a response curve (Figure 5.9 B). The linear region of the response curve was translated to a standard calibration curve with a high correlation co-efficient (R^2 = 0.99). The measurement offered a dynamic range of 1 pM–500 pM. An LOD of ~3.15 pM was calculated by using the relation, 3 × Sy/b, where Sy is the standard deviation (SD) of y-intercept, and b is the slope of the linear curve. With the discerned LOD the developed aptasensor could thus be applied to detect the target HRP-II in the infected malaria patients with high sensitivity. It is known that aptamers specifically binds to its target following conformation change guided by its energetically favourable folding process (Kimoto *et al*., 2013) The folding of B4 on HRP-II protein during their specific interactions likely to lower the exposed negative charge of the aptamer layers that facilitates the charge transfer on the electrode and thus, reduced the R_{CT} values (Elshafey *et al*.,2015). The ΔR_{CT} values were calculated by $R_{CT\ of\ blank} - R_{CT\ of\ sample}$ and then plotted

against $\log_{10}$ concentration of HRP-II as shown in figure 5.9 B. The applicability of the aptasensor to detect HRP-II in mimicked real sample was explored by spiking 500 pM HRP-II in 200 X diluted serum. The serum was obtained from a healthy volunteer and diluted accordingly. The ΔR_{ct} (%) was calculated by the following equation $\Delta Rct\ (\%) = (Rct_{(Blank)} - Rct_{(sample)} / Rct_{(Blank)}) * 100$. For bare serum and HRP-II spiked serum sample the corresponding signal change ware 2.3 % and 26 %. The results indicated that the developed aptasensor is highly sensitive as it could detect the target even after 200-fold dilution of the serum sample (Figure 5.10).

There has been no report on the use of aptamer as biorecognition element to fabricate malaria biosensor for detection of HRP-II. A plethora of HRP-II based sensors is available, which however, rely mostly on antibody (Sharma *et al*., 2008; Sharma *et al*., 2011; Castilho *et al*.,2011; Brince *et al*., 2016; Dutta *et al*.,2017 a; Dutta *et al*., 2017 b) and chemical techniques (Chakma *et al*., 2016) as the sensing systems. Our underlying motivation for substituting antibody with other recognition elements in the sensor platforms for malaria detection has already been explained elsewhere. An optical sensor developed by us for detecting HRP-II following a chemical principle was an impressive feat from the point of sensitivity (Gulka *et al*., 2015). However, when the diagnosis warrants high specificity and sensitivity of the sensors for the cases like, asymptotic malaria, the biological recognition elements are widely recognized as superior candidates. The aptamers imbibe the properties of the biological nucleic acids due to their common building blocks (nucleotides). Moreover, on demand, these recognition elements can be further chemically modified to enhance their specificity (Ni *et al*., 2017)

5.4 Conclusions

A specific ssDNA aptamer against HRP-II could be generated following a systematic molecular approach starting from SELEX, cloning and screening of the enriched candidates and then finally, validated the specificity by analysing the binding affinity. The aptamer was immobilized on a gold electrode surface following a rational chemical approach to maintain its natural flexibility for unrestricted binding to the target. A comprehensive scheme on the fabrication of the aptasensor is shown in figure 5.7. The developed aptasensor was found to be suitable for an impedimetric measurement of signal generated from its binding with the target HRP-II protein as no additional label is essential for this highly sensitive technique. The Faradic impedance technique we used here could detect HRP-II down to a picomolar level which can detect asymptomatic malaria patients. In case of asymptomatic malaria patients plasma HRP-II concentrations ranged between 0.2 and 121 $ng.mL^{-1}$ (Manning *et al*., 2017). The specificity of the developed aptasensor towards HRP-II in the presence of blood serum was also validated. This highly sensitive aptamer based electrochemical sensor thus has the potential to be developed as a viable product for specific diagnosis of malaria caused by *P. falciparum* at the pathophysiological concentration of HRP-II.

Figures

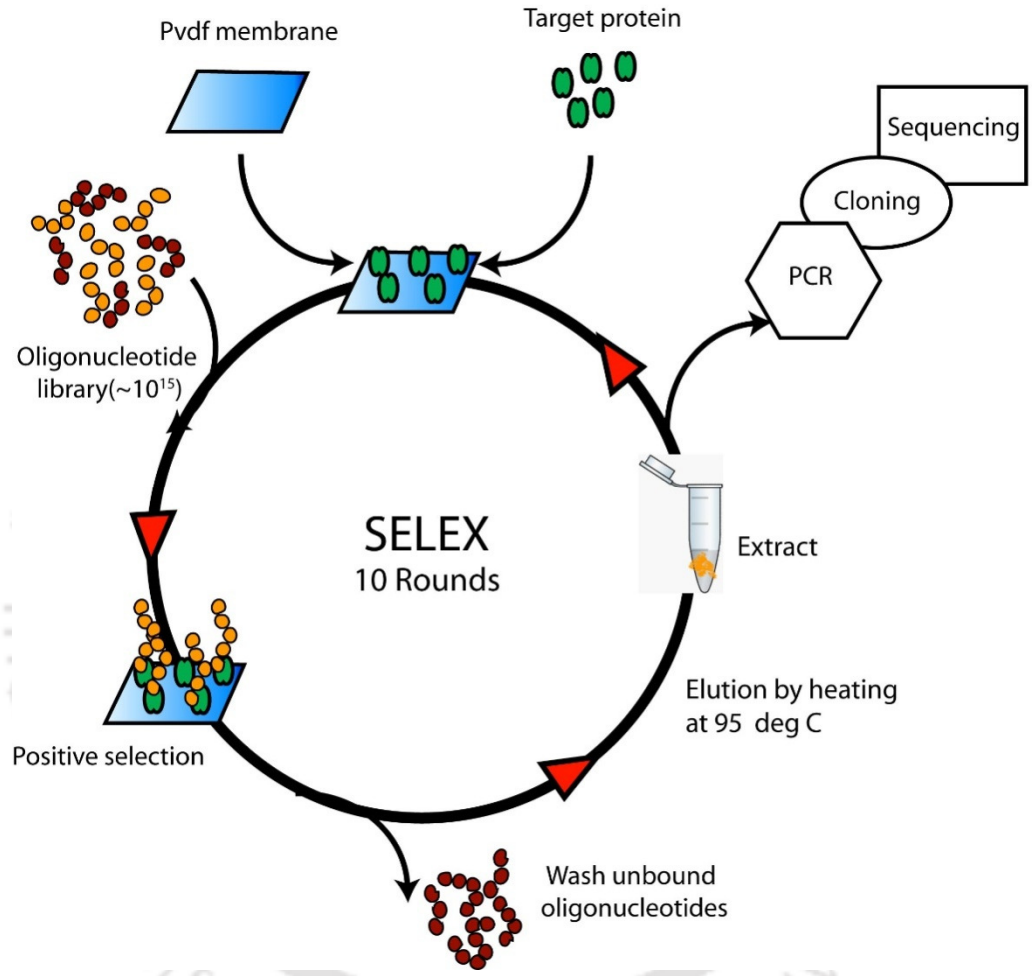

Figure. 5.1: Schematic representation of the SELEX process

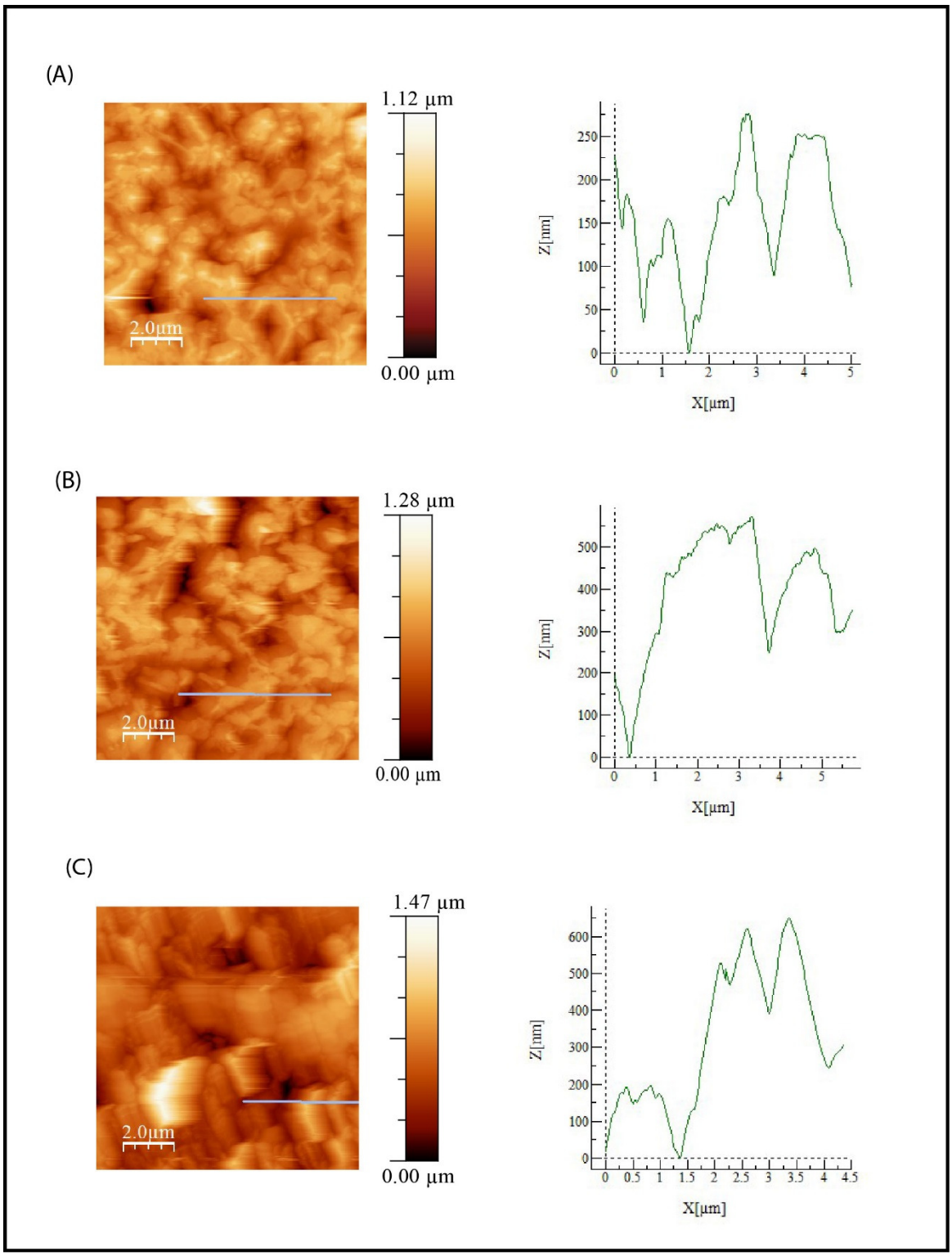

Figure 5.2: AFM topography and height profile of (A) bare PVDF membrane; (B) HRP-II immobilized on PVDF membrane; (C) after interaction with aptamer library with HRP-II treated PVDF membrane

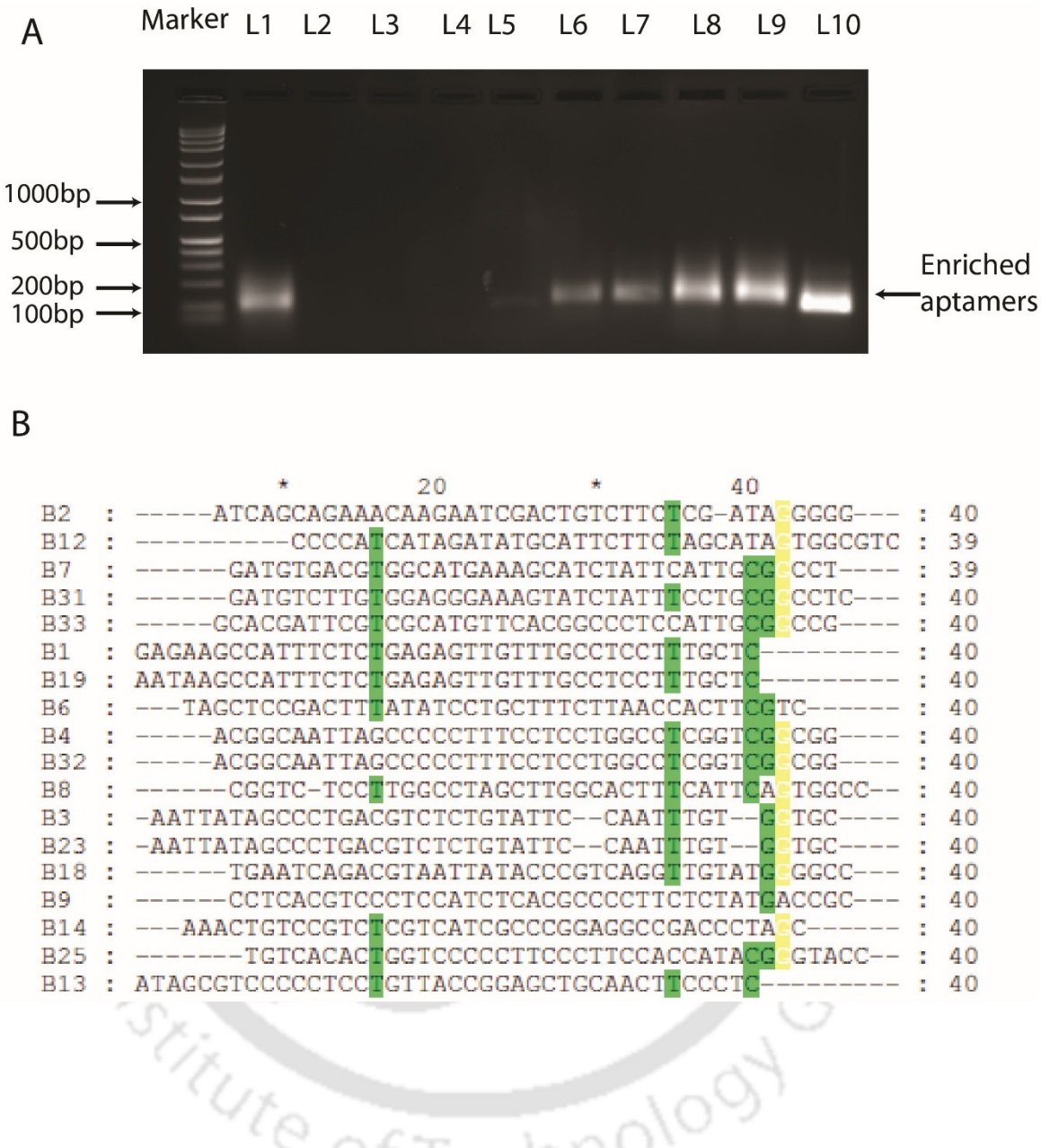

Figure 5.3: (A) PCR amplification of enriched aptamer population at the end of each positive cycle. L1: DNA marker, L2-L11: Amplified population after cycles 1-10, respectively, observed on a 2 % agarose gel. (B) Multiple sequence alignment of the random regions of selected candidates after SELEX process. Green and yellow coloured regions represent 70 % and 50 % sequence similarity, respectively

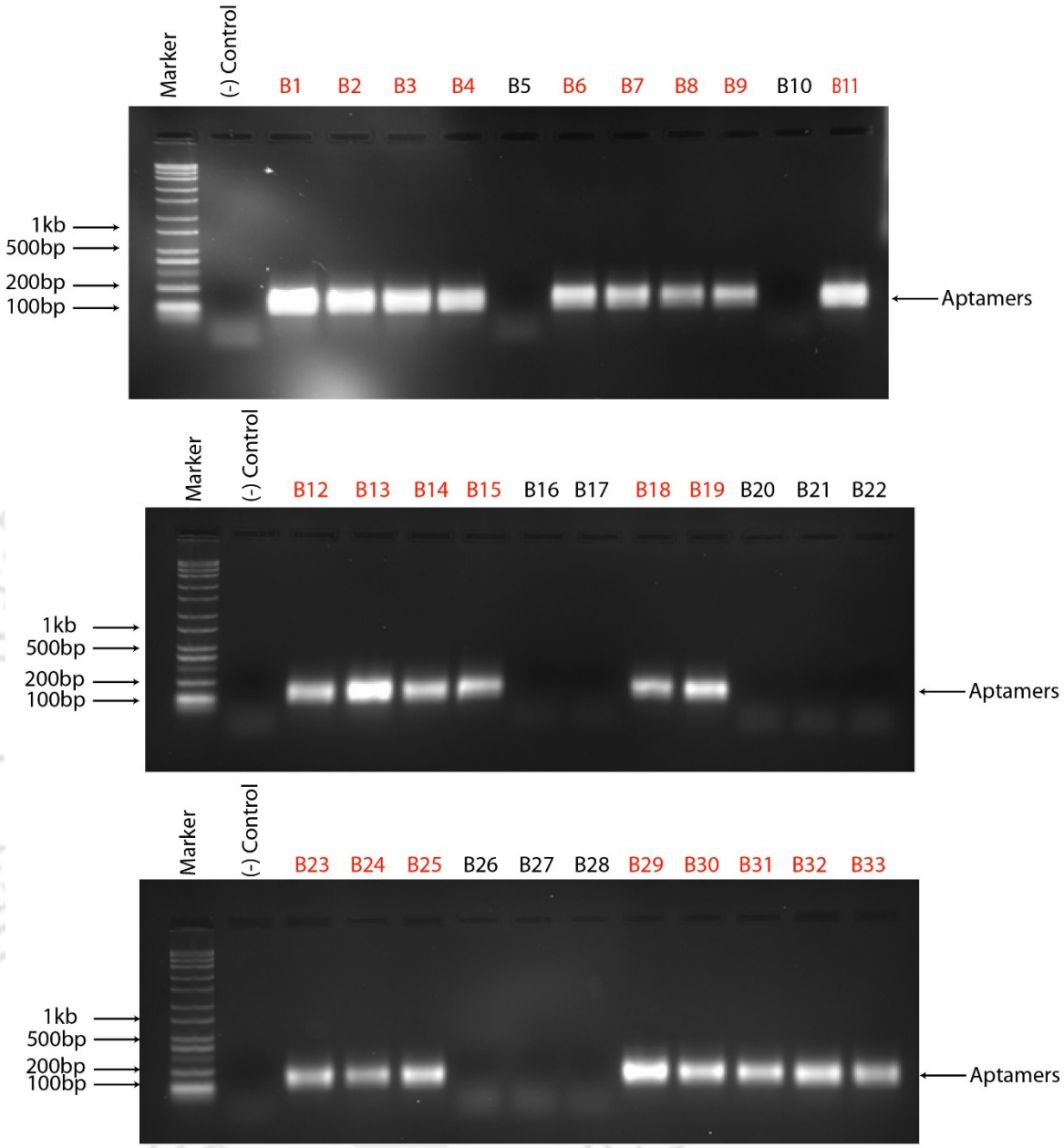

Figure 5.4: Screening of 33 white colonies by PCR. Lane 1: DNA marker; Lane 2: negative control, representing the amplification product from a blue colony. Other lanes are labelled as name of the colony screened, with positive colonies written in red.

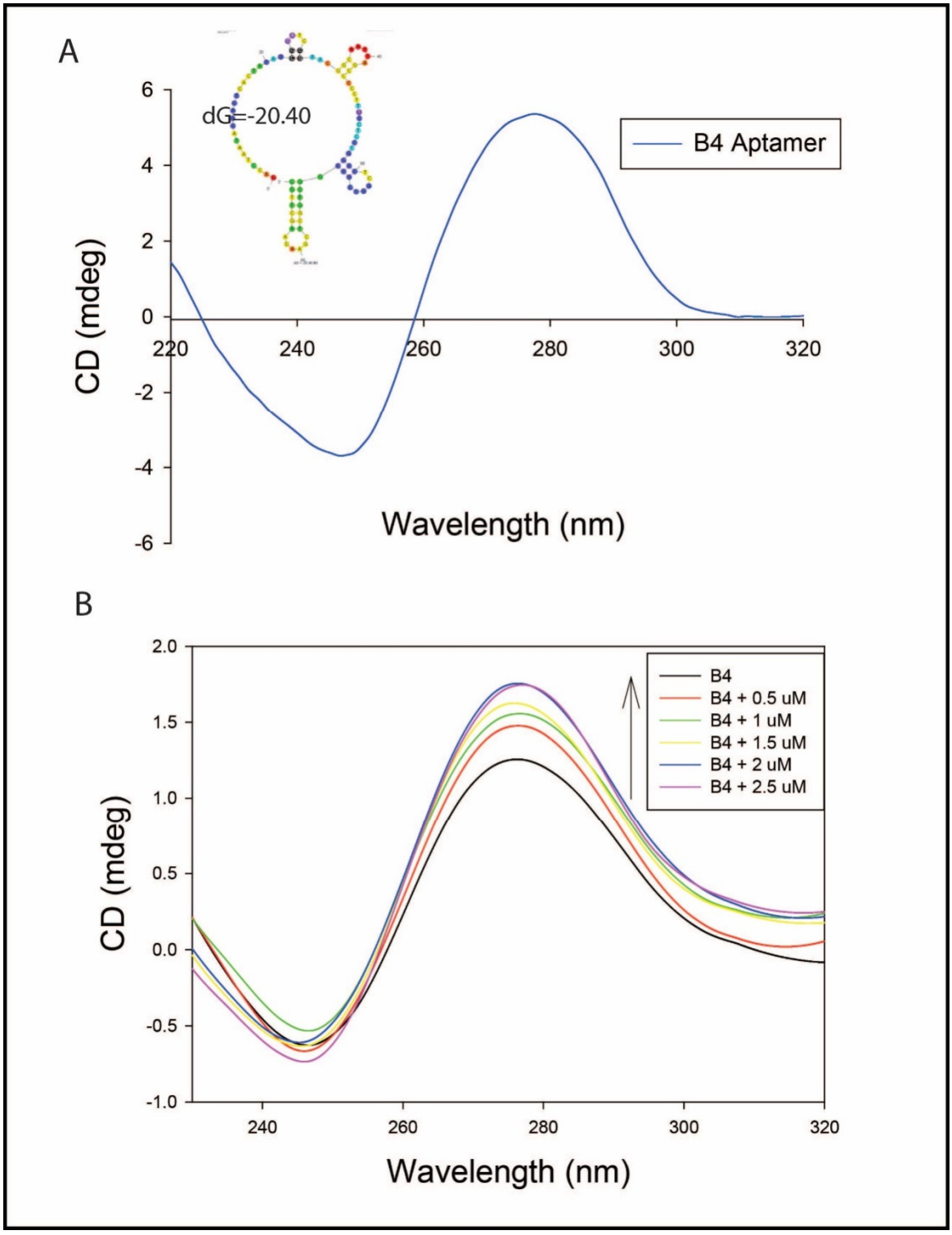

Figure 5.5: (A) CD spectra of B4 aptamer with (inset) secondary structure of B4 predicted by Mfold (B) CD Spectra of B4 with different concentrations of HRP-II. Spectra were recorded in 50 mM HEPES buffer, pH 7.4.

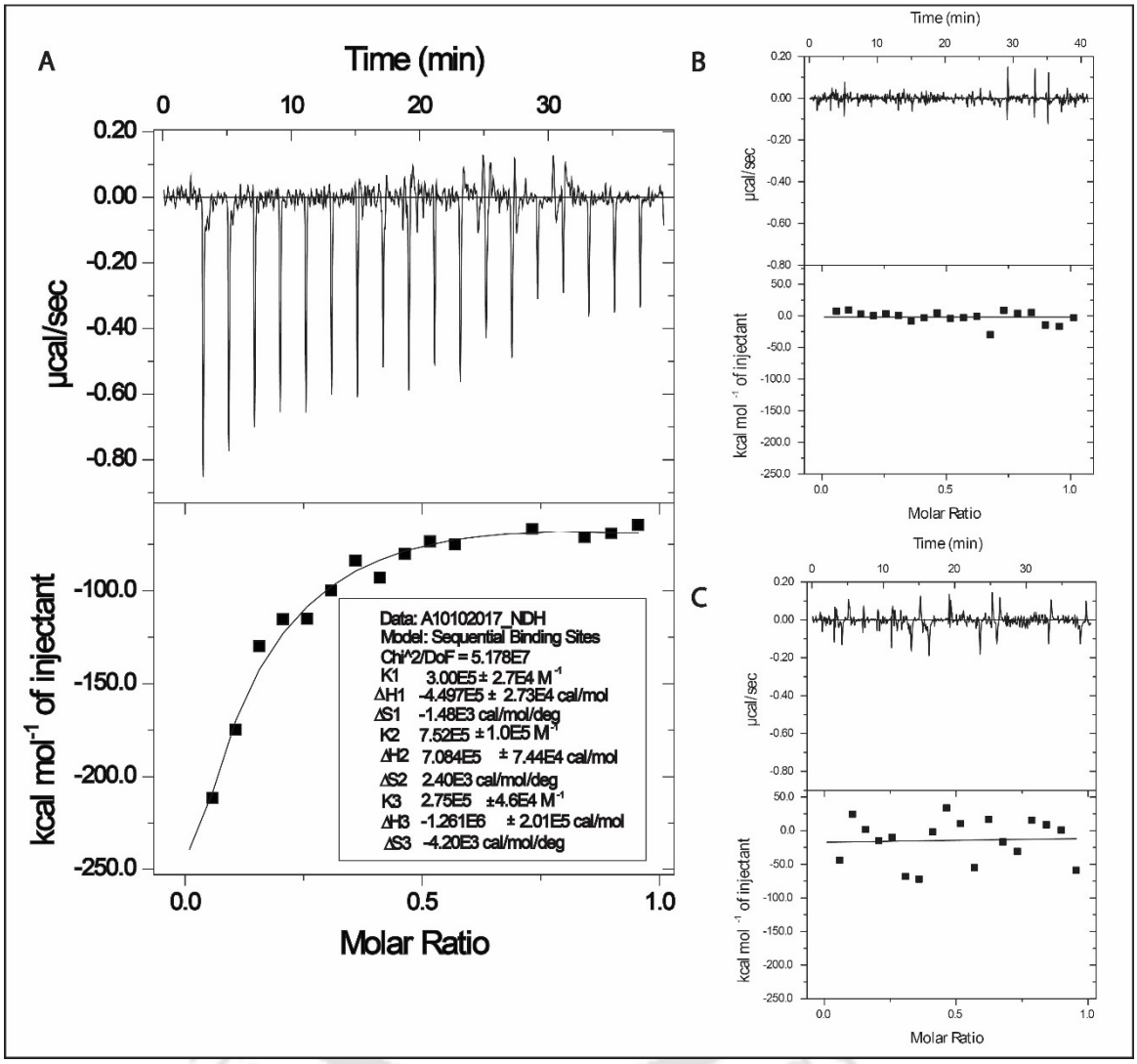

Figure 5.6: Isothermal binding curve for 20 µM B4 titrated into (A) 4 µM HRP-II (B) buffer only and (C) 4 µM HSA. All the experiments were performed in 50 mM HEPES buffer pH 7.4. Raw heat of binding curve is shown in the top part and fitted binding isotherm curve is shown in the bottom part of the graphs.

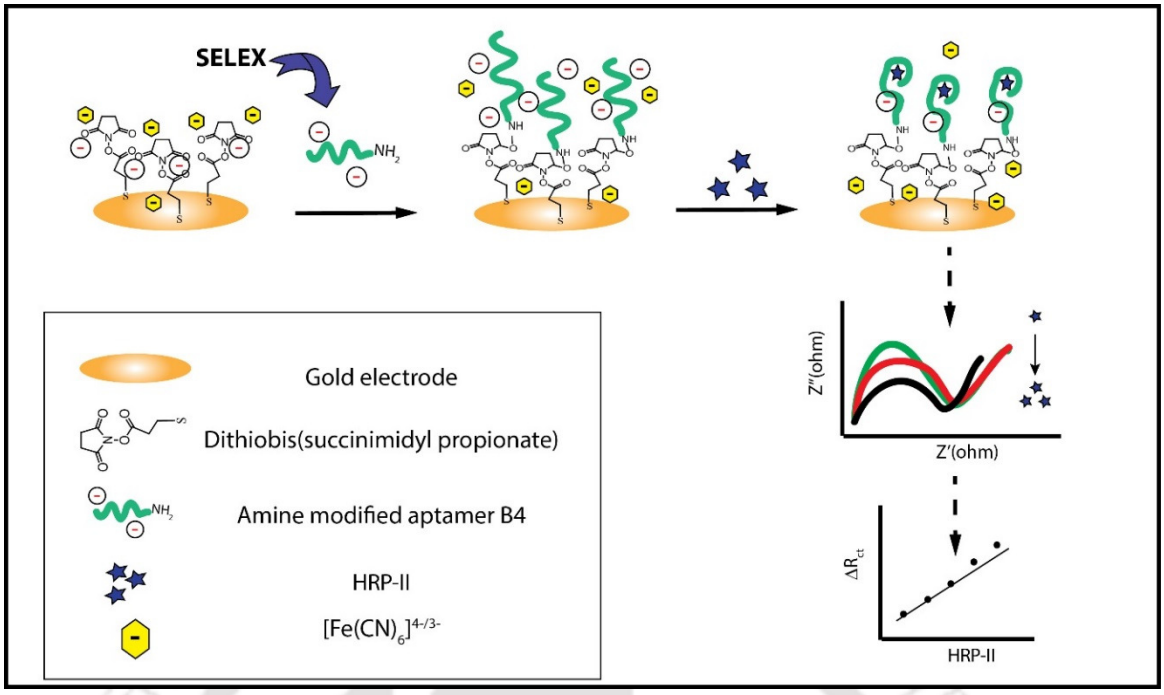

Figure 5.7: Schematic representation on the fabrication of the aptasensor and its application for the detection of HRP-II.

A

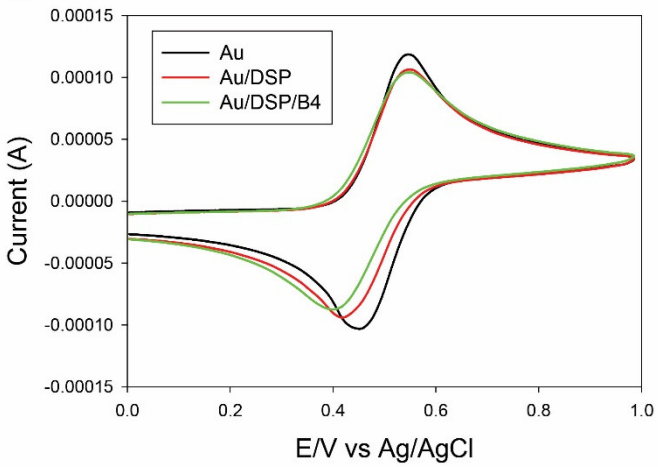

B

Electrode	Epa (V)	Epc (V)	Ipa(μA)	Ipa(μA)
Au	0.557	0.437	117	100
Au/DSP	0.557	0.418	106	94
Au/DSP/B4	0.557	0.398	104	88

Figure 5.8: (A) CV spectra of gold electrodes at different fabrication steps (B) Potential and current profiles discerned from the CV spectra of the gold electrodes at different fabrication steps.

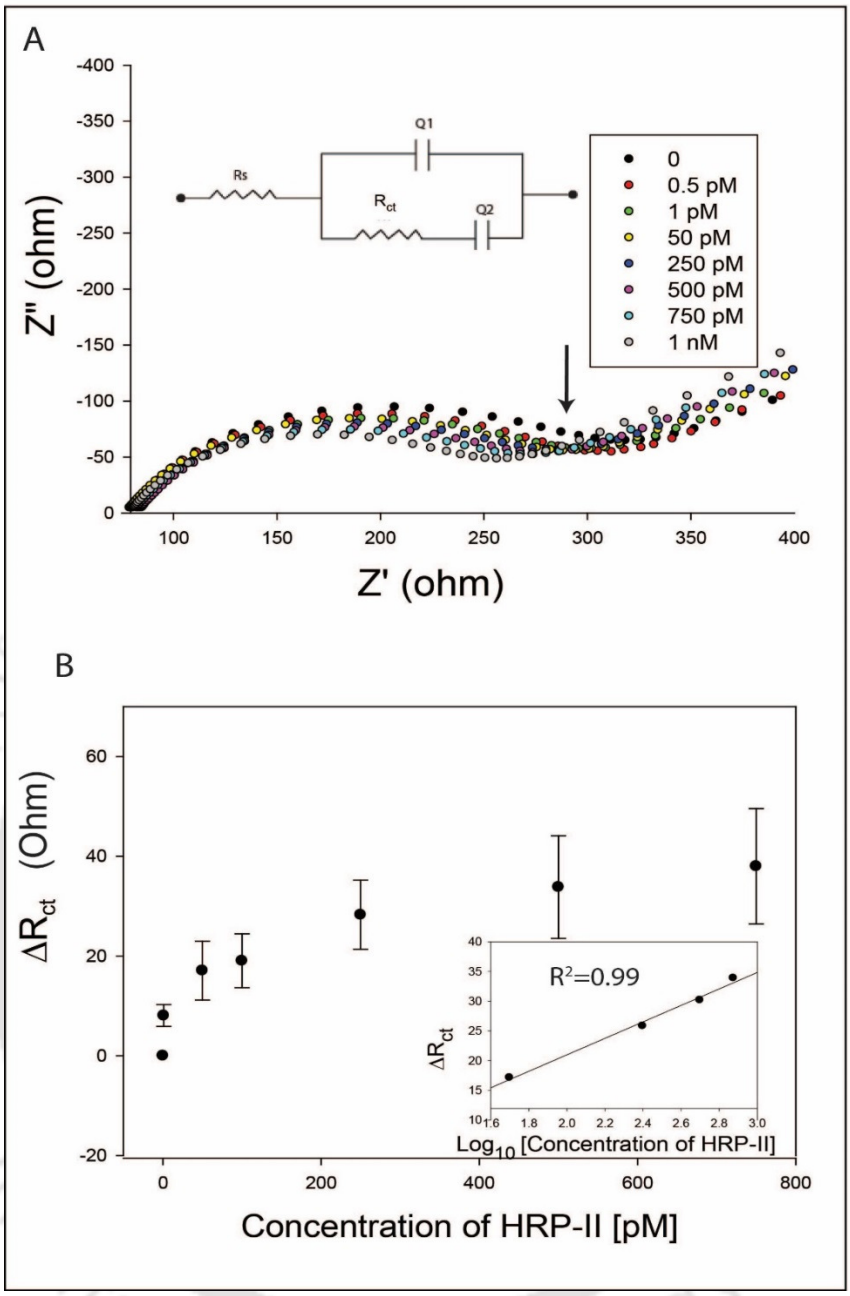

Figure 5.9: (A) Nyquist plots on the response of Au/DSP/B4 electrode towards HRP-II concentrations. Equivalent Circuit diagram is shown in the inset. (B) Response curve of ΔR_{ct} vs increasing HRP-II concentration. Each data point is an average of at least three individual experiments. Error bars indicate the SD.

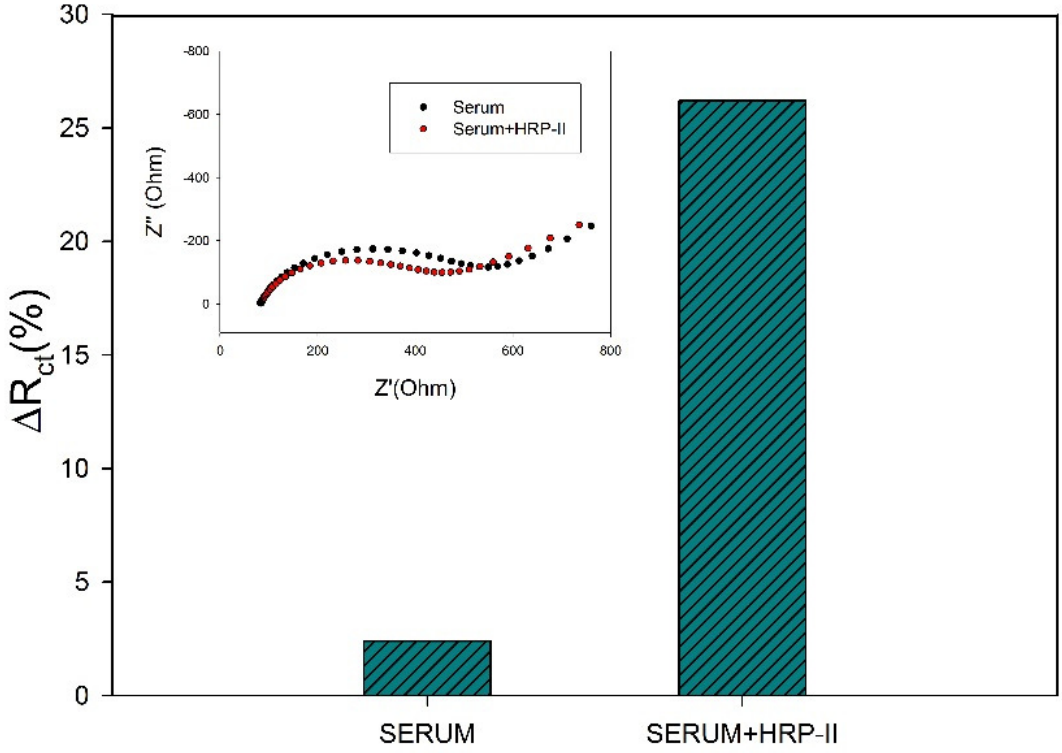

Figure 5.10: The performance of the developed aptasensor when challenged with bare serum and HRP-II spiked serum.

Conclusion and future directions of research

Conclusion and future directions of research

The major goal defined for the present work was to develop an efficient malaria detection system using *P.falciparum* HRP-II as the target biomarker. Our main concern was to explore a non-labile probe as an alternative to commonly used antibody for malaria detection system Therefore we looked into different non-labile probes that have not been reported so far. To achieve this goal we first expressed and purified the target protein (HRP-II) in our laboratory settings using molecular biology techniques and performed relevant experiments to confirm its purity and structural integrity. After successfully preparing the target protein, three independent proof-of-concepts for detecting HRP-II were successively explored: (i) Development of an indicator displacement based detection of malaria targeting HRP-II as biomarker for application in point-of-care settings, (ii) Quantitative detection of histidine-rich proteins using silver nanoparticle-based sensitive competitive binding assay at last (iii) Development of electrochemical impedance spectroscopy based aptasensor for malaria using HRP-II as target.

At first a colorimetric dye based assay which can detect HRP-II in solution as well as on a paper platform was interested. The murexide dye, which has the ability to form complexes with metal ions, was used for the assay (Sun et al., 2012). The assay which was based on competitive displacement of Ni^{2+} dye from the murexide-Ni^{2+} complex could detect HRP-II in a very broad

dynamic range. This offered an advantage of detecting malaria at high parasitaemia and to avoid false positive results due to prozone effect. The experiments were performed with increasing concentration of HRP-II and discerned the binding constants from the data. The specificity of the detection system was found to be high when compared to the analysis results of the non-specific target HSA, which is abundantly present in the blood serum. Additionally, the interference studies of the serum were performed by spiking the target protein in serum obtained from healthy volunteers. The results validated the potential of the method to be used for real blood serum samples. Further we upgraded the same detection system to a cheap paper based platform. The platform was prepared by modifying the ink cartridge to print hydrophobic microfluidic channels on chromatography paper using a deskjet printer. The paper platform so prepared was designed to be portable, cheap and amenable to perform multiple experiments simultaneously. Interestingly the sensitivity of the system was enhanced in the paper based format. Moreover, the detection sensitivity of the system could be enhanced to ascertain on demand such as, for early detection of malaria by simply increasing the pH of the reaction mixture from physiological state up to ~9 for low parasitaemia detection. Hence, this method would be suitable to reduce false negative results due to prozone effect at high concentration of HRP-II and cross contamination with other antibodies. Thus, there is a great scope of using the present detection system as an additional test along with the current RDTs to eliminate false negative results in the case of patients with high parasitaemia and patients suffering from auto immune diseases.

In the second proof of concept we used GS-AgNPS as a colorimetric probe to detect HisRPs by competitive binding event. Nanomaterials were used to enhance the sensitivity of detection systems. GS-AgNPs gives very sharp SPR signal to any event of aggregation caused by the target molecules. The GS-AgNPs competes with HisRPs to bind to Ni^{2+} and causes change in signal with aggregation as it binds to more Ni^{2+}. As the concentration of HisRPs increases the

extent of GS-AgNPs decreases which can be tracked spectrophotometrically. We validated this system with various proteins that had varying amount of histidine residues in different sequence. Additionally, the method was tested on HRP-II and showed sensitivity to as low as ~10 pM. The method also offerd to detect HRP-II in yes/no format following visual colorimetric signal and detects HRP-II in blood serum within 30 min at a low background noise (~4.4 %) to detect malaria. This method was successful in enhancing the sensitivity of HRP-II detection from the previous method due to the use of nanomaterials. Another great potential of this system found was its ability to quantitatively detect histidine tagged recombinant proteins in the laboratory

Though the aforementioned methods were fairly specific there was still scope for improvement since the systems were developed on the basis of histidine binding hence, there can be non-specific interactions from unknown proteins which have similar composition of histidine residues as in HRP-II. Therefore we moved forward to develop an aptasensor for which a novel aptamer was selected by the method of SELEX. Aptamers were generated against HRP-II, followed by TA cloning, blue white screening and sequencing. Finally a specific aptamer was identified based on computational and CD studies. The binding constant of B4 was calculated from ITC experiments. After successful screening of the aptamer B4 which is specific against HRP-II an aptasensor for an electrochemical impedance spectroscopy was constructed. The aptamer was immobilized on a gold electrode surface following a rational chemical approach to maintain its natural flexibility for unrestricted binding with the target and for reproducible fabrications of the aptasensor. The developed aptasensor was found to be suitable for an impedimetric measurement of signal generated from its binding with the target HRP-II protein and could detect the target protein down to a picomolar level. The specificity of the developed aptasensor towards HRP-II in the presence of blood serum was also validated.

Finally, we attempted to evaluate the different sensor platforms developed in this work by comparing the performance factors as shown in table C1.

Table C.1: Comparison of the performance of the developed analytical/biosensing methods mentioned in this thesis

Name of the method	**Detection probe**	**Detection platform**	**Sensitivity**	**Specificity**	**Dynamic range**	**Response time**	**Preparation time**
IDA in solution	Murexide dye	96 well plate	53 nM	Moderate	1 pM-3µM	10 mins	30 mins
Nanoparticles based competitive assay	GS-AgNPs	96 well plate	30 nM	Moderate	10 pM-1.2 µM	15 mins	5 h
Impedimetric Aptasensor	B4 Aptamer	Gold electrode	3.15 pM	High	1-500 pM	10 mins	24 h

As seen from the table C.1 the sensitivity achieved in terms of LOD by the optical methods namely IDA method and GS-AgNPs based competitive assay were in the clinically relevant range. However, the impedimetric aptasensor showed the lowest LOD which can be used for detecting malaria even in asymptomatic patients. The response time required for all the methods developed were comparably fast and could be used for POC settings. The impedimetric aptasensor had the highest preparation time because it required a lot of time in preparing the modified electrode which is one of its limitation. Though the selectivity and specificity of the optical methods were demonstrated over control proteins, there is a possibility that it can react with proteins that have high and contiguous His residues in the sequences thus making it less attractive. However the optical methods are very cheap, especially the paper based microfluidic method, which

can cost ~0.07 U.S. dollars including the cost of the reagents. The paper based platforms can be further improved by incorporating aptamer and dye to enhance its specificity.

The investigations in this thesis, entails a detailed study on the development of various detection methods for malaria biomarker HRP-II without the use of antibody. By doing so we were successful to improve the stability and reduce the cost as compared to RDTs. This study gives an idea on how different detection probes can be used as an alternative to antibodies to develop potential biosensors using different low cost platforms which can be used in low resource settings.

Future direction of research

The work presented over here enlists few potential biosensors/ methods as alternative detection strategies for malaria diagnosis. However, these strategies needs to be explored further to convert them into viable diagnostic products of commercial importance. Therefore, we need to address few critical points that can be further explored to project our study into commercial sensors. (i) In case of the paper based colorimetric platform some studies regarding covalent binding of dye to paper substrate should be done to reduce coffee ring effect and increase the sensitivity of the system. Also detailed study to digitalize the optical response in pixel intensity by simple device such as a phone and software may be done to increase its potential in a commercial settings. (ii) Secondly studies on enhancing the stability of GS-AgNPs which were employed for the corresponding colorimetric detection of malaria need to perform. Further this developed method should be translated into a low cost biocompatible sensor surface such as, paper and PDMS complying the ASSURED (Affordable, Sensitive, Specific, User-friendly, Rapid, Equipment free, Deliverable) mandate of WHO for expediency in the low income countries. (iii) Lastly we need to understand the exact mechanism of interaction between the aptamer and randomly coiled protein HRP-II. Till now no data on x-

ray crystal structure of HRP-II has been elucidated. There is a scope to solve the crystal structure of aptamer- protein complex to understand its exact mechanism of interaction. Furthermore, the stability studies of the aptamer following modifications with a suitable by various signal molecules by conserving its binding affinity is another area of focus to develop a low cost simple sensor device for detection of malaria.

Bibliography

Bibliography

Abeku, T., Kristan, M., Jones, C., Beard, J., Mueller, D., et al. Determinants of the accuracy of rapid diagnostic tests in malaria case management: evidence from low and moderate transmission settings in the East African highlands. Malar. J. 7, 202, (2008).

Accardo, A., Laurent, S.A.L., Mazarguil, H., Meyer, M., Robert, A., Meunier, B., Interaction of iron(II)-heme and artemisinin with a peptide mimic of Plasmodium falciparum HRP-II. J. Inorg. Biochem. 101, 1739–1747, (2007).

Adams, P.A., Egan, T.J., Ross, D.C., Silver, J., Marsh, P.J., The chemical mechanism of β-haematin formation studied by Mössbauer spectroscopy. Biochemical Journal, 318, 25–27, (1996).

Albertini, A., Lee, E., Coulibaly, S.O., Sleshi, M., Faye, B., Mationg, M.L., et al.. Malaria rapid diagnostic test transport and storage conditions in Burkina Faso, Senegal, Ethiopia and the Philippines. Malar. J. 11, 406, (2012).

Ameer, F.S., Varahagiri, S., Benza, D.W., Willett, D.R. Wen, Y., et al. Tuning Localized Surface Plasmon Resonance Wavelengths of Silver Nanoparticles by Mechanical Deformation , J. Phys. Chem. C. 120, 20886–20895, (2016)

Armah, H.B., Wilson, N.O., Sarfo, B.Y., Powell, M.D., Bond, V.C., et al. Cerebrospinal fluid and serum biomarkers of cerebral malaria mortality in Ghanaian children. Malar. J. 6, 147, (2007).

Avila, P.E., Kirchgatter, K., Brunialti, K.C.S., Oliveita, A.M., Siciliano, R.F., et al. Evaluation of a rapid dipstick test, Malar-CheckTM, for the diagnosis of *Plasmodium falciparum* malaria in Brazil. Rev Inst Med Trop Sao Paulo.44, 293–296, (2002)

Bae, D.R., Han, W.S., Lim, J.M., Kang, S., Lee, J.Y., Kang, D., Jung, J.H., Lysine-Functionalized Silver Nanoparticles for Visual Detection and Separation of Histidine and Histidine-Tagged Proteins. Langmuir. 26, 2181–2185, (2010)

Baker, J., McCarthy, J., Gatton, M., Kyle, D.E., Belizario, V., et al. Genetic diversity of Plasmodium falciparum histidine rich protein 2 (PfHRP2) and its effect on the performance of PfHRP2 based rapid diagnostic tests. J. Infect. Dis. 192, 870 –877, (2005).

Barbas III, F.C., Burton, R.D., Scott, K.J., Silverman, J.G., Quantitation of DNA and RNA, General Procedures, Appendix 3, Phage Display, Cold Spring Harbor Laboratory Press, Cold Spring Harbor, NY, USA, (2001).

Barlow, D.J., Thornton, J.M., Helix geometry in proteins. J. Mol. Biol. 201, 601–619, (1988).

Bartoloni, A., Zammarchi, L., Clinical Aspects of Uncomplicated and Severe Malaria. Mediterr J Hematol Infect Dis. 4, e2012026, (2012).

Bendezu, J., Rosas, A., Grande, T., Rodriguez, H., Llanos-Cuentas, A., et al. Field evaluation of a rapid diagnostic test (ParascreenTM) for malaria diagnosis in the Peruvian Amazon. Malar. J. 9, 154, (2010).

Bendrat, K., Berger, B.J., Cerami, A., Haem polymerization in malaria. Nature. 378, 138–139, (1995).

Benedetti, C.E., Kobarg, J., Pertinhez T.A., et al., Plasmodium falciparum histidine-rich protein II binds to actin, phosphatidylinositol 4,5-bisphosphate and erythrocyte ghosts in a pH-dependent manner and undergoes coil-to-helix transitions in anionic micelles. Mol. Biochem. Parasitol. 128, 157–166,(2003).

Bharti, P.K., Chandel, H.S., Ahmad, A., Krishna, S., Udhayakumar, V., Singh, N., Prevalence of pfhrp2 and/or pfhrp3 Gene Deletion in Plasmodium falciparum Population in Eight Highly Endemic States in India. PLoS ONE. 11, e0157949, (2016).

Biener, J., Wittstock, A., Baumann, T.F., Weissmüller, J., Bäumer, M., et al. Surface Chemistry in Nanoscale Materials. Materials, 2, 2404–2428, (2009).

Bjorkman, A. and Martensson, A., Risks and Benefits of Targeted Malaria Treatment Based on Rapid Diagnostic Test Results. Clin. Infect. Dis. 51, 512–514, (2010).

Bosshart, H. Heinzelmann, M., Endotoxin-neutralizing effects of histidine-rich peptides. FEBS Lett. 553, 135–140, (2003).

Bousema, T., Okell, L., Felger I., Drakeley C., Asymptomatic malaria infections: detectability, transmissibility and public health relevance. Nat Rev Microbiol. 12, 833-873, (2014).

Candiano, G., Bruschi, M., Musante, L., Santucci, L., Ghiggeri, G. M., et al. Blue silver: a very sensitive colloidal Coomassie G-250 staining for proteome analysis. Electrophoresis. 25, 1327-33 (2004).

Casals-Pascual, C., Idro, R., Gicheru, N., Gwer, S., Kitsao, B., et al. High levels of erythropoietin are associated with protection against neurological sequelae in African children with cerebral malaria. Proc Natl Acad Sci USA. 105, 2634 – 2639, (2008).

Centres for disease control and prevention (CDC) (http://www.cdc.gov/malaria/about/biology/parasites.html)

Chaikuad, A., Fairweather, V., Conners, R., Joseph-Horne, T., Turgut-Balik, D., et al. Structure of lactate dehydrogenase from Plasmodium vivax: Complexes with NADH and APADH. Biochem. 44, 16221–16228, (2005).

Chakma, B., Jain, P., Singh, N.K., Goswami, P., Development of an Indicator Displacement Based Detection of Malaria Targeting HRP-II as Biomarker for Application in Point-of- Care Settings. Anal.chem. 88, 10316–10321, (2016).

Chen, M.Z., Shi, L., Sullivan Jr., D.J., Haemoproteus and Schistosoma synthesize heme polymers similar to Plasmodium hemozoin and β-hematin. Mol. Biochem. Parasitol. 113, 1–8, (2001).

Cheung, Y.W., Kwok, J., Law, A., W., Watt, R., M., Kotaka, M., et al. Structural basis for discriminatory recognition of Plasmodium lactate dehydrogenase by a DNA aptamer PNAS. 110, 15967-72, (2013).

Chinnadayyala, S.R., Santhosh, M., Singh, N.K., Goswami, P., Alcohol oxidase protein mediated in-situ synthesized and stabilized gold nanoparticles for developing amperometric alcohol biosensor. Biosens. Bioelectron. 69, 155–161, (2015).

Chiodini, P.L., Bowers, K., Jorgensen, P., Barnwell, J.W., Grady, K.K., et al. The heat stability of Plasmodium lactate dehydrogenase-based and histidine-rich protein 2-based malaria rapid diagnostic tests. Trans. R. Soc. Trop. Med. Hyg. 101, 331–337, (2007).

Cho, E.J., Lee, J.W., Ellington, A.D., Applications of aptamers as sensors. Annu. Rev. Anal. Chem. 2, 241–264, (2009).

Choi, C.Y.H., Cerda, J.F., Hsiu-An, C., Babcock, G.T., Marletta, M.A., Spectroscopic characterization of the heme binding sites in Plasmodium falciparum histidine-rich protein 2. Biochemistry**.** 38, 16916–16924, (1999).

Choi, S., Lee, S.G., Lee, S.J., Kim, E., Rapid detection of 63-histidine-labeled recombinant proteins by immunochromatography using dye-labeled cellulose nanobeads. Biotechnol. Lett. 37, 627-632, (2015).

Chung, C.T., Niemela, S.L., Miller, R.H., One-step preparation of competent Escherichia coli: Transformation and storage of bacterial cells in the same solution. Proc. Natl. Acad. Sci. 86, 2172-2175 (1989).

Combes, V., Taylor, T.E., Juhan-Vague, I., Mège, J.L., Mwenechanya, J., et al. Circulating endothelial microparticles in malawian children with severe falciparum malaria complicated with coma. JAMA. 291, 2542–2544, (2004).

Conners, R., Schambach, F., Read, J., Cameron, A., Sessions, R.B., et al. Mapping the binding site for gossypol-like inhibitors of Plasmodium falciparum lactate dehydrogenase. Mol. Biochem. Parasitol. 142, 137–148, (2005).

Conroy, A., Lafferty, E., Lovegrove, F., Krudsood, S., Tangpukdee, N., et al. Whole blood angiopoietin-1 and -2 levels discriminate cerebral and severe (non-cerebral) malaria from uncomplicated malaria. Malar. J. 8,295, (2009).

Darain, F., Ban, C., Shim, Y.B., Development of a new and simple method for the etection of histidine-tagged proteins. Biosens. Bioelectron. 20, 857-863**,** (2004).

Davis, K.M., Bitting, A.L., Markwalter, C.F., Bauer, W.S., Wright, D.W., Iridium(III) Luminescent Probe for Detection of the Malarial Protein Biomarker Histidine Rich Protein-II. J. Vis. Exp. 22, 1–8, (2015).

de Oliveira, A.M., Skarbinski, J., Ouma, P.O., Kariuki, S., Barnwell, J.W., Performance of malaria rapid diagnostic tests as part of routine malaria case management in Kenya. Am. J. Trop. Med. Hyg. 80, 470 –474, (2009).

de Souza Castilho, M., Laube, T., Yamanaka, H., Alegret, S., Pividori, M.I., Magneto immunoassays for Plasmodium falciparum histidine rich protein 2 related to malaria based on magnetic nanoparticles. Anal. Chem. 83, 5570–5577, (2011).

Desakorn, V., Dondorp, A.M., Silamut, K., Pongtavornpinyo, W., Sahassananda, D., et al. Stage-dependent production and release of histidine-rich protein 2 by Plasmodium falciparum. Trans. R. Soc. Trop. Med. Hyg. 99, 517–524, (2005).

Dimeski, G., Interference testing. Clin. Biochem. Rev. 29 , 43–48. (2008)

Dirkzwager, R.M., Kinghorn, A.B., Richards, J.S., Tanner, J.A., APTEC: aptamer tethered enzyme capture as a novel rapid diagnostic test for malaria. Chem. Commun. 51, 4697-700, (2015).

Döbeli, H., Trzeciak, A., Gillessen, D., Matile, H., Srivastava, I.K., et al. Expression, purification, biochemical characterization and inhibition of recombinant Plasmodium falciparum aldolase. Mol Biochem Parasitol. 41, 259-68, (1990).

Dunn, C.R., Banfield, M.J., Barker, J.J., Higham, C.W., Moreton, K.M., The structure of lactate dehydrogenase from Plasmodium falciparum reveals a new target for anti-malarial design. Nat. Struct. Mol. Biol. 3, 912–915, (1996).

Dutta, G., Lillehoj, P.B., An ultrasensitive enzyme-free electrochemical immunosensor based on redox cycling amplification using methylene blue. Analyst. 142, 3492-3499, (2017).

Dutta, G., Nagarajan, S., Lapidus, L.J., Lillehoj, P.B., Enzyme-free electrochemical immunosensor based on methylene blue and the electro-oxidation of hydrazine on Pt nanoparticles. Biosens Bioelectron. 92, 372-377, (2017).

Eisen, D.P., Saul, A., Disappearance of pan-malarial antigen reactivity using the ICT Malaria P.f/ P.vTM kit parallels decline of patent parasitaemia as shown by microscopy. Trans. R. Soc. Trop. Med. Hyg. 94, 169–170, (2000).

Fakanya, W.M., Tothill, I.E., Detection of the inflammation biomarker C-reactive protein in serum samples: Towards an optimal biosensor formula. Biosensors. 4, 340–357, (2014).

Feldman, A.B., Progress toward rapid malaria screening based on mass spectrometry. Clin. Lab. Int. (2006).

Fitch, C.D., Cai G.Z., Chen, Y.F., Shoemaker, J.D., Involvement of lipids in ferriprotoporphyrin IX polymerization in malaria, Biochim. Biophys. Acta. 1454, 31-37, (1999).

Fleischer, B., Editorial: 100 years ago: Giemsa's solution for staining of plasmodia. Trop. Med. Int. Health. 9, 755–756, (2004).

Fogg, C., Twesigye, R., Batwala, V., Piola, P., Nabasumba, C., et al. Assessment of three new parasite lactate dehydrogenase (pan-pLDH) tests for diagnosis of uncomplicated malaria. Trans. R. Soc. Trop. Med. Hyg. 102, 25–31, (2008).

Forney, J.R., Magill, A.J., Wongsrichanalai, C., Sirichaisinthop, J., Bautista, C.T., et al. Malaria rapid diagnostic devices: performance characteristics of the ParaSight F device determined in a multisite field study. J. Clin. Microbiol. 39, 2884–2890, (2001).

Freyssinet, J.M., Cellular microparticles: what are they bad or good for? J. Thromb. Haemost. 1, 1655–1662, (2003).

Fry, M., Webb, E., Pudney, M., Effect of mitochondrial inhibitors on adenosinetri phosphate levels in Plasmodium falciparum. Comp. Biochem. Physiol. B. 96, 775–782, (1990).

Gamboa, D., Ho, M.F., Bendezu, J., Torres, K., Chiodini, P.L., et al. A large proportion of P. falciparum isolates in the amazon region of Peru lack pfhrp2 and pfhrp3: implications for malaria rapid diagnostic tests. PLoS ONE 5. e8091, (2010).

Geldert K.A., Zhang, X., Zhang, H., Lim, C.T., Highly Sensitive and Selective Aptamer Based Fluorescence Detection of a Malarial Biomarker Using Single-Layer MoS2 Nanosheets, ACS Sens. 1, 1315−1321, (2016).

Gibson, L.E., Wright, D.W., Sensitive Method for Biomolecule Detection Utilizing Signal Amplification with Porphyrin Nanoparticles. Anal. Chem. 88, 5928–5933, (2016).

Gikunoo, E., Abera, A., Woldesenbet, E., A Novel Carbon Nanofibers Grown on Glass Microballoons Immunosensor: A Tool for Early Diagnosis of Malaria, Sensors, 14, 14686-14699, (2014).

Gillet, P., Mori, M., Van Esbroeck, M., Van den Ende, J., Jacobs, J., Assessment of the prozone effect in malaria rapid diagnostic tests. Malar. J. 8, 271, (2009).

Goncalves, L., Subtil, A., de Oliveira, M.R., Rosario, V., Lee, P.W., et al. Bayesian latent class models in malaria diagnosis. PLoS ONE. 7, e40633, (2012).

Green, M.R., Sambrook, J., Molecular Cloning: a laboratory manual-4th ed. Cold Spring Harbour Laboratory Press, Cold Spring Harbour, New York, USA (2012).

Gulka, C.P., Swartz J.D., Trantum, J.R., Davis, K.M., Peak, C.M., et al. Coffee Rings as Low-Resource Diagnostics: Detection of the Malaria Biomarker Plasmodium falciparum Histidine-Rich Protein-II Using a Surface-Coupled Ring of Ni(II)NTA Gold-Plated Polystyrene Particles. ACS Appl. Mater. Interfaces. 6, 6257−6263, (2014).

Gulka, C.P., Swartz, J.D., Wright, D.W., Ni(II)NTA AuNPs as a low resource malarial diagnostic platform for the rapid colorimetric detection of Plasmodium falciparum Histidine- Rich Protein-2. Talanta. 135, 94–101, (2015).

Haest, C.W., Interactions between membrane skeleton proteins and the intrinsic domain of the erythrocyte membrane. Biochim. Biophys. Acta. 694, 331–352, (1982).

Hemben, A., Ashley, J., Tothill, I.E., Development of an Immunosensor for PfHRP 2 as a Biomarker for Malaria Detection. Biosensors. 7, 28-42. (2017).

Hendriksen, I.C.E., Mwanga-Amumpaire, J., von Seidlein, L., Mtove, G., White, L.J., et al. Diagnosing severe falciparum malaria in parasitaemic African children: A prospective evaluation of plasma PfHRP2 measurement. PLoS Med. 9, e1001297, (2012).

Howard, R.J., Uni, S., Aikawa, M., Aley, S.B., Leech, J.H., Secretion of a malarial histidine-rich protein (Pf HRP II) from Plasmodium falciparum infected erythrocytes. J. Cell Biol. 103, 1269–1277, (1986).

Hulka, B., Epidemiologic Studies Using Biological Markers - Issues for Epidemiologists. Cancer Epidemiol. Biomarkers Prev. 1, 13–19, (1991).

Hurdayal, R., Achilonu, I., Choveaux, D., Coetzer, T.H.T., Goldring, D.J.P., Antipeptide antibodies differentiate between plasmodial lactate dehydrogenases. Peptides. 31, 525–532, (2010).

Iqbal, J., Sher, A., Rab, A., Plasmodium falciparum histidine rich protein 2-based immunocapture diagnostic assay for malaria: cross-reactivity with rheumatoid factors. J. Clin. Microbiol. 38, 1184–1186, (2000).

Iqbal, J., Siddique, A., Jameel, M., Hira, P.R., Persistent histidine rich protein 2, parasite lactate dehydrogenase and pan malarial antigen reactivity after clearance of Plasmodium falciparum monoinfection. J. Clin. Microbiol. 42, 4237–4241, (2004).

Ireson, C.R., and Kelland, L.R., Discovery and development of anticancer aptamers. Mol. Cancer. Ther. 5, 2957-2962 (2006).

Jackson, K.E., Klonis, N., Ferguson, D.J.P., Adisa, A., Dogovski, C., Tilley, L., Food vacuole-associated lipid bodies and heterogeneous lipid environments in the malaria parasite Plasmodium falciparum, Mol. Microbiol. 54, 109–122, 2004.

Jain, P., Chakma, B., Goswami, P., Potential Biomarkers and Their Applications for Rapid and Reliable Detection of Malaria. Biomed Res. Int. 2014, 852645, (2014).

Jain, P., Chakma, B., Singh, N.K., Patra, S., Goswami, P., Aromatic surfactant as aggregating agent for aptamer-gold nanoparticle based detection of Plasmodium lactate dehydrogenase. Mol. Biotechnol. 58, 497–508, (2016).

Jelinek, T., Amsler, L., Grobusch, M., Nothdurft, H., Self-use of rapid tests for malaria diagnosis by tourists. The Lancet 354, 1609, (1999).

Jeon, W., Lee, S., Manjunatha, D., H., Ban, C., A colorimetric aptasensor for the diagnosis of malaria based on cationic polymers and gold nanoparticles. Anal. Biochem. 439, 11–16, (2013).

John, C.C., Panoskaltsis-Mortari, A., Opoka, R.O., Park, G.S., Orchard, P.J., et al. Cerebrospinal fluid cytokine levels and cognitive impairment in cerebral malaria. Am. J. Trop. Med. Hyg. 78, 198 – 205, (2008).

Jorgensen, P., Chanthap, L., Rebueno, A., Tsuyuoka, R., Bell, D., Malaria rapid diagnostic tests in tropical climates: the need for a cool chain. Am. J. Trop. Med. Hyg. 74, 750–754, (2006).

Kakoti, A., Siddiqui, M.F., Goswami, P., A low cost design and fabrication method for developing a leak proof paper based microfluidic device with customized test zone. Biomicrofluidics. 9, 502-524, (2015).

Kang J., Liu Y., Xie M.X., Li S., Jiang M., et al. Interactions of human serum albumin with chlorogenic acid and ferulic acid, Biochim. Biophys. Acta. 1674, 205–214, (2004).

Karpen, M.E., deHaseth, P.L., Neet, K.E., Differences in the amino acid distributions of 310-helices and α- helices, Protein. Sci.1, 1333–1342, (1992).

Kiatkumjom, T., Rattanarat, P., Sianghproh, W., Chailpakul, O., et al. Glutathione and l-cysteine modified silver nanoplates-based colorimetric assay for a simple, fast, sensitive and selective determination of nickel. Talanta. 128, 215–220, (2014)

Kilejian, A., A unique histidine rich polypeptide from the malaria parasite, Plasmodium lophurae. J. Biol. Chem. 249, 4650–4655, (1974)

Kilejian, A., Histidine-Rich Protein as a Model Malaria Vaccine. Science. 201, 922–924, (1978).

Kimoto, M., Yamashige, R., Matsunaga, K., Yokoyama, S., Hirao, I., Generation of high affinity DNA aptamers using an expanded genetic alphabet. Nat. Biotechnol. 31, 453-457, (2013).

Klein, R., Lin, E., Zhang, B., Luster, A., Tollett, J., et al. Neuronal CXCL10 directs CD8_ T-cell recruitment and control of west nile virus encephalitis. J. Virol. 79, 11457–11466, (2005).

Knecht, S.; Ricklin, D.; Eberle, A.N.; Ernst, B., Oligohis-tags : mechanisms of binding to Ni 2+ -NTA surfaces, J. Mol. Recognit. 22, 270–279, (2009).

Kraemer, S., Vaught, J. D., Bock, C., Gold, L., Katilius, E., et al. From SOMAmer-based biomarker discovery to diagnostic and clinical applications: a SOMAmer-based, streamlined multiplex proteomic assay. PLos One. 6, e26332, (2011).

Kyabayinze, D., Tibenderana, J., Odong, G., Rwakimari, J., Counihan, H., Operational accuracy and comparative persistent antigenicity of HRP2 rapid diagnostic tests for Plasmodium falciparum malaria in a hyperendemic region of Uganda. Malar. J. 7, 221, (2008).

Lab Tech. Link: http://www.cli-online.com/fileadmin/artimg/progress-toward-rapidmalaria-screening-based-on-mass-spectrometry.pdf

Laemmli, U.K., Cleavage of structural proteins during the assembly of the head of bacteriophage T4. Nature. 227, 680–685, (1970).

Laferi, H., Kandel, K., Pichler, H., False positive dipstick test for malaria. N. Engl. J. Med. 337, 1635–1636, (1997).

Lathwal, S., Sikes, H.D., Assessment of colorimetric amplification methods in a paper-based immunoassay for diagnosis of malaria. Lab Chip. 16, 1374-82, (2016).

Lau, Y.L., Fong, M.Y., Mahmud., R., Chang., P.Y., Palaeya, V., et al. Specific, sensitive and rapid detection of human Plasmodium knowlesi infection by loop mediated isothermal amplification in blood samples. Malar. J. 10,197, (2011).

Lee, J.H., Jang, J.W., Cho, C.H., Kim, J.Y., Han, E.T., Yun, S.G., Lim, C.S.,. False-Positive Results for Rapid Diagnostic Tests for Malaria in Patients with Rheumatoid Factor. J. Clin. Microbiol. 52, 3784–3787, (2014).

Lee, K., El-Sayed, M.A., Gold and Silver Nanoparticles in Sensing and Imaging : Sensitivity of Plasmon Response to Size, Shape , and Metal Composition, J. Phys. Chem. 110, 19220–19225, (2006).

Lee, N., Baker, J., Bell, D., McCarthy, J., Cheng, Q., Assessing the genetic diversity of the aldolase genes of Plasmodium falciparum and Plasmodium vivax and its potential effect on performance of aldolase detecting rapid diagnostic tests. J. Clin. Microbiol. 44, 4547–4549, (2006a).

Lee, N., Baker, J., Andrews, K.T., Gatton, M.L., Bell, D., et al. Effect of sequence variation in Plasmodium falciparum histidine rich protein 2 on Binding of specific monoclonal antibodies: implications for rapid diagnostic tests for malaria. J. Clin. Microbiol. 44, 2773–2778, (2006b).

Lee, P.W., Ji, D.D., Liu, C.T., Rampao, H.S., Rosario. V., et al. Application of loop mediated isothermal amplification for malaria diagnosis during a follow up study in Sao Tome. Malar. J.11, 408, (2012).

Lee, S., Manjunatha, H., D., Jeon, W., Ban, C., Cationic Surfactant-Based Colorimetric Detection of Plasmodium Lactate Dehydrogenase, a Biomarker for Malaria, Using the Specific DNA Aptamer. PLoS ONE. 7, e100847, (2014).

Lee, S., Song, K.M., Jeon, W., Jo, H., Shim, Y.B., Ban, C., A highly sensitive aptasensor towards Plasmodium lactate dehydrogenase for the diagnosis of malaria. Biosens. Bioelectron. 35, 291–296, (2012b).

Leech, J., Barnwell, J., Aikawa, M., Miller, L., Howard, R., Plasmodium falciparum malaria association of knobs on the surface of infected erythrocytes with a histidine-rich protein and the erythrocyte skeleton. J. Cell Biol. 98, 1256–1264, (1984).

Li, H., Cui, Z., Han, C., Glutathione-stabilized silver nanoparticles as colorimetric sensor for Ni^{2+} ion. Sens. Actuators, B. 143, 87–92, (2009)

Li, Y., Ning, Y.S., Li., L., Peng, D.D., Dong, W.Q., et al. Preparation of a monoclonal antibodies against Plasmodium falciparum glutamate dehydrogenase and establishment of colloidal gold-immunochromatographic assay. Di Yi Jun Yi Da Xue Xue Bao. 25, 435-8, (2005).

Lillehoj, P.B., Huang, M.C., Truongc, N., Hod , C.M., Rapid electrochemical detection on a mobile phone. Lab Chip.13, 2950-2955, (2013).

Lim, I.I.S., Mott, D., Ip, W., Njoki, P.N., Pan, Y., Zhou, S., Zhong, C.J., Interparticle interactions in glutathione mediated assembly of gold nanoparticles. Langmuir. 24, 8857–8863, (2008).

Lindblade, K.A, Steinhardt, L., Samuels, A., Kachur, S.P., Slutsker, L., The silent threat: asymptomatic parasitaemia and malaria transmission. Expert Rev Anti Infect. 11, 623–39. (2013).

Liu, J., Liu, H., Li, Y., Wang, H., Probing the coordination properties of glutathione with transition metal ions (Cr^{2+}, Mn^{2+}, Fe2+, Co^{2+}, Ni^{2+}, Cu^{2+}, $Zn^{2+,}$ $Cd^{2+,}$ Hg^{2+}) by density functional theory. J. Biol. Phys. 40, 313-323**,** (2014).

Love, J.C., Estroff, L.A., Kriebel, J.K., Nuzzo, R.G., Whitesides, G.M., Self-Assembled Monolayers of Thiolates on Metals as a Form of Nanotechnology. Chem. Rev. 105, 1103-1169. (2005).

Lovegrove, F.E., Tangpukdee, N., Opoka, R.O., Lafferty, E.I., Rajwans, N., et al. Serum angiopoietin-1 and -2 levels discriminate cerebral malaria from uncomplicated malaria and predict clinical outcome in African children. PLoS ONE 4, e4912, (2009).

Lucchi, N., Jain, V., Wilson, N., Singh, N., Udhaykumar, V., et al. Potential serological biomarkers of cerebral malaria. Dis. Markers. 31, 327–335, (2011).

Luchavez, J., Baker, J., Alcantara, S., Belizario, V., Cheng, Q., McCarthy, J.S., Bell, D., Laboratory demonstration of a prozone-like effect in HRP2-detecting malaria rapid diagnostic tests: implications for clinical management. Malar. J. 10, 286, (2011).

Lynn, A., Chandra, S., Malhotra, P., Chauhan, V.S., Heme binding and polymerization by Plasmodium falciparum histidine rich protein II: Influence of pH on activity and conformation. FEBS Lett. 459, 267–271, (1999).

Malleret, B., Claser, C., Ong A.S.M., Suwanarusk,R., Sriprawat, K., et al. A rapid and robust tri-color flow cytometry assay for monitoring malaria parasite development. Scientific reports. 1,118, (2011).

Maltha, J., Gamboa, D., Bendezu, J., Sanchez, L., Cnops, L., et al. Rapid diagnostic tests for malaria diagnosis in the Peruvian Amazon: Impact of pfhrp2 gene deletions and cross reactions. PLoS ONE 7, e43094, (2012).

Maltha, J., Gillet, P., Jacobs, J.,. Malaria rapid diagnostic tests in endemic settings. Clin. Microbiol. Infect. 19, 399–407, (2013).

Marangoni, K., Neves, A.F., Rocha, R.M., Faria, P.R., Alves, P.T., et al. Prostate-specific RNA aptamer: promising nucleic acid antibody-like cancer detection. Sci. Rep. 5, 12090, (2015).

Markwalter, C.F., Ricks, K.M., Bitting, A.L., Mudenda, L., Wright, D.W., Simultaneous capture and sequential detection of two malarial biomarkers on magnetic microparticle, Talanta. 161, 443–449, (2016).

Martin, S.K., Rajasekariah, G.H., Awinda, G., Waitumbi, J., Kifude, C., Unified parasite lactate dehydrogenase and histidine-rich protein ELISA for quantification of Plasmodium falciparum. Am. J. Trop. Med. Hyg. 80, 516–522, (2009).

Martinez, A.W., Phillips, S.T., Whitesides, G.M. Diagnostics for the developing world: microfluidic paper-based analytical devices. Anal. Chem. 82, 3–10 (2010).

Martinez, A.W., Phillips, S.T., Carrilho, E., Iii, S.W.T., Sindi, H., Whitesides, G.M., Simple Telemedicine for Developing Regions : Camera Phones and Paper-Based Microfluidic Devices for Real-Time , Off-Site Diagnosis. Anal. Chem. 80, 3699–3707, (2008).

Martinez, O., Bellard, E., Golzio, M., Mechiche-Alami, S., Rols, M.P., et al. Direct validation of aptamers as powerful tools to image solid tumor. Nucleic Acid Ther. 24, 217-225, (2014).

Mawili-Mboumba, D.P., Akotet, M.K.B., Ngoungou, E.B., Kombila, M., Evaluation of rapid diagnostic tests for malaria case management in Gabon. Diagn. Micr. Infec. Dis. 66, 162–168, (2010).

Mayxay, M., Pukrittayakamee, S., Chotivanich, K., Looareesuwan, S., White, N.J., Persistence of Plasmodium falciparum HRP-2 in successfully treated acute falciparum malaria. Trans. R. Soc. Trop. Med. Hyg. 95, 179–182, (2001).

McMorrow, M.L., Masanja, M.I., Kahigwa, E., Abdulla, S.M.K., Kachur, S.P., Quality assurance of rapid diagnostic tests for malaria in routine patient care in rural Tanzania. Am. J. Trop. Med. Hyg. 82, 151–155, (2010).

Meatherall, B., Preston, K., Pillai, D.R., False positive malaria rapid diagnostic test in returning traveler with typhoid fever. BMC Infect. Dis. 14, 377, (2014).

Melancon, M.P., Zhou, M., Zhang, R., Xiong, C., Allen, P., et al. Selective uptake and imaging of aptamer- and antibody-conjugated hollow nanospheres targeted to epidermal growth factor receptors overexpresses in head and neck cancer. ACS Nano. 8, 4530-4538, (2014).

Minami, T., Liu, Y., Akdeniz, A., Koutnik, P., Esipenko, N.A., Nishiyabu, R., et al., Intramolecular indicator displacement assay for anions: Supramolecular sensor for glyphosate. J. Am. Chem. Soc. 136, 11396–11401, (2014).

Moody, A., Rapid diagnostic tests for malaria parasites. Clin. Microbiol. Rev. 15, 66–78, (2002).

Morassin, B., Fabre, R., Berry, A., Magnaval, J.F., One year's experience with the polymerase chain reaction as a routine method for the diagnosis of imported malaria. Am. J. Trop. Med. Hyg. 66, 503–508, (2002).

Murray, C.K., Gasser, R.A., Magill, A.J., Miller, R.S., Update on rapid diagnostic testing for malaria. Clin. Microbiol. Rev. 21, 97–110, (2008).

National framework for malaria elimination Report 2016, (http://nvbdcp.gov.in/ Doc/National-framework-for-malaria-elimination-in-India2016%E2%80%932030 .pdf)

Ng, E.W., Adamis, A.P., Anti-VEGF aptamer (pegaptanib) therapy for ocular vascular diseases. Ann. N. Y. Acad. Sci. 1082, 151-171, (2006).

Nguyen, B.T., Anslyn, E.V., Indicator-displacement assays. Coord. Chem. Rev. 250, 3118–3127, (2006).

Nicastri, E., Bevilacqua, N., Schepisi, M.S., Paglia, M.G., Meschi, S., et al. Accuracy of malaria diagnosis by microscopy, rapid diagnostic test, and PCR methods and evidence of antimalarial overprescription in non-severe febrile patients in two Tanzanian hospitals. Am. J. Trop. Med. Hyg. 80, 712–717, (2009).

Nieba, L., Neiba-axmann, S.E., Persson, A., Hamalainen, M., et al. BIACORE Analysis of Histidine-Tagged Proteins Using a Chelating NTA Sensor Chip, Anal. Biochem. 228, 217–228, (1997).

Noedl, H., Yingyuen, K., Laoboonchai, A., Fukuda, M., Sirichaisinthop, J., et al. Sensitivity and specificity of an antigen detection ELISA for malaria diagnosis. Am. J. Trop.Med. Hyg. 75, 1205–1208, (2006).

Oh, J.H., Park, D.H., Joo, J.H., Lee, J.S., Recent advances in chemical functionalization of nanoparticles with biomolecules for analytical applications, Anal. Bioanal. Chem. 407, 8627-8645, (2015).

Oliveira, M.F., Silva, J.R., Dansa-Petretski, M., Souza, W. de Lins, U., et al. Haem detoxification by an insect. Nature. 400, 517–518, (1999).

Olszewski, K.L., Llinás, M., Central carbon metabolism of Plasmodium parasites. Mol. Biochem. Parasitol. 175, 95–103, (2011).

Pagola, S., Stephens, P.W., Bohle, D.S., Kosar, A.D., Madsen, S.K., The structure of malaria pigment β-haematin. Nature. 404, 307–310, (2000).

Pal, P., Balaban, A.E., Diamond, M.S., Sinnis, P., Klein, R.S., Goldberg, D.E., Plasmodium falciparum histidine-rich protein II causes vascular leakage and exacerbates experimental cerebral malaria in mice. PLoS One. 12 , e0177142, (2016).

Pal, P., Danielsd, B.P., Oskmanc, A., Diamonda, M.S., Kleinb, R.S., Goldberg, D.E., Plasmodium falciparum Histidine-Rich Protein II Compromises Brain Endothelial Barriers and May Promote Cerebral Malaria Pathogenesis. mbio.7, e00617, (2016)

Palmer, C.J., Lindo, J.F., Klaskala, W.I., Quesada, J.A., Kaminsky, R., et al. Evaluation of the OptiMAL test for rapid diagnosis of Plasmodium vivax and Plasmodium falciparum malaria. J. Clin. Microbiol. 36, 203–206, (1998).

Pandey, A.V., Bisht, H., Babbarwal, V.K., Srivastava, J., Pandey, K.C., Chauhan, V.S., Mechanism of malarial haem detoxification inhibition by chloroquine, Biochem. J. 355, 333–338, (2001).

Parekh, P., Kamble, S., Zhao, N.X., Portier, B.P., Zu, Y.L. Immunotherapy of CD30-expressing lymphoma using a highly stable ssDNA aptamer. Biomaterials. 34, 8909-8917, (2013).

Parra, M.E., Evans, C.B., Taylor, D.W., Identification of Plasmodium falciparum histidine-rich protein 2 in the plasma of humans with malaria. J Clin Microbiol. 29, 1629–1634, (1991).

Paul K.B., Kumar S., Tripathy S., Vanjari S. R.K., Singh V., et al. A highly sensitive self-assembled monolayer modified copper doped zinc oxide nanofiber interface for detection of Plasmodium falciparum histidine-rich protein-2: targeted towards rapid, early diagnosis of malaria, Biosens. Bioelectron. 80, 39–46, (2016).

Peeling, R.W., Holmes, K.K., Mabey, D., Ronald, A., Rapid tests for sexually transmitted infections (STIs): the way forward. Sex. Transm. Infect. 82, 1–6, (2006).

Peeling, R.W., Mabey, D., Point-of-care tests for diagnosing infections in the developing world. Clin. Microbiol. Infect. 16, 1062–1069, (2010).

Peng, Y., Wu, J., Wang, J., Li, W., Yu, S., Study and evaluation of Wondfo rapid diagnostic kit based on nano-gold immunochromatography assay for diagnosis of Plasmodium falciparum. Parasitol. Res. 110, 1421–1425, (2012).

Pisciotta, J.M., Coppens, I., Tripathi A.K. et al. The role of eutral lipid nanospheres in Plasmodium falciparum haem crystallization, Biochem. J. 402, 197–204, (2007).

Pisciotta, J.M., Ponder, E.L., Fried, B., Sullivan, D., Hemozoin formation in Echinostoma trivolvis rediae. Int. J. Parasitol. 35, 1037–1042, (2005).

Pologe, L.G., Pavlovec, A., Shio, H., Ravetch, J.V., Primary structure and subcellular localization of the knob-associated histidine-rich protein of Plasmodium falciparum, Proc. Natl. Acad. Sci. U. S. A, 84, 7139–7143, (1987).

Potyrailo, R.A., Murray, A.J., Nagraj, N., Pris, A.D., Ashe, J.M., et al. Towards maintenance-free biosensors for hundreds of bind/release cycles. Angew. Chem. Int. Ed. Engl. 54, 2174-2178, (2015).

Radom, F., Jurek, P.M., Mazurek, M.P., Otlewski, J., Jeleń, F., Aptamers: molecules of great potential. Biotechnol. Adv. 31, 1260-1274, (2013).

Rakotonirina, H., Barnadas, C., Raherijafy, R., Andrianantenaina, H., Ratsimbasoa, A., et al. Accuracy and reliability of malaria diagnostic techniques for guiding febrile outpatient treatment in malaria endemic countries. Am. J. Trop. Med. Hyg. 78, 217–221, (2008).

Ramutton, T., Hendriksen, I., Mwanga-Amumpaire, J., Mtove, G., Olaosebikan, R., et al. Sequence variation does not confound the measurement of plasma PfHRP2 concentration in African children presenting with severe malaria. Malar. J., 11,276, (2012).

Ratha, A., Glibowicka, M., Nadeaua, V.G., Chena, G., Debera, C.M., Detergent binding explains anomalous SDS-PAGE migration of membrane proteins. Proc. Natl. Acad. Sci. U.S.A. 106, 1760-1765, (2009).

Ravindran, A., Chandran, P., Khan, S.S., Biofunctionalized silver nanoparticles : Advances and prospects. Colloids Surf. B. 105, 342–352, (2013).

Richardson, D.C., Ciach, M., Zhong, K.J.Y., Crandall, I., Kain, K.C., Evaluation of the Makromed dipstick assay versus PCR for diagnosis of Plasmodium falciparum malaria in returned travelers. J. Clin. Microbiol. 40, 4528–4530, (2002).

Rock, E.P., Marsh, K., Saul, A.J., Wellems, T.E., Taylor, D.W., et al. Comparative analysis of the Plasmodium falciparum histidine-rich proteins HRP-I, HRP-II and HRP-III in malaria parasites of diverse origin. Parasitology. 95, 209–227, (1987).

Rodríguez-Acosta A., Domínguez., N.G., Aguilar I., Girón. M.E., Characterization of Plasmodium falciparum glutamate dehydrogenase-soluble antigen. Braz. J. Med. Biol. Res. 31, 1149-1155, (1998).

Rogier, E., Plucinski, M., Lucchi, N., Mace, K., Chang, M., Lemoine, J.F., et al. Bead-based immunoassay allows sub-picogram detection of histidine-rich protein 2 from Plasmodium falciparum and estimates reliability of malaria rapid diagnostic tests. PLoS One. 12, e0172139, (2017).

Roth, E., Plasmodium falciparum carbohydrate metabolism - a connection between host cell and parasite. Blood Cells. 16, 453–460, (1990).

Rubach, M.P., Mukemba, J., Florence, S., John, B., Crookston, B., Lopansri, B.K., et al. Plasma Plasmodium falciparum histidine-rich protein-2 concentrations are associated with malaria severity and mortality in Tanzanian children. PLoS One 7, 3–7, (2012).

Santos, L., Pereira, N.R., Andrade, P., Dias, P.F., Alves, C.L., Abreu, C., et al. Prozone-like phenomenon in travellers with fatal malaria: Report of two cases. J. Infect. Dev. Ctries. 9, 321–324, (2015).

Schneider, E.L., Marletta, M.A., Heme binding to the histidine-rich protein II from Plasmodium falciparum. Biochemistry. 44, 979-86, (2005).

Sessions, R.B., Dewar, V., Clarke, A.R. and Holbrook, J., A model of Plasmodium falciparum lactate dehydrogenase and its implications for the design of improved antimalarials and the enhanced detection of parasitaemia. Protein. Eng. 10,301-6, (1997).

Sun, S.K, Tu, K.X., Yan, X.P., An indicator-displacement assay for naked-eye detection and quantification of histidine in human urine. Analyst. 137, 2124-8, (2012).

Sharma, M.K., Agarwal, G.S., Rao, V.K., Upadhyay, S., Merwyn, S., et al., Amperometric immunosensor based on gold nanoparticles/alumina sol-gel modified screen-printed electrodes for antibodies to Plasmodium falciparum histidine rich protein-2. Analyst. 135, 608-614, (2010).

Sharma, M.K., Rao, V.K., Merwyn, S., Agarwal, G.S., Upadhyay, S., et al. A novel piezoelectric immunosensor for the detection of malarial Plasmodium falciparum histidine rich protein-2 antigen. Talanta. 85, 1812–1817, (2011).

Sharma, M.K., Rao, V.K., Agarwal, G.S., Rai, G.P., Gopalan, N., et al. Highly sensitive amperometric immunosensor for detection of Plasmodium falciparum histidine rich protein 2 in serum of humans with malaria: comparison with a commercial kit. J. Clin. Microbiol. 46, 3759–3765, (2008).

Shear, H.L., Wanidworanun, C.C., Nagel, R.L., Antisense oligonucleotides targeting malarial aldolase inhibit the asexual erythrocytic stages of Plasmodium falciparum," Mol. Biochem Parasitol. 102, 91–101, (1999).

Singh, N., Saxena, A., Awadhia, S.B., Shrivastava, R., Singh, M.P., Evaluation of a rapid diagnostic test for assessing the burden of malaria at delivery in India. Am. J. Trop. Med. Hyg. 73, 855–858, (2005).

Slater, A.F., Swiggard, W.J., Orton, B.R., Flitter, W.D., Goldberg, D.E., et al. An iron carboxylate bond links the heme units of malaria pigment. Proc. Natl. Acad. Sci. USA. 88, 325–329, (1991).

Solomonov, I., Osipova, M., Feldman, Y., Baehtz, C., Kjaer, K., et al. Crystal nucleation, growth, and morphology of the synthetic malaria pigment β-hematin and the effect thereon by quinoline additives: The malaria pigment as a target of various antimalarial drugs. J. Am. Chem. Soc. 129, 2615–2627, (2007).

Song H.O., Lee, B., Bhusal, R.P., Park, B., Yu, K., et al. Development of a Novel Fluorophore for Real-Time Biomonitoring System, Plos One. 7, e48459, (2012).

Srivastava, I.K., Schmidt, M., Certa, U., Döbeli ,H., Perrin, L.H., Specificity and inhibitory activity of antibodies to Plasmodium falciparum aldolase. J. Immunol. 144:1497– 503, (1990).

Stahl, H.D., Kemp, D.J., Crewther P.E. et al., Sequence of a cDNA encoding a small polymorphic histidine- and alanine-rich protein from Ptasmodium falciparum, Nucleic Acids. Res. 13, 7837–7846, (1985).

Stauga, S., Hahn, A., Brattig, N.W., Herr, J.F., Baldus, S., Burchard, G.D., Cramer, J.P., Clinical relevance of different biomarkers in imported plasmodium falciparum malaria in adults: a case control study, Malar. J. 12, 246-254, (2013)

Stoltenburg, R., Nikolaus, N., Strehlitz, B., Capture-SELEX: Selection of DNA Aptamers for Aminoglycoside Antibiotics. J. Anal. Methods. Chem. 2012, 415697, (2012).

Storm, J., Perner, J., Aparicio, I., Patzewitz, E.M., Olszewski, K., et al. Plasmodium falciparum glutamate dehydrogenase a is dispensable and not a drug target during erythrocytic development, Malar. J. 10, 193-205, (2011).

Sui, Y., Potula, R., Dhillon, N., Pinson, D., Li, S., et al. Neuronal apoptosis is mediated by CXCL10 overexpression in simian human immunodeficiency virus encephalitis. Am. J. Pathol. 164, 1557–1566, (2004).

Sullivan, D.J., Gluzman, I.Y., Goldberg, D.E., Plasmodium hemozoin formation mediated by histidine-rich proteins. Science. 271, 219–222, (1996).

Sun, H., Zu, Y.A., Highlight of Recent Advances in Aptamer Technology and Its Application. Molecules. 20, 11959-11980, (2015).

Swartz, J.D., Gulka, C.P., Haselton, F.R., Wright, D.W., Development of a Histidine-Targeted Spectrophotometric Sensor Using Ni(II)NTA-Functionalized Au and Ag Nanoparticles, Langmuir, 27, 15330–15339, (2011).

Tangpukdee, N., Duangdee, C., Wilairatana, P., Krudsood, S., Malaria Diagnosis: A Brief Review. Korean J Parasitol. 47, 93-102, (2009).

Tjitra, E., Suprianto, S., Dyer, M., Currie, B.J., Anstey, N.M., Field evaluation of the ICT malaria P.f/P.v immunochromatographic test for detection of Plasmodium falciparum

and Plasmodium vivax in patients with a presumptive clinical diagnosis of malaria in Eastern Indonesia. J. Clin. Microbiol. 37, 2412–2417, (1999).

Tnag, L., Li, J., Plasmon-Based Colorimetric Nanosensors for Ultrasensitive Molecular Diagnostics. ACS Sens. 2, 857-875, (2017).

Toedter, G., Hayden, K., Wagner, C., Brodmerkel, C., Simultaneous detection of eight analytes in human serum by two commercially available platforms for multiplex cytokine analysis. Clin. Vaccine Immunol. 15, 42–48, (2008).

Trampuz A., Jereb M., Muzlovic I., Prabhu R.M., Clinical review: Severe malaria, Crit. Care, 7, 315-323, (2003).

Uguen, C., Rabodonirina, M., De Pina, J.J., Vigier, J.P., Martet, G., et al. ParaSight-F rapid manual diagnostic test of Plasmodium falciparum infection. Bull World Health Organ. 73, 643–649, (1995).

Valenti, L.E., De Pauli, C.P., Giacomelli, C.E., The binding of Ni(II) ions to hexahistidine as a model system of the interaction between nickel and His-tagged proteins. J. Inorg. Biochem. 100, 192–200, (2006).

Valle, M.R., Quakyi, I.A., Amuesi, J., Quaye, J.T., Nkrumah, F.K., et al. Detection of antigens and antibodies in the urine of humans with Plasmodium falciparum malaria. J. Clin. Microbiol. 29, 1236–1242, (1991).

Wagner, J.T., Ludeman, H., Farber., P.M., Lottspeich, F., Krauth–Siegel, R.L., Glutamate dehydrogense, the marker protein of Plasmodium falciparum : cloning, expression and characterization of malarial enzyme. Eur. J .Biochem . 258, 813-819, (1998).

Wasowicz, M., Milner, M., Radecka, D., Grzelak, K., Radecka, H., Immunosensor Incorporating Anti-His (C-term) IgG F(ab') Fragments Attached to Gold Nanorods for Detection of His-Tagged Proteins in Culture Medium. Sensors. 10, 5409-5424, (2010).

Wasowicz, M., Viswanathan, S., Dvornyk, A., Grzelak, K., Kludkiewicz, B., Radecka, H., Comparison of electrochemical immunosensors based on gold nano materials and immunoblot techniques for detection of histidine-tagged proteins in culture medium, Biosens. Bioelectron. 24, 284-289, (2008).

Wellems, T.E., Howard, R.J., Homologous genes encode two distinct histidine-rich proteins in a cloned isolate of Plasmodium falciparum. Proc. Natl. Acad. Sci. USA. 83, 6065–6069, (1986).

Wenisch, C., Spitzauer, S., Florris-Linau, K., Rumpold, H., Vannaphan, S., et al. Complement Activation in Severe Plasmodium falciparum malaria. Clin. Immunol. Immunopathol. 85, 166–171, (1997).

Willets, K.A., Duyne, R.P., Localized Surface Plasmon Resonance Spectroscopy and Sensing, Angew. Chem., 58, 267–297, (2006).

Wongsrichanalai, C., Barcus, M.J., Muth, S., Sutamihardja, A., Wernsdorfer, W.H., A review of malaria diagnostic tools: microscopy and rapid diagnostic test (RDT). The Am. J.Trop. Med. Hyg. 77, 119 –127, (2007).

Wongsrichanalai, C., Rapid diagnostic techniques for malaria control. Trends Parasitol. 17, 307–309, (2001).

Wood, O.D., Dinsmore, J.M., Bare, A.G, Lee, S.J., M-DNA is stabilised in G•C tracts or by incorporation of 5-fluorouracil. Nucleic Acids Res. 30, 2244–2250, (2002).

World Malaria Report, 2016, (http://apps.who.int/iris/bitstream/10665/252038/1/9789241511 711-eng.pdf?ua=1)

Xiong, X.L., Lv, Y.F., Chen, T., Zhang, X.B., Wang, K.M., et al. Nucleic acid aptamers for living cell analysis. Annu. Rev. Anal. Chem (Palo Alto Calif). 7, 405-426 (2014).

Li, X., Tian, J., Garnier, G., Shen, W., Fabrication of paper-based microfluidic sensors by printing. Colloids Surf B Biointerfaces. 76, 564-70, (2010).

Yang, Q., Goldstein, I.J., Mei, H.Y., Engelke, D.R. DNA ligands that bind tightly and selectively to cellobiose. Proc. Natl. Acad. Sci. U S A. 95, 5462-5467 (1998).

Yang, S., Parmley, S.F., Toxoplasma gondii expresses two distinct lactate dehydrogenase homologous genes during its life cycle in intermediate hosts. Gene. 184, 1–12, (1997).

Yeo S.J., Huong D.T., Han J.H., Kim J.Y., Lee W.J., et al. Performance of coumarin derived dendrimer-based fluorescence-linked immunosorbent assay (FLISA) to detect malaria antigen. Malar. J.13,266, (2014).

Yu, Y., Hong, Y., Gao, P., Nazeeruddin, M.K., Glutathione Modified Gold Nanoparticles for Sensitive Colorimetric Detection of Pb^{2+} Ions in Rainwater Polluted by Leaking Perovskite Solar Cells. Anal. Chem. 88, 12316-12322, (2016).

Zhang B., Chan Y., Lu B., Diamond M., Klein R., CXCR3 mediates region-specific antiviral T cell trafficking within the central nervous system during west nile virus encephalitis, J. Immunol,180:2641-2649, (2008).

Ziegler, J., Chang, R.T., Wright D.W., Multiple-antigenic peptides of histidine-rich protein II of Plasmodium falciparum: dendrimeric biomineralization templates, J. Am. Chem. Soc, 121, 2395–2400, (1999).

List of Publications

- **Babina Chakma**, Priyamvada Jain and Naveen K. Singh and Pranab Goswami. Development of electrochemical impedance spectroscopy based aptasensor for malaria using HRP-II as target biomarker. (Manuscript submitted).
- **Babina Chakma**, Naveen K. Singh, Priyamvada Jain and Pranab Goswami. Detection of histidine rich proteins following silver nanoparticle based sensitive competitive binding assay. (**2017**) (Manuscript under review).
- **Babina Chakma**, Priyamvada Jain, Naveen K. Singh and Pranab Goswami. Development of an indicator displacement based detection of malaria targeting HRP-II as biomarker for application in point-of-care settings. Analytical Chemistry.88, 10316-1032 (**2016**).
- Priyamvada Jain, **Babina Chakma** (equal 1st author contribution), Sanjukta Patra, and Pranab Goswami Potential biomarkers and their applications for rapid and reliable detection of malaria. BioMed Research International. ID 852645 (**2014**).
- Priyamvada Jain, **Babina Chakma**, Naveen K. Singh, Sanjukta Patra, Pranab Goswami*, Metal-DNA interactions improve signal in high resolution melting of DNA for species differentiation of Plasmodium parasite, Molecular Biotechnology.59,179-191 (**2017).**
- Priyamvada Jain, **Babina Chakma**, Sanjukta Patra, Pranab Goswami Hairpin stabilized fluorescent silver nanoclusters for quantitative detection of NAD^+ and monitoring NAD^+/NADH based enzymatic reactions. Analytica Chimica Acta 956, 48–56 (**2017).**

- Priyamvada Jain, **Babina Chakma**, Naveen Kumar Singh, Sanjukta Patra, Pranab Goswami, Aromatic surfactant as aggregating agent for aptamer-gold nanoparticle based detection of Plasmodium lactate dehydrogenase. Molecular Biotechnology.58, 497-508 **(2016**).
- Priyamvada Jain, Smita Das, **Babina Chakma**, Pranab Goswami, Aptamer-graphene oxide for highly sensitive dual electrochemical detection of Plasmodium lactate dehydrogenase, Analytical Biochemistry, 514, 32–37(**2016**).

Table A1: List of bacterial strains

Strain	Description
Escherichia coli DH5α (Novagen)	F'ϕ80dlacZΔM15 Δ (lacZYA-argF) U169 endA1 recA1 hsdR17 (rk^-mk^+) deoR thi-1 phoA supE44 λ^- gyrA96 relA1
Escherichia coli BL21 (DE3) (Novagen)	F^- ompT hsdSB (rB^- mB^-) gal dcm (DE3). Derivation of B834. (Parental strain: B834; Resistance: none)

Table A2: Culture medium for bacteria

Medium Composition	**Composition**
Luria Bertani broth (LB) (1 L)	Casein enzymic hydrolysate 10 g, Yeast extract 5 g, NaCl 10 g, pH 7.5 + 0.2
Casein enzymic hydrolysate 10 g, Yeast	Casein enzymic hydrolysate 10 g, Yeast extract 5 g, NaCl 10 g, Agar 15 g, pH 7.5 ± 0.2

Table A3: Buffers and solutions

Solutions for plasmid isolation

Solution I	50 mM glucose, 25 mM Tris-Cl buffer, 10 mM EDTA, pH 8.0
Solution II	0.2 N NaOH, 1 % SDS
Solution III	5 M potassium acetate, pH adjusted to 4.8 with acetic acid

Buffer for agarose gel electrophoresis

TAE buffer (50X) 1L	242 g Tris base, 57.1 ml glacial acetic acid, 100 ml 0.5 M EDTA (pH 8), adjust final volume to 1L with water

Solution for competent cell preparation

Transformation and storage solution (TSS)	10 % (w/v) polyethylene glycol, 5 % (v/v) dimethyl sulfoxide and 50 mM $MgCl_2$ in LB broth, pH 6.5

Buffers for protein purification

Lysis/Equilibration buffer	20 mM Tris buffer, 500 mM NaCl pH 8
Washing buffer	20 mM Tris buffer, 500 mM NaCl, supplemented with varying concentration of imidazole (50 mM, and 100 mM), pH 8
Elution buffer	20 mM sodium phosphate buffer, 500 mM NaCl, 350 mM imidazole

Buffers/solutions for SDS-PAGE

30 % acrylamide-bisacrylamide gel solution (100 ml)	29.2 g acrylamide, 0.8 g bisacrylamide
Tris-HCl, pH 6.8, 0.5 M (100 ml)	6.06 g Tris base, pH adjusted to 6.8 with 2 N HCl
Tris-HCl, pH 8.8, 1.5 M (100 ml)	18.18 g of Tris base, pH adjusted to 8.8 with 2 N HCl
Gel running buffer (10X)	30.0 g of Tris base, 144.0 g of glycine, and 10.0 g of SDS in 1000 ml of water.
SDS gel loading buffer (2X)	100 mM Tris/HCl (pH 6.8), 4 % (w/v) SDS, 0.2% (w/v) bromophenol blue dye, 20 % (v/v) glycerol, 200 mM DTT or β-mercaptoethanol
Staining solution (blue silver staining) (100 ml)	10 ml ortho phosphoric acid, 10 g w/v ammonium sulfate, 0.12 g w/v

Composition of Biuret solution

Biuret solution	1.50 g of cupric sulfate pentahydrate ($CuSO_4.5H_2O$) with 6.0 g sodium potassium tartrate tetrahydrate ($NaKC_4H_4O_64.H_2O$) in 500 ml of H_2O. Add 300 ml 10 % (w/v) NaOH and make the volume to 1 litre with water

Solutions for SELEX

Binding buffer	50 mM sodium phosphate buffer, pH 7.4, 50 mM NaCl, 5 mM KCl, 2.5 mM $MgCl_2$
Coupling buffer	20 mM Tris HCl, pH 7.5, 0.5 M NaCl, 1 mM EDTA
TBE buffer (5X)	54 g of Tris base, 27.5 g of boric acid, 20 mL of 0.5 M EDTA (pH 8.0)
10 % acrylamide bisacrylamide Gel solution (75:1), 15 ml	5 ml of 30 % acrylamide-bisacrylamide solution (75:1), 3 ml, TBE buffer (5X), 105 µl 10 % APS, 10 µl TEMED, 6.8 ml water

Table A4: List of primers

Name	Sequence (5'-3')
F1	CACCTAATACGACTCACTATAGCGGA
R1	GCAAGCTTGTTCGAGCCAG
R1-biotin	biotin-GCAAGCTTGTTCGAGCCAG